Microfluidic Chip Design for Studying Ultrafiltration Failure in the Fibrotic Peritoneum

A Major Qualifying Project report submitted to the faculty of Worcester Polytechnic Institute in partial fulfillment of the requirements for the Degree of Bachelor of Science in Biomedical Engineering

Submitted by:
Araceli Baeza González
Cleo Caldwell
Alison Drapeau
Gabriel Rivera

Submitted to:
Dr. Catherine Whittington
Dr. Diana Alatalo

April 27, 2023

Table of Contents

List of Figures

List of Tables

Authorship

Report Section	Primary Author	Primary Editor
1.0 - Introduction		
1.1 - Statement of Problem and Clinical Need	Gabriel	Araceli
1.2 - Project Goals	Gabriel	Araceli
2.0 - Literature Review		
2.1 - Kidney Failure Treatments	Alison	Gabriel
2.1.1 - Kidney Transplant	Alison	Gabriel
2.1.2 - Hemodialysis	Alison	Gabriel
2.1.3 - Peritoneal Dialysis	Alison	Gabriel
2.2 - Ultrafiltration Failure	Alison	Gabriel/Cleo
2.3 - Physiological Changes to the Peritoneum during Peritoneal Dialysis Treatment	Alison	Araceli
2.4 - Lymphangiogenesis May Lead to Ultrafiltration Failure	Alison	Araceli
2.5 - Prior Art	Gabriel	Alison
2.5.1 - Gold Standards for Ultrafiltration Failure Models	Gabriel	Cleo
2.5.2 - Microfluidic Device Models	Gabriel	Cleo
2.6 - Microfluidic Models	Araceli/Cleo	Alison
2.6.1 Benefits and Limitations	Cleo	Alison
2.6.2 Fabrication Techniques	Gabriel	Cleo
3.0 - Project Strategy		
3.1 - Initial Client Statement	All	All
3.2 - Design Requirements	Araceli/Cleo	Gabriel
3.2.1 - Objectives	Araceli	Gabriel/Alison

3.2.2 - Functions	Araceli	Gabriel/Alison
3.2.3 - Constraints	Araceli	Alison
3.2.4 - Means	Cleo	Araceli
3.3 - Revised Client Statement	All	All
3.4 - Relevant Industry Standards	Alison	Araceli
4.0 - Design Process		
4.1 - Needs Analysis	Araceli	Cleo
4.1.1 - Needs	Araceli	Cleo
4.1.2 - Wants	Araceli	Cleo
4.2 - Conceptual Designs	All	Gabriel
4.2.1 - Three-Chamber Chip Conceptual Design	Cleo	Araceli
4.2.2 - Cross Flow 3D Chip Conceptual Design	Alison	Cleo
4.2.3 - Multi-Microfluidic Channel Chip Conceptual Design	Araceli	Gabriel
4.2.4 - Lumen Multi-Microfluidic Channel Chip Conceptual Design	Araceli	Gabriel
4.2.5 - Daisy Chained Chip Conceptual Design	Gabriel	Alison
4.3 - Front-Running Alternative Design Selection	Araceli	Alison
4.4 - Feasibility Testing and Final Design Selection Criteria	Araceli	Alison
4.4.1 - Preliminary Designs Manufacturing and Assembly	All	All
4.4.2 - Hydrogel Formulation	Araceli	Cleo
4.4.3 - Hydrogel Seeding	Araceli	Gabriel

4.4.4 - Final Design Selection	Alison	Gabriel
5.0 - Final Model Manufacturing and Formulation		
5.1 - Final Manufacturing Process	Alison	Araceli
5.2 - Fluid Addition	Alison/Araceli	Gabriel/Alison
5.3 - Syringe Pump Flow Setup	Araceli	Alison
6.0 - Final Model Verification Testing		
6.1 - Stiffness Characterization of Hydrogel Using Rheology	Gabriel	Alison
6.1.1 - Rheology Testing Methods	Gabriel	Alison
6.1.2 - A Stiffness Greater Than the Stiffness in the Healthy Peritoneum is Achieved	Gabriel	Alison
6.2 - Permeability Characterization of Hydrogel using Transwell System	Cleo	Alison
6.2.1 - Permeability Characterization of Hydrogel Methods	Cleo/Araceli	Alison
6.2.2 - Permeability Coefficient Obtained from Transwell Assay	Cleo	Araceli
6.2.3 - Parameter Optimization in COMSOL Multiphysics Estimated the Diffusion Coefficient Across the Collagen Hydrogel	Araceli	Alison
6.3 - Standard Peritoneal Permeability Assay	Cleo	Alison
6.3.1 - Experimental MTAC Methods	Cleo	Alison
6.3.2 - Simulated MTAC in COMSOL Multiphysics Estimates Dwell Time of 6 Hours	Araceli	Alison
6.3.3 - MTAC in the	Araceli	Alison

Microfluidic Model Differs from Predicted Values in the Simulation		
6.4 - Sterility Testing	Alison	Gabriel
6.4.1 - Sterility Testing Methods	Alison	Gabriel
6.4.2 - Higher Absorbance Measured in Non-Sterile Control Chips Compared to Sterilized Chips	Alison	Gabriel
6.4.3 - High Number of Round Colonies Seen in Agar Plating of All Groups	Alison	Gabriel
7.0 - Final Design and Validation		
7.1 - Assessment of Objectives	Alison	Gabriel
7.1.1 - Representative of *in vivo* Conditions	Cleo	Alison
7.1.2 - Accessible for Research Purposes	Araceli	Cleo
7.1.3 - Production	Alison	Araceli
7.1.4 - Cost Effectiveness	Alison	Araceli
7.1.5 - Reusability	Gabriel	Alison
7.2 - Ethical Impact of Designs	Cleo	Araceli
7.2.1 - Economic Impact	Gabriel	Cleo
7.2.2 - Environmental Impact	Gabriel	Alison
7.2.3 - Social Impact	Cleo	Alison
7.2.4 - Global Impact	Alison	Araceli
7.2.5 - Health and Safety Concerns	Araceli	Alison
7.2.6 - Manufacturability	Araceli	Alison
7.2.8 - Sustainability	Alison	Gabriel
8.0 - Discussion		

8.1 - Discussion of Stiffness Results	Gabriel	Alison
8.2 - Discussion of Permeability Results	Cleo	Araceli
8.3 - Discussion of Standard Peritoneal Permeability Assay and MTAC Results	Alison	Araceli
8.4 - Discussion of Sterility Test Results	Alison	Araceli
9.0 Conclusion and Recommendations		
9.1 - Future Work - Permeability Assay	Cleo	Gabriel
9.2 - Future Work - Optimize Pump Set-Up	Alison	Araceli
9.3 - Future Work - Device Cellularization	Cleo	Gabriel
9.4 - Future Work - Reducing Dwell Time and Further SPA Experimentation	Cleo	Araceli
9.5 - Future Work - Reusability	Araceli	Gabriel

Acknowledgements

Abstract

Approximately 15% of adults in the United States alone have gradual loss of kidney function due to chronic kidney disease (CKD) [1]. The closest option to a cure for CKD is a kidney transplant and current treatment methods include hemodialysis and peritoneal dialysis (PD) while patients wait for a transplant. However, 18% of patients who start on PD ultimately switch to hemodialysis due to ultrafiltration failure (UFF), which results in failure to provide adequate waste product filtration of the blood [10]. Ultrafiltration failure is thought to occur so frequently with PD due to physiological changes, including fibrosis and increased lymphatic vascular growth, in the peritoneum from repeat exposure to dialysate fluid. In order to increase the viability of PD as a treatment option for a larger percentage of patients, these physiological changes and the effect of more biocompatible dialysate solutions on ultrafiltration rate need to be completely understood. There is currently no high throughput in vitro model that includes a fibrotic environment and incorporates interstitial flow to study this exact condition. Therefore, there exists a need to develop a microfluidic model for this purpose.

The design that satisfied objectives to begin accurately modeling the physiological condition consists of a three chamber microfluidic chip manufactured using soft lithography. The first chamber is a vascular fluidic channel that accommodates for the flow of a blood analog fluid via a syringe pump system to mimic the function of a capillary. The middle chamber accommodates a bovine collagen hydrogel (Telocol®-10) with an average stiffness of 5.04 kPa akin to the fibrotic peritoneum after approximately three months of PD treatment [55]. This hydrogel has a theoretical mass area transfer coefficient (MTAC) for urea within the range of 22.9 ± 7.04 mL/min after a dwell time of six hours that was confirmed with a COMSOL simulation of the microfluidic model [52]. The final chamber is a reservoir for dialysate fluid, where waste products from the blood analog diffuse across the hydrogel and can be removed after the dwell time.

The model is determined to be representative of the in vivo conditions of interest through the stiffness and mass transfer area coefficient transport property characterizations. It is a cost effective option that is able to be produced in a standard academic lab. It is accessible for research purposes in the sense that preliminary sterility testing confirms the ability to create a sterile environment for future cellularization of the model. The identification of an adequate sterilization method lays the framework for re-sterilization of the chips following a cleaning after an experiment, indicating the model is potentially reusable. In addition to cellularization of the model to allow for studying the effect of increased lymphatic vessel growth, future work could optimize the dwell time with simple chamber dimension changes to allow for quicker diffusion and higher throughput screenings of ultrafiltration.

1.0 Introduction

1.1 Statement of Problem and Clinical Need

Chronic kidney disease (CKD) is described as the gradual loss of kidney function estimated to affect 15% of adults in the U.S [1]. The kidneys are responsible for removing waste products and excess fluids from the blood through the urine. Kidney failure and CKD causes dangerous levels of waste products to build up inside the body causing poisoning and rapid eventual death unless treated. Current treatments for CKD focus on slowing the progression of kidney damage, and end stage CKD is treated by kidney transplantations or using an artificial filtering method known as dialysis. Even though transplantation is the treatment of choice, there is a shortage of donors for a high demand. Therefore, dialysis is the only alternative despite the fact that patients undergoing this treatment have 15-20% mortality rates. There are two main types of dialysis: hemodialysis and peritoneal dialysis. On one hand, hemodialysis uses an artificial kidney or dialysis machine to filter the waste products; and on the other, peritoneal dialysis uses dialysate flowing through a catheter into the abdominal cavity. Here the peritoneum acts as a filter removing waste products from the blood, and after a set period of time the dialysate is removed from the abdominal cavity and discarded. However, there is a common complication associated with long term peritoneal dialysis known as ultrafiltration failure (UFF) which causes insufficient filtration rates in the peritoneum mainly because of non biocompatible dialysis which leads to inflammation and fibrosis [2].

Fibrosis is a process characterized by progressive accumulation of extracellular matrix eventually leading to scar tissue formation and organ dysfunction [3]. Recent research has shown that kidney's that underwent injury, often fail to repair themselves completely often leading to fibrosis [4]. Fibrosis is a significant health problem present in many diseases affecting millions of people worldwide. The incidence of fibrotic diseases and fibrotic related deaths is predicted to increase exponentially as there is a correlation with the increasing prevalence of obesity and kidney diseases. Currently, there are no therapies available to reverse chronic fibrosis or CKD, and the persistence of this clinical need is mostly due to the complexity of the disease process and lack of reliable and reproducible in vitro models. Therapies that have proved potentially effective in animal fibrosis models have failed clinical trials, suggesting a disparity between animal and human models [3].

The lymphatic system also plays a pivotal role regulating kidney function. Kidney's have a large network of lymphatic vessels that clear fluid and small molecules from the renal interstitium. Lymphatic vessels are thus linked with the progression and maintenance of kidney disease [5]. In the case of peritoneal dialysis, lymphatic vessels can uptake the dialysate fluid counteracting peritoneal ultrafiltration and leading to type 4 UFF. Lymphangiogenesis or new lymphatic vessel formation is generally observed during tissue fibrosis. Therefore,

lymphangiogenesis can lead to more dialysate being removed by lymphatic vessels and insufficient ultrafiltration [6].

Due to the important role that lymphangiogenesis and fibrosis play in peritoneal dialysis, it is pivotal that an *in vitro* model be developed which incorporates both processes for the understanding and development of treatments. Where both physiological changes contribute to ultrafiltration failure, it is the hope that understanding of these changes will lead to mitigation or even reversal strategies and, in turn, strategies to prevent ultrafiltration failure. Prevention of ultrafiltration failure will allow peritoneal dialysis to be a viable treatment option for a larger subset of the population living with CKD.

1.2 Project Goals

There is an overwhelming clinical need for *in vitro* models that can accurately model the complexity of disease processes like lymphangiogenesis and fibrosis. Accurate *in vitro* modeling of lymphangiogenesis and fibrosis, would be revolutionary for the health and medicine field as understanding the disease processes can lead to therapeutic treatment developments potentially impacting millions of patients affected by CKD and other fibrotic related diseases. For these reasons, the goal of our project is to develop a microfluidic chip model of peritoneal fibrosis to study the role of lymphatic absorption on ultrafiltration failure.

2.0 Literature Review

In order to accurately identify the disease state of PD and modeling PD using microfluidic chips, an extensive literature review was performed. The literature review includes information on the clinical problem, physiological changes that occur as a result of the clinical problem, and current models used to study the clinical problem.

2.1 - Kidney Failure Treatments

Although chronic kidney disease (CKD) is often thought of as a condition that primarily affects older adults whose kidney function has begun to decline naturally, it is a progressive disease that can affect patients of any age, including pediatric patients [7]. Some factors that increase a patient's risk for developing CKD include comorbidities such as cardiovascular disease, diabetes, hypertension, and obesity, which are prevalent in nearly 20% of adults over age 20 in the United States [8]. Kidney failure is characteristic of the final phase of CKD, called end-stage renal disease (ESRD). In kidney failure, the kidneys are unable to perform their main function - ultrafiltration of the blood - which leads to detrimental effects from the accumulation of waste products in the body [8]. Fluid and electrolyte balance is also disturbed during kidney failure due to the lack of ultrafiltration [8].

2.1.1 - Kidney Transplant

A kidney transplant is one way to restore this filtration function to the body and combat end-stage renal disease, but relies on the availability of a healthy kidney from a donor and subjects both donor and recipient to an extremely invasive procedure with significant risk. While time is crucial in stopping the progression of chronic kidney disease, the nature of the cure increases the likelihood that a patient will have to wait for a kidney. The health of both the donor and recipient may also be limiting factors for the willingness of a surgeon to perform the transplant procedure and increase the time a patient has to wait for transplant [8]. Transplant procedures are expensive and although insurance will cover some costs, both donor and recipient can expect high out-of-pocket costs [8]. Coupled with long recovery times that both may be out of work and losing wages, lack of funds emerges as an unfortunate deterrent for the procedure. For these reasons, interim treatment must include some method to alternatively filter the blood and remove the harmful waste products using a filtration system at another site in the body or an artificial filtration system outside the body while the patient waits for transplant.

2.1.2 - Hemodialysis

Dialysis is a method of treatment that accomplishes the ultrafiltration function at an alternative site to the kidneys. There are two main types of dialysis - hemodialysis and peritoneal dialysis. Both treatments impact the lifestyle of the patient and significant adjustments must be made. Hemodialysis involves filtering the blood through a semipermeable membrane in a hemodialysis machine outside the body, where the blood is accessed through a fistula in the patient's forearm [8]. Patients undergoing treatment with this method can expect to spend at least three hours, three to four times each week sitting with the hemodialysis machine, not factoring in travel times to a hemodialysis center where this process is usually performed under the care of a trained medical professional [8]. As such, this treatment method is not preferred for patients with a more active lifestyle or those who do not have access to a hemodialysis treatment center. The vasculature of the patient must be exceptionally strong to form the fistula, and hemodialysis may not be a good option for patients with weakened or underdeveloped vasculature, such as pediatric patients [7]. For patients unable to endure hemodialysis, peritoneal dialysis is the preferred method of treatment.

2.1.3 - Peritoneal Dialysis

Peritoneal dialysis involves introducing dialysate fluid into the abdominal cavity through a catheter that is permanently inserted in the abdomen [8] (Figure 1). The peritoneum serves as the semi-permeable membrane to filter the waste products from the blood, restore electrolyte balance, and remove excess fluid from the blood through concentration gradients and diffusion [9]. The dialysate fluid itself contains sodium, chloride, and magnesium ions at low concentrations relative to the peritoneal tissue [7]. This allows a flow of these ions down their

concentration gradient from the peritoneal tissue into the dialysate fluid to be removed during the peritoneal dialysis treatment as seen in Figure 2.
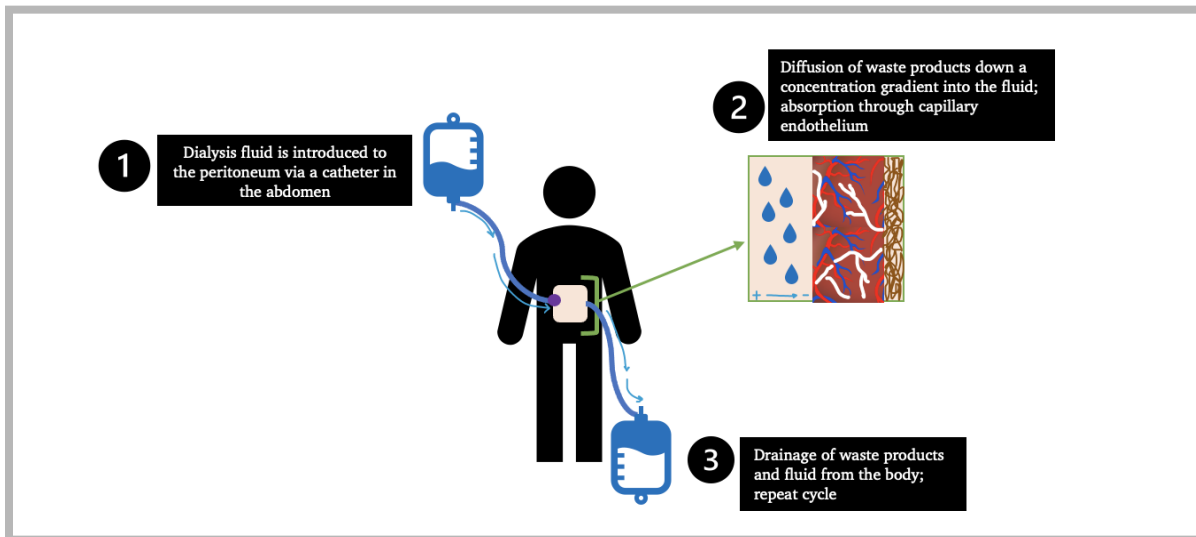
Figure 1: Peritoneal dialysis exchange process.
Dialysis fluid (dialysate) is introduced to the peritoneum via a catheter inserted in the abdomen. Due to the composition of the fluid, concentration gradients form that allow for exchange of ions, waste products, and fluid using the peritoneum as a semipermeable membrane. Last, after the specified dwell time, the dialysate fluid is drained from the body via the catheter.

Dialysate also contains extremely high levels of glucose, where concentrations of 4250 mg/dL (typically 4.25% glucose solution) are commonly used [7, 10]. The glucose in the dialysate creates an osmotic pressure gradient, where osmolality in the dialysate is high relative to the excess water in the tissue. This allows for the removal of excess water from the body to restore fluid balance, as the excess water is pulled into the dialysate to flow towards osmotic equilibrium. When the excess fluid flows into the dialysate, water-soluble waste products from the blood are carried into the dialysate as well [7]. This exchange happens across the capillary endothelium in the submesothelial layer of the peritoneum, where the vasculature is located [7], as seen in Figure 1.

The dialysate fluid typically stays in the body for a dwell period of four to six hours before being drained from the catheter to discard. The dwell period is determined by the patient's physician as well as how many exchanges, or repeats of the peritoneal dialysis process, are needed per day [8]. With proper sterilization training and precautions, patients can perform peritoneal dialysis at home, either manually or automatically with a cycler machine, making it the preferred treatment method for patients to maintain their independence [8].

2.2 - Ultrafiltration Failure in Peritoneal Dialysis

Peritoneal dialysis is a treatment that utilizes the peritoneum essentially as the kidneys to replace the ultrafiltration function lost during kidney failure. However, the peritoneum is not

meant to naturally function in this capacity for prolonged periods. As such, ultrafiltration failure (UFF), or the inability of the peritoneum to achieve appropriate filtration rates can occur after prolonged exposure to dialysate fluid during the exchange processes [11]. Clinically, ultrafiltration failure is diagnosed as the inability to achieve a minimum of 400 mL net ultrafiltration from a single exchange in a four hour dwell time using a 4.25% dextrose (chemically identical to glucose) [10]. These values are known as the "rule of fours." There are four main types of ultrafiltration failure differentiated by the mechanisms reducing filtration.
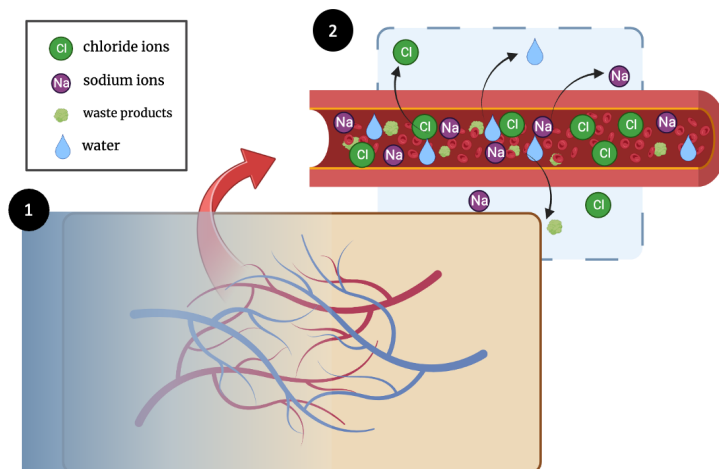
Figure 2: How dialysate fluid accomplishes ultrafiltration in the peritoneum.
1) Dialysate fluid enters the peritoneum and surrounds the capillaries in the submesothelial layer. 2) Excess sodium, chloride, and magnesium (not pictured) ions move down the concentration gradient into the dialysate fluid. Excess water is pulled into the dialysate due to the osmotic gradient, which carries water-soluble waste products. Created with BioRender.com.

Type 1 UFF, or high effective peritoneal surface area, reduces filtration when an increased surface area of the peritoneum is utilized for filtration and solute transport is rapid across the capillary endothelium [10]. Essentially, too many electrolytes and water enters the dialysate fluid, reducing the ability of peritoneal dialysis treatment to achieve a balance of these substances through the exchange process. Type 2 UFF, or low osmotic conductance to glucose, reduces the ability of the osmotic gradient to transport excess water from the body into the dialysate [10]. Type 3 UFF, or low effective peritoneal surface area, reduces filtration when a decreased surface area of the peritoneum is utilized for filtration and solute transport is sluggish across the capillary endothelium [10]. This is the opposite scenario that happens in Type 1 UFF, where too few electrolytes and water enter the dialysate fluid and waste products accumulate in the body, again reducing the effectiveness of peritoneal dialysis in achieving the balance through adequate filtration. Type 4 UFF, or high total peritoneal fluid loss, involves an increased uptake of the dialysate fluid in the submesothelial layer of the peritoneum by lymphatic vessels [10]. In

this scenario, the "potential" of some of the dialysate is wasted, as it is unable to surround the capillaries and complete the solute exchange.

At the point when a patient is diagnosed with any type of UFF, the peritoneum has been exposed to the dialysate fluid for numerous exchange cycles. The high glucose concentration renders the dialysis fluid bioincompatible, where glucose degradation products attack the structural integrity of the peritoneum over time and travel through systemic circulation to result in a decline of overall health of the individual [7]. Traditional dialysate also has a low pH and contains advanced glycation end products which similarly affect the tissue after prolonged exposure [9]. While biocompatible dialysis solutions are under development using alternative molecules to glucose, glucose-based, bioincompatible dialysis fluids remain the gold standard for peritoneal dialysis treatment and are the most readily available [7]. As such, it is important to understand exactly how prolonged exposure to high-glucose dialysate causes physiological changes in the peritoneum that lead to ultrafiltration failure.

2.3 - Physiological Changes to the Peritoneum during Peritoneal Dialysis Treatment

The peritoneal membrane consists of two layers - the mesothelial layer and the submesothelium, as seen in Figure 3 [9]. The mesothelial layer consists of a single layer of mesothelial cells with microvilli on the apical surface, facing away from the submesothelial layer [9]. As previously stated, the submesothelial layer in the healthy peritoneum contains the vasculature where solute transport across the capillary endothelium occurs. The submesothelial layer also contains a few fibroblasts in low concentration and some lymphatic vessels to drain excess fluid from the tissue through interstitial flow [9]. Both the mesothelial and submesothelial layers are affected during peritonitis, which is inflammation of the peritoneum. Peritonitis is a serious complication of peritoneal dialysis and occurs for a variety of reasons. Prolonged exposure to the bioincompatible dialysate is one main cause of peritonitis in peritoneal dialysis patients [9].

During peritonitis, the inflammation response increases production of vascular endothelial growth factor (VEGF) which increases the amount of vasculature in the submesothelium (angiogenesis) [9] (Figure 3). Additionally, new cell types such as myofibroblasts, fibrocytes, and cells that have undergone epithelial to mesenchymal transdifferentiation migrate to the submesothelium and even into the mesothelial layer upon detection of inflammatory factors, effectively stiffening the tissue [9]. The original layer of mesothelial cells undergo transdifferentiation and new gaps emerge [9, 12]. Connective tissue growth factor (CTGF) present in the fibrotic tissue and exclusively induces lymphangiogenesis [11]. This series of changes results in a peritoneum that differs significantly from the healthy peritoneum. Thus, the properties of the tissue, most importantly the ability of the peritoneum to serve as a semipermeable membrane to achieve ultrafiltration, change as a result of inflammation

from prolonged exposure to the bioincompatible dialysate. These changes reduce the ability of the peritoneum to achieve ultrafiltration and can ultimately lead to ultrafiltration failure.
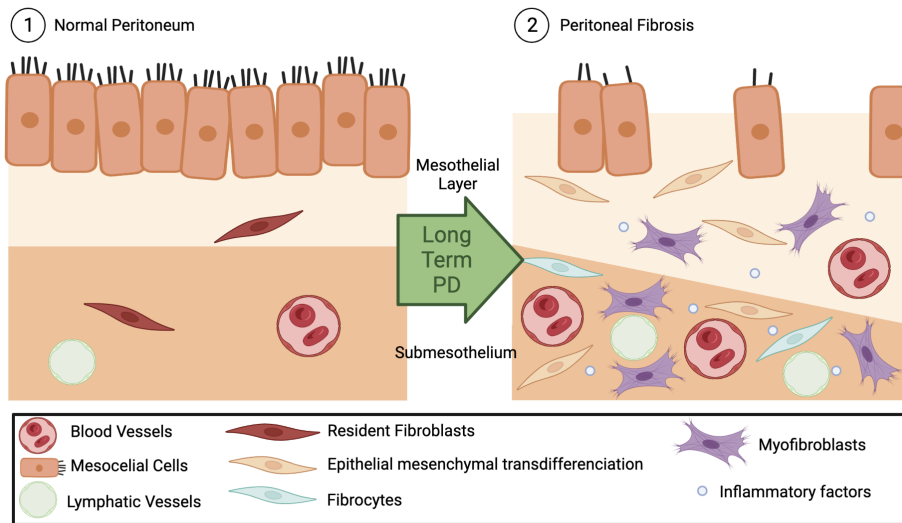
Figure 3: Comparison of the structure of healthy and fibrotic peritoneum.
New cell types migrate to the submesothelium during the inflammatory response of peritonitis caused by prolonged peritoneal dialysis treatment. These cells stiffen the peritoneum. Additionally, increased vasculature (angiogenesis) and increased lymphatic vessels (lymphangiogenesis) are seen in the fibrotic peritoneum. All of these changes can contribute to ultrafiltration failure. This figure is adapted from Zhang et al. [9]. Created with BioRender.com.

2.4 - Lymphangiogenesis May Lead to Ultrafiltration Failure

Each of the aforementioned physiological changes to the peritoneum could be connected to the different types of ultrafiltration failure. For example, both type 1 and type 3 UFF involve a change in the rate of solute transport across the peritoneum. Increased angiogenesis and a change in the stiffness of the tissue due to the migration of new cell types to the area could change the rate at which diffusion across the capillary endothelium into the dialysate happens. With more capillaries present, there is a greater surface area that serves as the barrier to transport. Additionally, solutes could encounter new barriers to diffusion into the dialysate fluid and target levels of ultrafiltration may not be achieved.

Type 4 UFF presents an interesting area for study, as the loss in ultrafiltration function is perceived to occur as a result of increased uptake of dialysate in the lymphatic vessels. It is known that lymphatic absorption of the dialysis fluid counteracts ultrafiltration [6]. Lymphatic absorption is an inherent feature of peritoneal dialysis due to the anatomical proximity to the diaphragm. When the diaphragm relaxes, dialysate fluid is able to move past the mesothelial cells through gaps and into the lacunae of the lymphatic vessels [6]. The net ultrafiltration is reduced by this lymphatic absorption of the fluid and in order to increase ultrafiltration, therapeutic approaches could aim to reduce lymphatic absorption. In peritoneal fibrosis, there is an increase in lymphatic vessels and a likely increase of lymphatic absorption, although the rate

at which this occurs has not been quantified definitively [9, 10]. Therefore, there is a need to understand and quantify the rate at which lymphatic absorption occurs in the fibrotic peritoneum to determine if this is a potential target for treating ultrafiltration failure. If ultrafiltration failure can be addressed, peritoneal dialysis would continue to be a treatment option for patients currently undergoing this treatment. Additionally, quantifying lymphatic absorption in this fibrotic state could provide an understanding of the effects of increased lymphangiogenesis in other fibrotic tissues beyond the peritoneum, whether they are helpful or harmful to the progression of disease.

2.5 - Prior Art

Animal models and in vitro devices like microfluidic chips are some of the methods used by scientists to study disease states. These can be used to study fibrosis and lymphangiogenesis in multiple tissues. Some of these methods are well established and considered as gold standards in industry and academic labs, and others are under development to try to fill the gaps from the gold standards.

2.5.1 Gold Standards for Ultrafiltration Failure Models

There are multiple models, either in vivo or in vitro, used in industry and academia to model peritoneal tissue and dialysis environments. These are needed to screen for different drugs to treat conditions like ultrafiltration failure. These models are listed below as gold standards, as they present multiple advantages, but they are not perfect and also present some disadvantages.

Table 1: Advantages and disadvantages of peritoneum model gold standards.

	Advantages	Disadvantages
In Vivo Animal Models	- Accurate physiological conditions - Can be used for drug screening	- Expensive models - Ethical considerations - Human conditions may not be represented accurately
In Vitro Tissue Cell Cultures	- Cheaper than animal models - Good for biocompatibility testing	- Lack of physiological conditions - Does not allow for drug screening for peritoneal fibrosis and/or ultrafiltration failure specifically

2.5.1.1 In Vivo Models

The gold standard to screen for peritoneal fibrosis and angiogenesis drugs is the use of animal models, specifically rats and mice. There are multiple studies using these animals to test drugs by inducing fibrosis and introducing dialysis fluid in the animal's peritoneal cavity [14, 15]. Animal testing may be influenced by many factors such as the cost, sizes, and similarities to humans. Rats and mice are the most advantageous because they are cheaper, as they reproduce quickly, and are a stable model that endure surgical procedures. However, they may not be the most accurate model and small size makes catheter usage complicated when they get blocked. Larger models like rabbits have a more similar peritoneum to humans; however, they do not reproduce quickly and are fairly expensive [16].

2.5.1.2 In Vitro Models

In vitro models for peritoneal dialysis are used by researchers to test biocompatibility and cytotoxicity of the dialysate. Firstly, scholars have used human tissues extracted from biopsies where they discovered that mesothelial cells are closely related to peritoneal injury. Therefore, in vitro models are obtained by culturing peritoneal mesothelial cells. This technique has multiple advantages such as low cost and a clear target; however, this model does not represent the complete physiological environment of the peritoneum, as it is a single cell model only used for toxicity [16]. Because of this, this model cannot be used to test drugs to treat fibrosis in the peritoneum, but only to test for possible improvements made by changes in the dialysis solution.

2.5.2 Microfluidic Device Models: What They Are

Microfluidic chips are an emerging tool in the field of disease modeling and biomedical engineering. Microfluidic chips consist of groves and microchannels engraved on different materials. The microchannels are interconnected with each other and designed to achieve specific functions. The microchannels are associated with the macroworld through a series of inlets and outlets. Microfluidic chips, with the help of pumps or pressure gradients can induce flow of fluids through the microchannels to study behavioral changes of the fluids. Additionally, microfluidic chips can be used in combination with cell culture techniques to model interactions between cells and external stimuli [13]. In the case of peritoneal dialysis, the microfluidic chip is a suitable tool for modeling this process as the microchannels can be used in combination with lymphatic endothelial cells and a stiffening hydrogel (LEC) to study the effects of LECs and fibrosis on the absorption of dialysate solution.There are no microfluidic chips that model the peritoneum, fibrosis, and lymphangiogenesis concurrently. However there are gold standards that model these three states separately that can be used for reference.

2.5.2.1 Lymphangiogenesis

Lymphangiogenesis is mainly used in the study of tumor models. Utilizing mainly photolithography for the creation of initial master molds, these models such as the one utilized by Cho *et al.*, incorporate interstitial flow and growth factors to induce lymphatic endothelial cell (LEC) sprouting [17]. As seen in Figure 4, LECs are seeded in a channel adjacent to a hydrogel that can be seeded with other cell types. The channel on the opposite side of the hydrogel is filled with media containing growth factors which diffuse through the hydrogel and cause growth in toward it. The main hydrogel used in these studies is a fibrin gel or fibrin collagen hybrid. The growth into the hydrogel also supports extracellular matrix (ECM) remodeling. This design is utilized by other studies looking at lymphangiogenesis, especially at the interplay between LECs and other cell types in the progression of disease such as cancer.
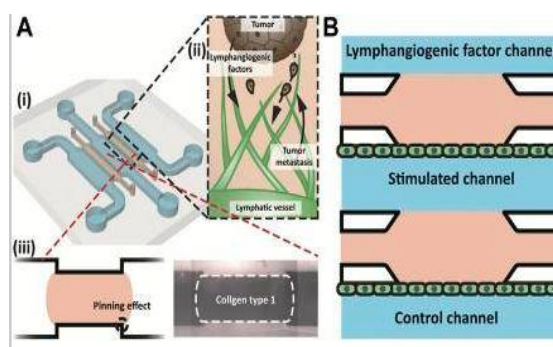
Figure 4: Lymphangiogenesis microfluidic chip design from Cho *et al*.
This chip was designed to model the interactions between lymphangiogenesis and the tumor cell environment. As seen above, the three channels hold either lymphatic endothelial cells or growth factors. These channels are separated by a hydrogel which holds a tumor microenvironment for the study of tumor interactions [17]. Image used under Creative Commons License (CC BY 4.0).

2.5.2.2 Peritoneum

The peritoneum does not have extensive modeling. Only one microfluidic chip was found that modeled relevant features. The omentum-on-a-chip modeled by Ibrahim *et al.* models the omentum as a part of the peritoneum defined as a fatty layer lining the intraperitoneal organs [18]. This chip has three channels. The middle channel holds a hydrogel seeded with adipose cells to mimic the ECM environment. The top of the hydrogel is seeded with mesothelial cells, the principal cell type lining the peritoneum. The side channels are seeded with endothelial cells for endothelial capillary infiltration into the hydrogel. This model is used for tumor modeling, but provides a novel design for modeling the anatomy of the peritoneum.

2.5.2.3 Fibrosis

Fibrosis is modeled mainly by the inclusion of fibroblasts into a hydrogel coculture. Fibroblasts are treated with pro-fibrotic factors such as TGF-**β**1, then seeded into a hydrogel with other cell types such as pluripotent stem cells [19]**.** Once treated with supplemented media, the

fibroblast starts to remodel to the ECM environment. This event is marked by increased collagen type I or III deposition. For the use of this project which will be modeling fibrosis acellularly, the mechanics of this tissue are the most important. Using atomic force microscopy, fibrotic tissue is generally found to have stiffness uniformly between 0.6 to 9.2kPa [19].

2.6 - Microfluidic Models

Microfluidic devices are a great tool for experimental modeling because of four main reasons they are: cost effective, highly customizable, allow for high throughput testing, and allow for high control of experimental conditions. Microfluidic chips are usually in the range of 1-10 cm in size with microchannels ranging from 0.1-1.5 mm in diameter. This compact size allows for experiments to be run with very low reagent volumes making it extremely cost effective.

2.6.1 Benefits and Limitations

Microfluidic chips are used in a wide variety of applications like drug discovery, diagnostics, and disease modeling. Pattanayak *et al.* classifies microfluidic chips into four broad categories: droplet based, 3D cell culture based, hydrogel based, and detection instrument based [13]. Microfluidic chips have different designs for different purposes suggesting the tool is highly customizable. Microfluidic chips can also be designed to incorporate several systems in one chip allowing multiple analytes or experiments to be run at once or high throughput testing. Lastly, *in vitro* models like the microfluidic chips lack some of the complexity that *in vivo* models have when it comes to disease modeling. But that also means that *in vitro* models are able to isolate specific features of interest or have high control over experimental conditions.

2.6.2 Fabrication Techniques

The research team found that for microfluidic chips used in disease modeling, the most common manufacturing techniques included: soft lithography, photolithography, micromachining, and injection molding. Photolithography involves the use of excimer laser lithography machines to selectively expose photosensitive polymers to light making a latent image of the polymer. Photolithography has excellent resolution in the 100 nm range but the highly specialized equipment reduces the accessibility of this manufacturing method. Micromachining is a manufacturing technique that involves the subtractive fabrication of devices or features through geometrically defined cutting edges. The resolution of micromachining is in the micrometer range. Micromachining also involves the use of low accessible machines and the features depend on the available cutting edge geometry. Injection molding is a manufacturing process involving the use of an injection molding machine. The material of choice is fed into a heated barrel where it is then mixed with a helical screw and finally injected into a mold.

Injection molding has a resolution of 2-4 mm and is mostly used to standardize and mass produce structures once the design has been tested and is functional. Injection molding also involves the use of low accessible machines. Soft lithography is a technique for fabricating or replicating structures using molds. Elastomeric materials are usually poured over the mold and cured to achieve the desired structure. Soft lithography has a resolution of approximately 25 μm. Soft lithography is the most inexpensive manufacturing technique out of the four, as only a mold and the material is needed. For the purposes of our project, soft lithography is likely the technique that will be applied due to its accessibility and ease of use.

3.0 Project Strategy

Considering the clinical need and the fact that prior art fails to provide a high throughput testing solution to researchers looking to improve peritoneal dialysis specifically, a project strategy was developed that would result in considerations for a final design to address this gap.

3.1 Initial Client Statement

There exists a need for a microfluidic chip to accurately model lymphangiogenesis in the fibrotic peritoneum caused by peritoneal dialysis. Specifically, the model needs to accommodate interstitial flow, a stiffened extracellular matrix, and be able to model receiving large quantities of dialysate. The model needs to be manufactured with an attainable method for a standard academic lab and must be accessible in operation of the device, with the possibility of reuse.

3.2 Design Requirements

After completing a literature review on disease states with connections to lymphangiogenesis the scope of the project was able to be narrowed. The following objectives were in consideration with modeling the peritoneum during ultrafiltration failure, a period of increased ECM fibrosis and lymphangiogenesis. A summary of design objectives and how they relate to the design functions and means is included in Table 3.

3.2.1 Objectives

In order to design the desired microfluidic chip that satisfies the needs listed in the client statement, a set of objectives were established as follows:

1. *Cost Effective:* The effectiveness of the microfluidic chip should justify the cost.

2. *Representative of In Vivo Conditions:* Model organization mimics stiffening extracellular matrix, interstitial flow and lymphangiogenesis aspects of ultrafiltration failure in Humans

3. *Accessible for Research Purposes:* Model can be used to test treatment options for ultrafiltration failure.

4. *Production:* Model can create ultrafiltration failure with traditional academic laboratory resources.

5. *Reusable*: Model has sterilization properties that allow for reuse.

The importance of these objectives was evaluated using a pairwise comparison chart, which shows the relative significance between objectives (Table 2). The ranking of these objectives will be used to prioritize design features.

Table 2: Pairwise comparison chart of microfluidic chip design objectives.

	Cost Effective	Representative of In Vivo Conditions	Accessible for Research Purposes	Production	Reusable
Cost Effective		1	0	0.5	0
Representative of In Vivo Conditions	0		0	0	0
Accessible for Research Purposes	1	1		1	0
Production	0.5	1	0		0
Reusable	1	1	1	1	
TOTAL (Weight)	2.5	4	1	2.5	0

In the pairwise comparison chart, the objectives in the first row were compared with each row of objectives in the first column. On one hand, if the objective in the first row was seen with a higher priority than the one being compared to in the first column, a 1 value was assigned in its corresponding intersecting cell. On the other hand, if the objective in the first column was more important than the one being compared to in the first row, a value of 0 was assigned to the interesting cell. As a result, the summation of all the values in each objective column provided the level of importance of that objective. The two higher ranked objectives were *representative of in vivo conditions* and *manufacturable*, which will be the most important criteria to take into account when designing the microfluidic device. When evaluating and comparing the alternative designs, the priority of these objectives will be taken into account to determine the best approach.

It is important to note that the decisions on the objectives' importance was made as a team according to what was considered a priority for the project. This process was guided by the objective descriptions provided earlier but ultimately, subjective decisions of importance were made. The reasoning behind the teams choices on the ranked objectives can be found below:

Representative of In Vivo Conditions (4): One of the biggest gaps identified in the existing *in vitro* models for peritoneal dialysis is the representation of the physiological conditions that can be achieved in animal testing. This is the main reason why there is not an adequate *in vitro* model for this disease. Because of this, the team determined that representing the *in vivo* conditions should be one of the highest priorities. The device must be manufacturable and biocompatible; but if at the end of the day the microfluidic device does not meet the client needs of an *in vitro* model that represents physiological conditions, there will be no use for it.

Production(2.5): In order to deliver the final product, it needs to be manufacturable. Using available techniques is a must, as if there is no method to fabricate the device, it will be impossible to deliver the microfluidic chip. This was ranked as the second most important objective, surpassing biocompatibility, because in order to meet that there is a need for a physical product.

Cost Effectiveness (2.5): Due to budget constraints that the team has, cost was determined as an objective that needs to be met. The team needs to ensure that the device is effective, but also stays within the budget. Comparing this to other objectives, it was considered as less important but something to keep in mind when focusing on achieving higher ranked objectives.

Accessible for Research Purposes (1): Besides being one of the client needs, this objective will depend on the higher ranked ones, if previous objectives are not achieved there will either be no product to perform research on. Once there is a product that fits within the budget, the team will ensure that it can be used for research.

Reusable (0): Reusability is an important feature to improve any negative environmental impact; however, this is not an essential criteria for the function and client needs. Reusability would be something that the team will like to achieve but not prioritize. Once the other objectives are met, the incorporation of reusability will be considered.

3.2.2 Functions

1. *Model Peritoneal Dialysis:* The microfluidic chip will provide a structure that allows to model the conditions used in peritoneal dialysis treatment.

2. *Mimic Physiological Environment of Peritoneal Fibrosis:* The microfluidic chip will incorporate the matrix stiffness found in ultrafiltration failure at the same time as provide similar interstitial flow conditions. The microfluidic chip will also promote lymphangiogenesis as observed in ultrafiltration failure.

3. *Accessible to use in Research:* The microfluidic chip will be used for drug screening and testing. It will be imageable using traditional methods (i.e. microscopy).

3.2.3 Constraints

In order to satisfy the client's needs, the design objectives must be met. Therefore, there is a list of specifications that will act as constraints and that the team needs to take into account when designing the microfluidic chip.

1. *The microfluidic chip must be biocompatible:* According to the ISO 10993 standard, reduction of 30% viability when culture material is tested will result in cytotoxicity [20]. Thus, materials chosen for the design should not cause this response. For that it is important to have a sterile design.

2. *The microfluidic chip must be cost effective:* The materials and resources used for the fabrication and testing of the microfluidic chip must not cost more than the project budget of $1,000.00.

3. *The microfluidic chip must be manufacturable:* The fabrication techniques used for the manufacturing of the microfluidic must be accessible in the team's academic lab. The team had access to all equipment and materials needed for making 3D-printed molds for soft-lithography of polydimethylsiloxane microfluidic chips. The team did not have access to more advanced technology, such as instruments and materials needed for the photolithography process.

4. *The microfluidic chip must align with physiological benchmarks:* The hydrogel used must reach a stiffness of 8kPa and have a mass transfer area coefficient proportional to 22.9 ± 7.04 mL/min, as found in the peritoneum [55, 52]. The blood flow should be equivalent to 6.2 ± 1.2 mL/min per 100g in the peritoneum.

3.2.4 Means

The functions and constraints of the microfluidic chip were defined from the objectives and their various weights. The objectives dealing with clinical needs were defined as functions while the objects based on manufacturing became design constraints. Based on these functions the team developed a range of means to accomplish them and aid in the future development of the conceptual design.

The first functions fall under modeling peritoneal dialysis. The chip layout must provide a structure that is able to mimic the peritoneal environment during dialysis. This function will be achieved by modeling the microfluidic design off an existing chip that models the omentum , as well as taking in account the peritoneal anatomy [18]. The chip design should incorporate three

different elements in order to model the different places where the dialysate fluid moves through. These elements are the ECM, peritoneal cavity with dialysate, and capillaries with blood. Using these criteria this design we will be able to study the movement of fluid through the peritoneal membrane as well as mimic solute exchange by varying media concentrations across the chip. The chip design could also vary based on the direction of the flow. The chip could utilize flow in a horizontal direction while other chips could utilize flow vertically. The model however must incorporate an ECM and have some forces such as gravity or hydrostatic pressure to create interstitial flow.

Table 3: Design objectives, functions, and means

Objectives	Functions	Means
Representative of *in vivo* conditions	● Achieve matrix stiffness seen in UF cases ● Promote lymphangiogenesis/lymphatic absorption of dialysate ● Achieve filtration ● Achieve interstitial flow	● Hydrogel with different concentrations of crosslinker ● LEC seeding in hydrogel, growth factors in media ● Dialysate fluid and blood analog channels ● Flow from blood analog through hydrogel to LECs
Accessible for Research Purposes	● Able to be imaged with a microscope ● Can be used for drug screening	● Bonded to glass microscope slide ● Single layer of PDMS and channels ● Channels allow for research options (different dialysate fluids, drugs in blood channel, etc.)
Production	● 3D, resin printed molds to produce PDMS chips ● Reproducible, can make multiple chips	● Molds are 3D printed from resin ● Easy to print multiple molds - potentially reuse molds
Cost Effectiveness	● Within the project budget	● Material choices and manufacturing processes are within the project budget
Reusable	● Molds are reusable ● Chips are reusable	● Resin molds can be reused to pour multiple PDMS chips ● Chips can be re-sterilized

The second group of functions was defined as physiological functions to mimic the physiological environment of peritoneal fibrosis seen in UFF. The first in this group is incorporating peritoneal interstitial flow (IF). In order to incorporate IF a pressure gradient will be incorporated into the design. Creating a hydrostatic pressure difference would cause the fluid to flow in a defined direction according to the pressure gradient. Peritoneal dialysis utilizes hydrostatic pressure to aid in solute exchange incorporating a gradient would help better mimic the physiological functions involved in fibrosis. IF can also be incorporated via pumps such as a peristaltic or syringe pump. The second function needed is the ability to support lymphangiogenesis. Lymphangiogenesis could be achieved in many ways. LEC's have been shown to sprout in a 3D hydrogel matrix. Therefore, seeding LEC in a 3D gel matrix that mimics native tissue would also allow for more physiologically relevant behavior. In addition to that, LEC's could also be seeded in a channel adjacent to a hydrogel and be allowed to infiltrate into the hydrogel. This process has been demonstrated before by Cho Y. et al In their paper outlining LEC tumor cell interactions [17]. The final function needing to be accomplished is mimicking the fibrotic environment with ECM at a stiffness above 2kPA. This function could be accomplished using either a natural material such as fibrin and collagen or synthetic material such as polyethylene glycol. Fibrotic environments are stiffer than normal healthy tissue. This effect can be replicated acellularly by varying the ratios of agents like thrombin and fibrinogen in a fibrin gel to replicate fibrotic tissue changing concentration. Polyethylene glycol can vary its stiffness by photocrosslinking.

The final function involves research use. This function defines the chip's useability in the research field, meaning you must be able to easily collect data from this chip. This will be carried out by making sure the chip is imageable as well as able to have drug screening or histological assays run on it. This will be accomplished by basing the microfluidic chip design on the gold standard chip which already allows for imaging and assays.

To accomplish the main constraints behind the microfluidic chip, manufacturing, sterilizations and biocompatibility, the chip was designed around these "must haves" to ensure its function. To accomplish these design constraints the microfluidic chip will be made from biocompatible material such as PDMS as it is the main material used in research for soft lithography. The chip must be sterilizable using methods such as isopropyl alcohol sterilization or UV sterilization, as it is the standard used in the fabrication of these devices. Finally, the chip must be manufacturable, which means that it is accessible to any lab and does not exceed the team budget of $1000. Using molds is a great method to accomplish this, as once the master mold is made, microfluidic chips can be essentially manufactured at a low cost by only taking the materials price into consideration. The master mold however, must be made using a process that does not require special accommodations such as a clean room. Techniques such as injection molding and photolithography are somewhat inaccessible. To navigate this constraint the microchip design will be able to be created using a 3D printer or CNC machine to manufacture the master mold.

3.3 Revised Client Statement

There exists a need for an *in vitro* testing tool that accurately represents the *in vivo* conditions of peritoneal fibrosis caused by prolonged exposure to dialysate fluid during peritoneal dialysis. Specifically, the model needs to accommodate interstitial flow, a stiffened extracellular matrix, and lymphangiogenesis with future cellularization of the model. The model needs to be manufactured with an attainable method for a standard academic lab and must be accessible in operation of the device, with the possibility of reuse.

3.4 Relevant Industry Standards

In considering the design process for the microfluidic model, there are some relevant industry standards that provide guidelines that could be helpful in maximizing the performance of our model and ensuring that it can undergo future cellularization. For example, ISO 22916:2022 is a standard that provides guidelines on microfluidic devices specifically, as this is becoming an emerging field [43]. This standard gives information to aid in designing microfluidic chip dimensions in order to integrate the microfluidic chip with additional parts of a model. For example, a microfluidic model that is connected to a pump system to allow for a specific flow rate of a solution would need to have a connection from the pump system to the microfluidic chip itself. This standard would provide information about dimensions for connections in order to do this. Using correct dimensions for flow connections would help minimize the risk of turbulent flow and pressurization within the system in the case flow is constricted too much from the connecting device to the microfluidic chip.

Additionally, ISO 22916:2022 gives guidelines on initial device classification and how to name the microfluidic device [43]. The information provided in this regard could be helpful for regulatory submission processes and deciding how to classify the device for the submission. For example, if the chip is classified as an *in vitro* diagnostic device, it may require additional labeling and a specific name in order to go through the regulatory submission process to the FDA and be sold in the United States. This standard may help decide if this classification and naming is necessary depending on the final design and intended uses of the chip. Along these lines, a second standard, ISO 10991, provides definitions of terms associated with microfluidic device manufacturing and final device classifications as they are used in industry [44]. If the final design is to be marketed to investors or submitted to regulatory agencies, it is important to use the correct terminology to accurately convey what the purpose of the developed microfluidic model is. The definitions outlined in this standard would provide clarity in any final descriptions of the device for the aforementioned purposes.

In consideration of future cellularization of the device, there are a few standards that could be helpful in determining methods for testing if the microfluidic model is biocompatible and will allow for cell growth and proliferation. ISO 10993-5 includes guidelines on methods for

testing in vitro cytotoxicity of medical devices and ISO 10993-4 provides methods for selecting tests for blood compatibility with medical devices [45, 46]. Where part 5 of ISO 10993 provides strategies for quantitatively measuring cytotoxicity when cells come in contact with any part of a medical device, picking one of the strategies outlined in the standard would allow for assessment of the material selection in the microfluidic model. These tests would determine if the chip allows for cell proliferation and growth. This is an important consideration in future cellularization of the model to evaluate fluid uptake by lymphatic vessels. Where part 4 of ISO 10993 provides tests that show if a medical device interacts negatively with blood, the guidelines in this standard could determine if the microfluidic chip could be used as an in vitro diagnostic device. If the chip is determined to be compatible with blood, samples of a patient's blood could potentially be used in place of a blood analog solution to screen different dialysate solutions or different pharmaceuticals for effectiveness in achieving ultrafiltration in peritoneal dialysis.

In consideration of creating a sterile environment for cells to grow, regardless of if the device is classified as an in vitro diagnostic device, USP 71 provides guidelines on direct transfer sterility testing that could help develop test methods to evaluate the adequacy of the chosen sterility method following the manufacturing process [47]. The direct transfer sterility method typically involves submerging a biopharmaceutical product in tryptic soy broth to evaluate pathogenic growth after 3, 7 and 14 days [47]. A similar method could be used for the finished microfluidic device, where the broth would be in contact with all sterilized surfaces and evaluate if bacteria and fungi are eliminated prior to cell seeding.

4.0 Design Process

The design process facilitates the consideration of objectives, functions, and means for the identification of features needed in the final design. From this weighting process, a set of conceptual designs was developed with the most important needs in mind. These conceptual designs were then evaluated in a selection matrix against the gold standard on the design objectives with weights applied. The two highest scoring conceptual designs moved forward to be front-running designs. From here, the front-running designs went through the desired manufacturing process and preliminary feasibility testing to ultimately determine the final design, which emerged as best meeting the objectives, incorporating the needs and some wants.

4.1 Needs Analysis

Using the objectives priorities from the previous chapter, a need analysis was performed to determine what is needed versus what is wanted. The must have design features are determined as the need and the features that are favorable but not critical are determined as the wanted.

4.1.1 Needs

The needs were determined by choosing the features that the microfluidic chip needed to function. The device must be biocompatible to support cell growth and lymphangiogenesis. The device must be manufacturable using techniques available to the team. The device must model the peritoneal dialysis environment to accurately represent the disease that needs to be studied. The design must mimic a fibrotic environment that promotes lymphangiogenesis. The design cost must stay within the budget.

4.1.2 Wants

The wants were established with the lower ranked objectives and based on what the team wanted to incorporate to the design. Ideally, the design will be maintained as acellular. Ideally, the design will be used for research and drug screening. Ideally the design will have a high throughput, where low quantities will provide abundant results. Ideally, the design could be reusable to eliminate as many negative environmental effects as possible.

4.2 Conceptual Designs

The following conceptual designs were developed with the design objectives and functions in mind. Each design seeks to create means to achieve the design objectives and functions using a combination of previously documented microfluidic chip features and novel features relevant to the desired applications of this project. Consideration of all model components as a whole were taken into account when developing conceptual designs. Channels and chambers with specified fluid flows are included along with channel and chamber design. Additionally, a compartment to seed a hydrogel and culture cells is incorporated in each design. These conceptual designs were evaluated after development using a Pugh selection matrix to determine the two preliminary designs that best provide the means to meet device objectives and functions.

4.2.1 Three-Chamber Chip Conceptual Design

Based on the final objectives and functions, a conceptual model was created to model the peritoneal environment. This chip has three chambers as seen in Figure 5. The chip was designed to support solute exchange using interstitial flow (IF). To account for this, the dialysate chamber to the left is much bigger than the side chambers holding the hydrogel and "capillaries". This will create a hydrostatic pressure difference causing the dialysate fluid to flow toward the capillaries for solute exchange similar to in the peritoneal environment during peritoneal dialysis. The hydrogel mimics the peritoneal ECM environment and can be augmented to better represent fibrosis to model ultrafiltration failure (UFF). Additionally, the model can be cellularized to even more closely resemble the peritoneum. A mesothelial layer could be added between the dialysate

chamber and hydrogel. The channel to the right is the vascular channel which will hold simulated blood fluid containing key solutes such as urea. This design was inspired by the design described by Ibrahim *et. al* of the omentum-on-a-chip [18]. However, this design visualizes dialysis horizontally. This will allow for easier fluid sampling once the dialysate is introduced, initiating filtration. The horizontal view also allows for the hydrogel to be visualized much easier in permeability assays where fluorescence is involved. In order to manufacture this chip, a resin 3D-printed mold will be made for the PDMS negatives. This chip has small posts needed to keep the hydrogel from flowing out of the hydrogel chamber. Because the designs are so small these post might serve as a source of error in manufacturing the chip as the PDMS might break, not fully form, or stick to the mold.
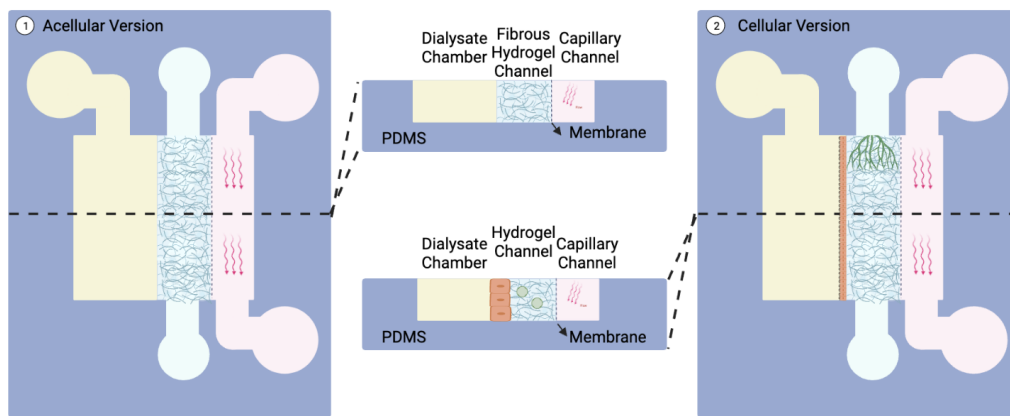
Figure 5: Three chamber chip conceptual design.
First conceptual design of microfluidic chip designed to mimic the peritoneum physiological environment. This design uses a three chamber system and a horizontal view of dialysis.

4.2.2 Cross Flow 3D Chip Conceptual Design
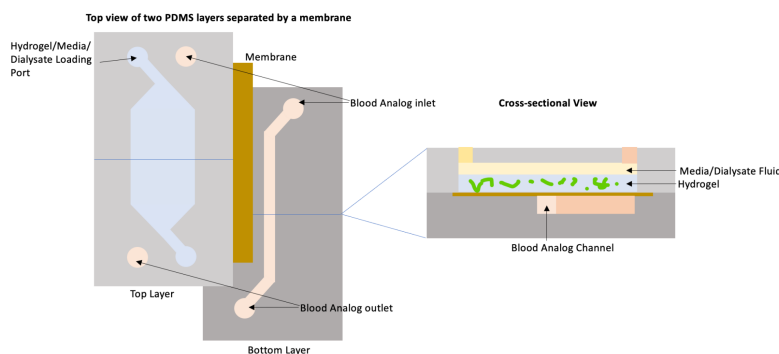
Figure 6: Cross flow chip conceptual design.
Blown-apart schematic drawing of the cross flow 3D chip conceptual design. Two layers of PDMS are separated by a membrane to allow for filtration between the blood analog channel and dialysate/hydrogel chamber. Lymphatic endothelial cells seeded in the hydrogel interact with the dialysate.

The cross flow 3D chip conceptual design features two chambers on top of one another separated by a membrane, which allows for different fluid flows across the top and bottom of the membrane and filtration of the blood analog fluid (Figure 6). The top and bottom layers in gray are made of PDMS. This design requires two distinct molds for manufacturing the PDMS layers, where the channel patterns are unique to each layer. The top layer contains a hydrogel chamber where lymphatic endothelial cells (LECs) would be seeded. There is also an inlet for flowing cell culture media formulated for LECs and for dialysate to flow in, sit within the chip for a specified dwell time, and be drained through the same channel as an outlet. To prevent mixing of media and dialysate, media would be removed prior to addition of dialysate. The bottom layer contains an inlet and outlet for constant "blood" flow, where the "blood" would contain a solute of interest that would get filtered into the dialysate fluid. This solute, or marker, would flow down its concentration gradient, across the membrane, and into the dialysate in the chamber within the top layer of the chip. The primary purpose of the semipermeable membrane is to separate the top and bottom flow layers, allowing for passage of the solute into the dialysate but not for the fluids in either layer across the membrane. As such, choice of membrane pore size must take the fluid and solute molecule sizes into account.

The inspiration for this chip is the PreciGenome Cross Flow Membrane Chip Cell, which is marketed for cell culture applications [21]. The channel pattern has been modified to fit the specific applications for this project. The cross flow design allows for addition of the necessary fluids to be able to determine filtration rates achieved by a specific dialysate solution across the membrane. The hydrogel chamber where LECs can be seeded allows for lymphatic absorption of the dialysate. This conceptual design theoretically allows for the addition and drainage of dialysate, accounts for matrix stiffness with the hydrogel chamber, and accounts for interstitial flow from the blood vessel chamber into the LECs in the hydrogel chamber, which is representative of in vivo conditions.

The materials and manufacturing method have been modified to fit project objectives. The PreciGenome chip is manufactured with injection molding [21]. Although this is feasible for large scale manufacturing, a more accessible technique for this project would be to 3D-print the top and bottom layer molds. A polyethylene terephthalate (PETE) membrane is used in the PreciGenome chip [21]. The membrane used in this conceptual design would have to have similar properties, such as hydrophilicity, and could be made of a hydrophilic polyester material. In order to get the membrane to adhere in between the top and bottom layer, the PDMS around the hydrogel chamber and the blood vessel channel would be heated and the membrane inserted into the molten silicone. Upon cooling, the membrane would be fixed in the silicone. The PDMS layers would adhere to each other and to a glass microscope slide after oxygen plasma treatment.

This design involves constant flow across the bottom "blood vessel" channel. A system would have to be designed to account for this constant flow, such as using a pump to continuously achieve the desired flow rate. A second idea would be to design a reservoir where fluid would drain into the inlet and out through the outlet due to gravity, where the height of the

starting reservoir and collection reservoir could be designed to achieve the desired flow rate. The dialysate would have to be removed after the dwell time from the top layer. A pipette aid could help to draw the dialysate fluid out for further analysis of filtration rates. The chip would have to be sterilized before use with LECs. Autoclave sterilization may be a good method to accomplish this.

There are some questions that arise when considering this conceptual design. First, where does the dialysate fluid absorbed by the LECs go? Where there is no channel for lymphatic vessel drainage, there is a concern that fluid could build up and damage the lymphatic sprouts or not adequately measure the absorption rate. Second, will imaging be possible where multiple layers are stacked on top of each other? The overlay of channels may make it difficult to visualize lymphatic absorption with fluorescent markers and a traditional microscope. Last, will components of the fluids used clog the membrane and affect filtration capabilities or the ability of the membrane to separate fluid flows? The charge of the ions in the fluid and interactions with the membrane material emerges as a concern to address in additional iterations of this conceptual design or in development of subsequent conceptual designs.

4.2.3 Multi-Microfluidic Channel Chip Conceptual Design
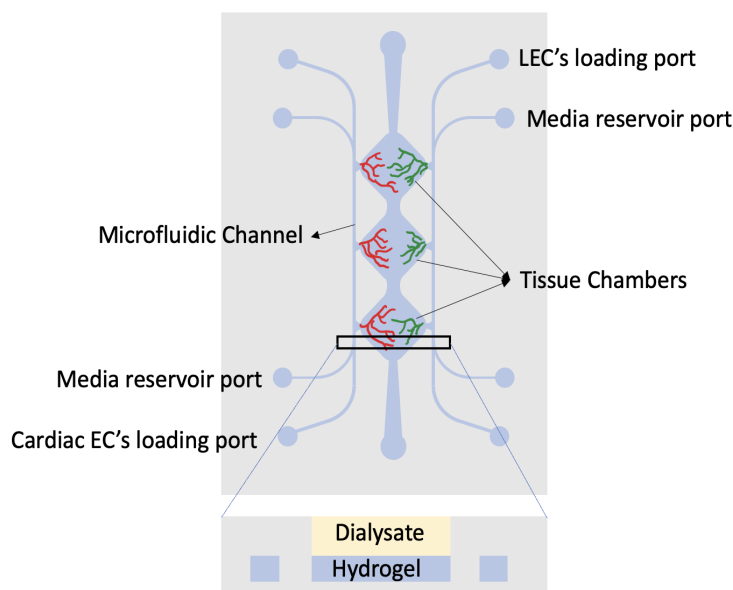
Figure 7: Multi-microfluidic channel chip conceptual design.
Top and cross sectional view of the multi-microfluidic channel chip conceptual design.

The multi-microfluidic channel chip features three connected, diamond-shaped hydrogel chambers situated between microfluidic channels (Figure 7). The microfluidic channels connect with the hydrogel chamber through the edges of the diamonds which allows for cell culture and sprouting through the hydrogel. Both microfluidic channels have the same structure but play different roles. One of the channels represents the lymphatic system and the other one represents

the cardiovascular system.The channels have a cell loading port to introduce lymphatic endothelial cells for the lymphatic system and cardiac endothelial cells for the cardiovascular system. The channels also include media ports that introduce the media for the cells needed for proliferation and sprouting towards the hydrogel.

In order to mimic the disease state of peritoneal dialysis, dialysate fluid will be introduced on top of the hydrogel and will not be in direct contact with the channels. This way the dialysate will diffuse through the hydrogel into the sprouted capillaries and lymph vessels. The hydrogel located on the bottom will experience interstitial flow through pressure difference between the media reservoir inlet and outlet channels.

This design was inspired by a paper from Wang et. al where researchers evaluate a method for generating an intact and perfusable microvascular network that connects to microfluidic channels without leakage through the use of a microfluidic chip [22]. The microfluidic chip in this paper did not mimic the peritoneum, but it is a generic model for vasculature that could be adapted to our purposes as they were able to sprout endothelial cells into the hydrogel and produce biological channels or vessels [22].

In order to manufacture this chip, a resin 3D-printed mold where to pour PDMS will be needed due dimensions as small as 0.05mm used in the perfusable microfluidic design. This design is also highly dependent on cells and it will require co-culture of LECs and ECs. Without the use of cells, there is no room to evaluate the potential performance of the chip, which is its main drawback.

4.2.4 Lumen Multi-Microfluidic Channel Chip Conceptual Design

The lumen multi-microfluidic channel chip was developed as an iteration of the previous design, the multi-microfluidic channel chip. This was done in order to eliminate the concern of coculture of LEC's and cardiac EC's. This design features the same amount of channels as the previous conceptual design. However, both of the channels in this design are used to seed LECs. Another main difference this design has in comparison to the previous one is in the addition of a lumen through the hydrogel that mimics a blood capillary. This was done because the culture of ECs was removed and there was still a need for a channel that mimicked this system for representative in vivo conditions. As seen with the previous design, this design also has diamond shaped chambers where the hydrogel is added and where the LECs will sprout. The dialysate fluid will sit on top of this hydrogel in order to represent peritoneal dialysis.

When it comes to the manufacturing of this design, the model will be identical to the previous conceptual design. However, when the hydrogel is poured, there will be a needle acting as a lumen that when removed, will result in a new channel that runs through the hydrogel. This adds some extra complication to the production of this chip, but removes co-culture concerns and facilitates testing performance without the use of cells.
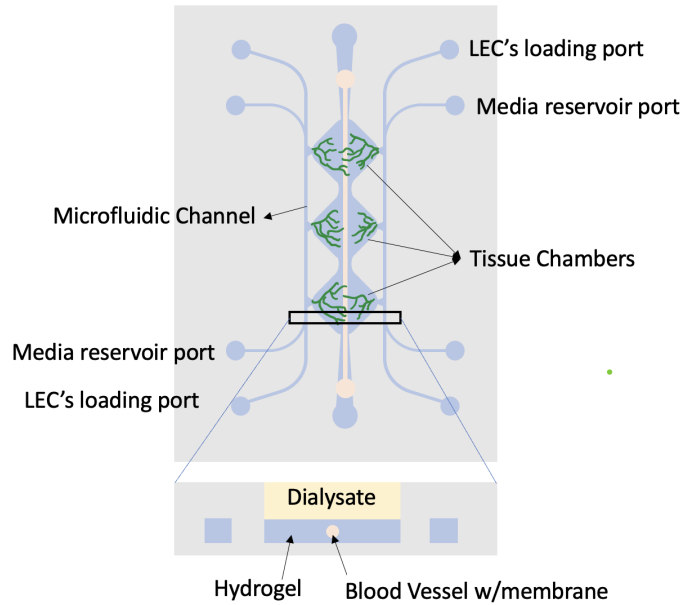
Figure 8: Lumen multi-microfluidic channel chip conceptual design.
Top and cross sectional view of the lumen multi-microfluidic channel chip conceptual design.

4.2.5 Daisy Chained Chip Conceptual Design
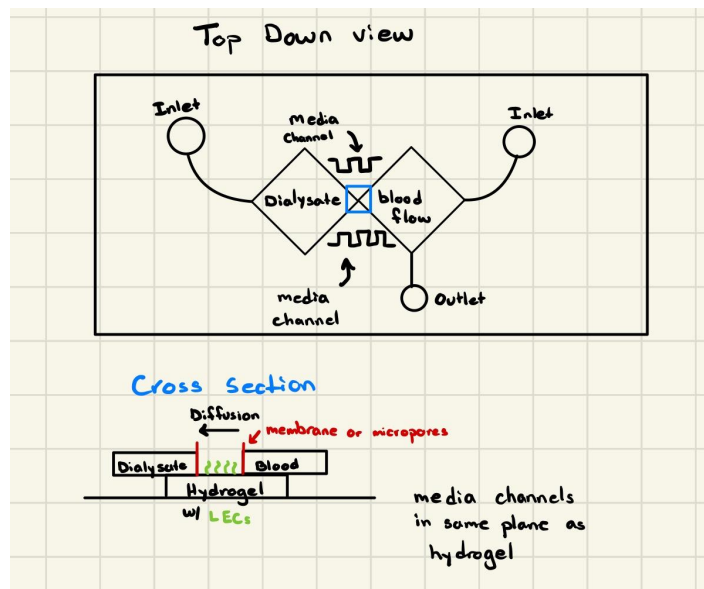
Figure 9: Daisy-chained chip conceptual design.
Schematic top down and cross section view of the daisy chained chip conceptual design.

The daisy chained chip was inspired by the Alonzo *et al.* interstitial flow-mediated homotypic and heterotypic cellular communication. The daisy chained chip features two daisy chained channels [54]. The dialysate fluid would flow into one chamber while the blood analog would flow into the other. The chambers would be separated by a membrane or micropore that

would allow diffusion to occur via the concentration gradient established by the blood analog and dialysate. The hydrogel chamber is located directly under the diffusion area and the vascular and dialysate chambers. Media channels would be on the same plane as the hydrogel which can be used to feed the any cells seeded within the hydrogel as well as introduce growth factors. The main idea of this design was to have LECs proliferate and invade the diffusion area between the dialysate and vascular channel and study how the LECs would affect the diffusion process between the dialysate and blood analog.

4.3 Front-Running Alternative Design Selection

Using the objective weights determined with the pairwise comparison of objectives, the conceptual designs were evaluated and ranked in comparison to the gold standard using a Pugh Selection matrix (Table 4). The gold standard, which is an in vivo rat model for ultrafiltration failure, was ranked with all zeroes as a baseline. If an in vitro microfluidic chip was significantly better than the gold standard in its respective category, a ranking of 1 was assigned. If the microfluidic chip being compared was only slightly better than the gold standard, a ranking of 0.5 was awarded. If the gold standard and microfluidic chip were comparable one another in its respective objective, a ranking of 0 was assigned. If the in vitro conceptual design was slightly worse than the in vivo gold standard, a ranking of -0.5 was awarded. Finally, a ranking of -1 was only awarded if the proposed conceptual design performed significantly worse than the gold standard in the respective objective. In order to assign these values, the rubric in Appendix A was used.

After all the objectives were ranked in all conceptual designs, the values were multiplied with its respective objective weight and added together. The front-running designs were found to be the three chamber chip with a value of 9.5 and the lumen multi-microfluidic channel chip with a ranking of 8.75. These designs were chosen as preliminary designs and underwent feasibility testing to evaluate their performance in critical areas of functionality for the desired model.

4.4 Feasibility Testing and Final Design Selection Process

In order to choose the final model, the manufacturability of both preliminary designs was evaluated based on the desired manufacturing methods. The criteria used for the final design selection is outlined in Appendix B. In summary, feasibility testing consisted of an assessment of whether or not soft lithography was possible with the different resin mold designs in regard to chip breakage during PDMS removal from the molds. From here, hydrogel retention in the molds was evaluated and lumen manufacturing was assessed for the lumen design. The design that would advance to be the front-running design would have to retain a hydrogel (with or without a lumen depending on the design).

Table 4: Pugh selection matrix to evaluate conceptual designs.

	Weight	Gold Standard - In Vivo (Rat UF Model)	Three Chamber Chip	Cross Flow 3D Chip	Multi-Microfluidic Channel Chip	Lumen Multi-Microfluidic Channel Chip	Daisy Chained Microfluidic Chip
Representative of In Vivo Conditions	4	0	0.5	0.5	1	1	-1
Production	2.5	0	1	0.5	0	0.5	0.5
Cost Effective	2.5	0	1	1	1	1	1
Accessible for Research Purposes	1	0	0.5	0.5	1	1	0.5
Reusable	0	0	0	0	0	0	0
TOTAL	-	0	**9.5**	**6.25**	**7.5**	**8.75**	**0.25**

4.4.1 Preliminary Designs Manufacturing and Assembly

Molds of the front running chip designs were modeled using SolidWorks, 3D-printed in resin, excess UV cured, and fluorination-treated for success in peeling PDMS. Following additive manufacturing to create the molds, soft lithography using PDMS was used to create the PDMS microfluidic chips. In order to create complete channels, oxygen plasma treatment was used to bond the PDMS microfluidic chips to a glass microscope slide. The hydrogel was then seeded in the hydrogel chamber of the bonded chip at the point of partial gelation and placed in a 37℃ incubator for complete gelation.

4.4.1.1 Mold Design and Treatment

After choosing our two front-running designs, the chips were modeled using SolidWorks and creating a negative of the desired chip. The drawing views of these designs can be found in Appendix C. The models were first scaled up and printed in PLA using a Replicator + printer as

a rough prototype to check for any design flaws. The final design was printed in resin using the Objet260 Connex printer.

The molds were further surface treated to facilitate soft lithography. After speaking with graduate students in the field of biomedical microfluidics using the same manufacturing technique, it was recommended that the resin molds be excess UV cured and fluorination surface treated to avoid cure inhibition. Cure inhibition occurs when surface contaminants prevent a material from curing as expected. Since our method for manufacturing these chips involves pouring PDMS into the molds, cure inhibition could be a problem if not accounted for. Excess UV curing consisted of exposing the molds for 30 mins to light at a wavelength of approximately 380 nm to ensure the resin molds were not under cured. After excess UV curing, the molds were oxygen plasma treated. Following oxygen plasma treatment, the molds were fluorinated by exposing the molds to a fluorine derivative inside a degassing chamber overnight. The fluorine atoms will partially replace the hydrogen atoms in the materials surface. The main effect of fluorination is improved bonding and adhesion as well as reduced friction and stickiness, both of which help combat cure inhibition.

Three Chamber Chip

The first iteration of the three chamber chip had overall dimensions of 24 mm, 22.15 mm and 6 mm (x, y, and z respectively). The hydrogel channel, vascular, and dialysate channel have a width of 1.30 mm. The inlets and outlets for the vascular and dialysate channels (side channels) have a diameter of 6 mm while the hydrogel inlet has a diameter of 4 mm to allow for certain size pipette tips to fit in the inlets/outlets. The trapezoidal features in the hydrogel channel are micropores designed to keep the hydrogel from leaking into the other channels. The gap between each micropore is 0.2 mm (Figure 11(b)).

After printing a first iteration of the mold, some faulty features were identified leading to design changes and a second iteration. This design only had three outer walls, and thus PDMS pouring for soft lithography was performed vertically between a piece of acrylic and ceramic tile (Figure 10). This method led to leakage and a full chip could not be formed. Another observation was that the trapezoidal features blended together due to the tolerance of the 3D printer. Finally, the intel and outlet diameters were too large for the pipette tips and component addition. All these lead to a second iteration shown in Figure 11(c), where a fourth wall was added, the shape of the trapezoids was adjusted to two different crescent shapes, and the inlets and outlets diameter was adjusted to 1 mm.
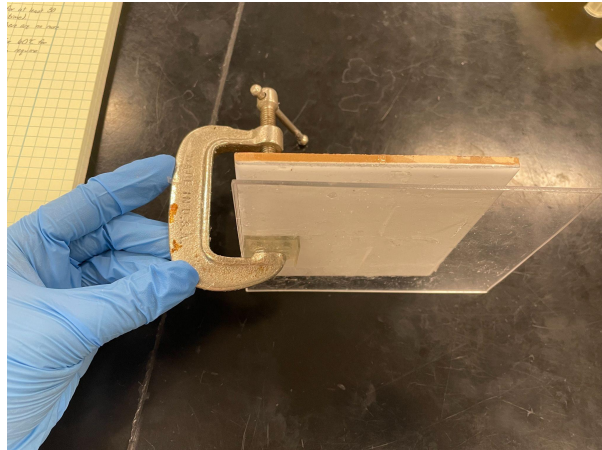
Figure 10: Vertical PDMS-pouring setup.
Vertical PDMS pouring setup for the first iteration of the three-chamber design that contained three outer walls. PDMS was poured down into the mold from the top in between the ceramic tile and acrylic piece.

After obtaining the print of this new iteration, there were still flaws in the design, such as the features that separate the hydrogel chamber from the fluidic channels were still blended together. This led to the final design in Figure 11(d) where the previous model was scaled up by a magnitude of 2 in the x and y direction, but not the height (z direction), to allow for these features to meet the printer tolerance. In addition, the hydrogel chamber height was increased to further avoid leakage problems between channels, and four chip setups were added to a single mold, resulting in a master mold for faster production.
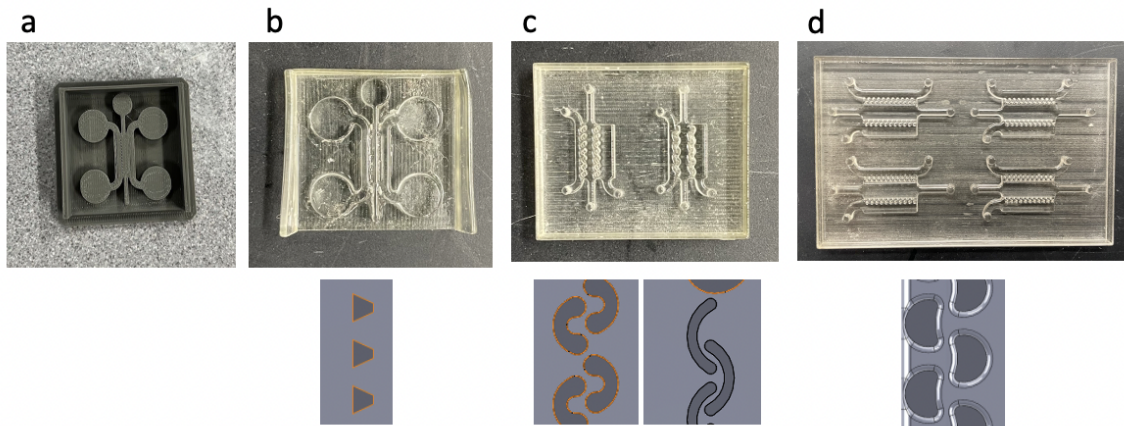
Figure 11: Iterations of 3D-printed three chamber chip mold.
(a) PLA Print of first iteration, (b) resin print of first iteration, (c) resin print of second iteration, (d) resin print of final iteration. The drawings under (b), (c), and (d) show the hydrogel retention feature design for each mold and are located at the boundaries where the hydrogel chamber meets the vascular and dialysate chambers.

Lumen Multi-Microfluidic Chip

For the first iteration of the lumen multi-microfluidic channel chip, channels were designed with a width of 0.1mm, inspired by the dimensions in Wang *et al.* [42]. The area where the channels connect with the diamond shapes in the hydrogel chamber to deliver media to cells seeded here is 50 μm, and the cross sectional area of the diamond shapes that separates both channels is 1 mm. The connection channel between the diamond shapes is 200 μm wide. In order to print this design in PLA first, the design was scaled up 2 times to fit the printer's tolerances. When the design was printed in resin, the original dimensions described were used.

The first iteration of this design had all the features well-defined. However, the smallest feature of the hydrogel chamber was too small to allow for a needle to go through for the lumen manufacturing. Because of this, a second and final iteration of this design was made by scaling up the mold by a magnitude of two in the x and y direction, maintaining the height constant. In addition to this change, the mold also was designed to accommodate four chips with the goal of facilitating production of more chips at one time, effectively creating a master mold.
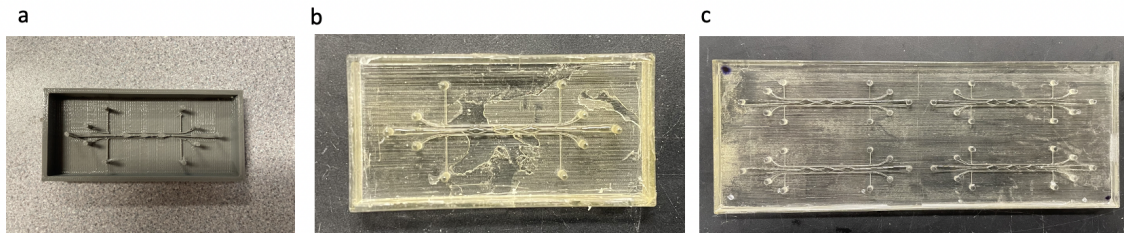
Figure 12: Iterations of 3D-printed lumen multi-microfluidic channel chip.
(a) PLA print of first iteration, (b) Resin print of first iteration, (c) Resin print of final iteration.

4.4.1.2 Soft Lithography

PDMS was mixed in a 10:1 Sylgard silicone elastomer base mass to Sylgard elastomer curing agent ratio in plastic weigh boats. The PDMS was degassed in a vacuum chamber at 25 mmHg vacuum pressure for 40-60 minutes until no air bubbles remained. The prepared PDMS was poured into fluorination-treated resin molds where care was taken to make sure all features were covered completely with PDMS and an even layer was poured across the mold. The mold containing PDMS was placed on aluminum foil and placed in a 70℃ incubator for curing overnight (at least 15 hours).

Following curing overnight, the mold was removed from the incubator and placed on the benchtop. Using a scalpel blade, cuts through the PDMS along the outer walls of the mold were made, taking care not to cut or scratch the bottom layer of the mold. Cuts were also made vertically and horizontally down the middle of the mold to separate four distinct chips. Starting in the corner of one of the chips near the wall, a 200 μL disposable pipette tip was used to lift the

PDMS from the mold. The pipette tip was used to carefully apply upward pressure to gently free the PDMS from the mold around the features and ensure no PDMS remained in the mold. The pipette-tip peeling process was repeated until all chips were removed from the mold. Following chip removal, excess PDMS was removed from the bottom of the mold by peeling to prepare for reuse in the next round of soft lithography.

This process helped determine if the mold designs were adequate to obtain all desired features. The lumen chip showed no challenges during peeling off as it retained every design feature. However, the three chamber chip did not retain every feature, as the dents that were designed to prevent the hydrogel from leaking into the other channels got stuck on the molds. As an alternative method to retain the hydrogel in its chamber, a membrane out of sports pre wrap was placed instead of the dents. In order to place this in the chip, small incisions were made on the PDMS using a scalpel, and a small piece of the pre wrap was placed there using tweezers. The PDMS pinched the pre wrap pieces holding them in place as shown in Figure 13 below.

Figure 13: Sports pre-wrap membrane addition

4.4.1.3 Plasma Bonding

In order to create working channels for the microfluidic chip, the PDMS chips prepared using soft lithography needed to be bonded to a substrate to seal off the channels from the bottom for hydrogel and fluid addition. The substrate of choice in this model is glass, specifically glass microscope slides. The size of the microscope slides is convenient for imaging purposes and the glass is thinner and easier to image through compared to a secondary layer of PDMS, making it favorable over PDMS. In order to permanently bond the PDMS chips to the glass, an oxygen plasma reactor was used. When the PDMS surface is treated with oxygen plasma, the high-energy molecules in the chamber dislodge the methyl groups and form silanol groups, which can then bond to silanol groups on the surface of the glass slide [38]. When full bonding is achieved, separation of the PDMS from the glass slide following treatment becomes essentially impossible, successfully creating the desired channels and chambers.

Prior to oxygen plasma treatment, the PDMS chips and glass slides were cleaned using antimicrobial soap and warm tap water. The substrates were dried first using paper towels and then set to air dry for 5-10 minutes. Following air-drying, the PDMS chips were tapped gently against a folded Kimwipe to remove any remaining water from the chip features. Once it was determined that both substrates were completely dry, they were placed on the two halves of a 60 mm culture plate to ensure they did not come into contact with the bottom of the chamber. The PDMS chip was placed with the channels facing upward so this surface would receive the oxygen plasma treatment. The culture plate halves were loaded into the chamber of a Harrick benchtop oxygen plasma reactor using forceps. A vacuum seal was created within the chamber using a vacuum pump and the rf setting was turned to 'Hi' for 15 seconds before turning 'Off.' A pink glow was observed within the chamber while the rf setting was on, indicating good quality plasma. The chamber was carefully re-pressurized and the culture plate halves were removed with forceps. Taking care to only touch the sides of the PDMS chip and not the treated surface, the PDMS chip was flipped over onto the glass slide for bonding to occur. Pressure was applied for 15-30 seconds until full bonding occurred and it became impossible to separate the substrates by peeling. Both chip designs (three-chamber chip with the pre-wrap membrane addition and the lumen multi-microfluidic chip) were able to be plasma bonded using this process, which allowed continuation to the hydrogel seeding step of the final design selection criteria.

4.4.1.4 Plasma Bonding Feasibility Testing - Dye Leakage

The dye leakage test was designed to verify multiple aspects of the model manufacturability under the production objective. The first goal was to assess the bond formed between the PDMS and the glass microscope slide following oxygen plasma treatment. To prepare the visualization dye, food-grade blue dye was mixed with deionized water. The chip was placed on a white paper towel to aid in dye visualization. A phone camera was placed above the chip on a stand to remain steady and record video observations of the dye leakage test. In the first phase of the test, the blue dye was injected with a pipette into the chip bonded to the glass slide. After running the test, the recording was inspected to qualitatively identify points of leakage out of the channels, which would indicate an inadequate bond between the glass slide and PDMS chip. Results have shown that there is proper bonding between the PDMS and the glass slide, as no leakage was identified (Figure 14).

An observation made when running the dye through the hydrogel inlet in the lumen design is that the dye flowed through the chamber and exited through the outlet with minimal flow into the media channels (Figure 14 (a)). However, if the outlet was plugged, the dye ran through the media channels without restriction (Figure 14 (b)). Finally, the three chamber chip also showed no leakage after more than a hour of testing, the only observable leak was around the cut made to place the membrane which does not affect the performance of the device (Figure 14 (c)). This indicates all channels formed correctly during soft lithography.
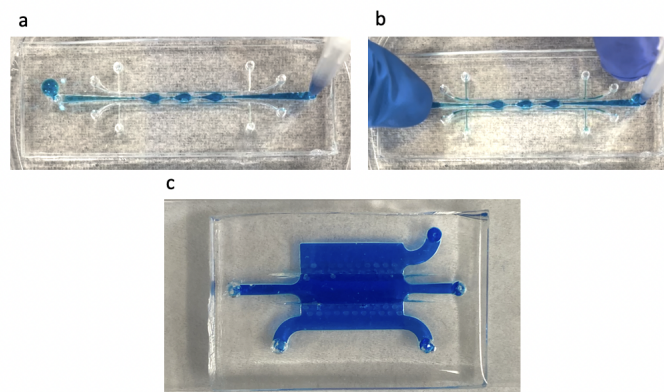
Figure 14: Dye leakage test for plasma bonding assessment.
Dye leakage test to assess plasma bonding in (a,b) Lumen design and (c) Three Chamber design.

4.4.2 Hydrogel Formulation

Before the hydrogel seeding step could occur in the final design selection process, it was important to choose a hydrogel that would mimic physiological conditions. The target stiffness for the hydrogel should mimic the stiffness of fibrotic peritoneum as a patient undergoes peritoneal dialysis treatment, which has an average stiffness of around 8.25kPa over the duration of treatment [55]. Gupta *et al.* were able to achieve this high stiffness through using a gelatin hydrogel crosslinked with microbial transglutaminase (TGA). Using 5-8% gelatin and 2-4% transglutaminase, they achieve a range of stiffness between 20-100 kPa [41]. Gelatin crosslinked with TGA appeared to be a good candidate to achieve the stiffness of a hydrogel to mimic the fibrotic peritoneum and was thus evaluated for the model. It is important to note that the hydrogel seeded in microfluidic chips for the purposes of this project will remain acellular for the duration of study. In future use of the model, addition of cells could further affect the stiffness of the hydrogel and cause deviation from the desired stiffness.

The TGA was extracted from the Moo Gloo RM Transglutaminase meat-binder product manufactured by Modernist Pantry, LLC following a procedure obtained from a professor in the field. This extraction consisted of diluting 2 parts of Moo Gloo to 10 parts of DBPS(-), to obtain a 20% solution of Moo Gloo in DPBS(-). It is important to note that the exact concentration of TGA in the Moo Gloo was unknown, and thus the concentration in the extraction is also unknown, but assumed to be 20%. After the dilution, the solution was left mixing in a vertical tube rotator overnight inside the incubator at 37℃. The solution was centrifuged the next day and the supernatant was obtained and stored in the fridge as the final extraction containing 20% TGA.

The formulation chosen for characterization consisted of 4% TGA with 4% Gelatin diluted on DBPS(-). Depending on the amount of chips being seeded with hydrogel, a different

volume of this was prepared to further pipette into the hydrogel the chambers: 116 μL for the three-chamber chip, and 31 μL for the lumen multi-microfluidic channel chip. Both the stock solutions of gelatin and TGA were 20%. To prepare a 100 μL volume of hydrogel, 60 μL of DBPS(-) was added to a tube, then 20 μL of TGA, then 20 μL of gelatin. The solutions were mixed in the tubes using repeat pipetting.
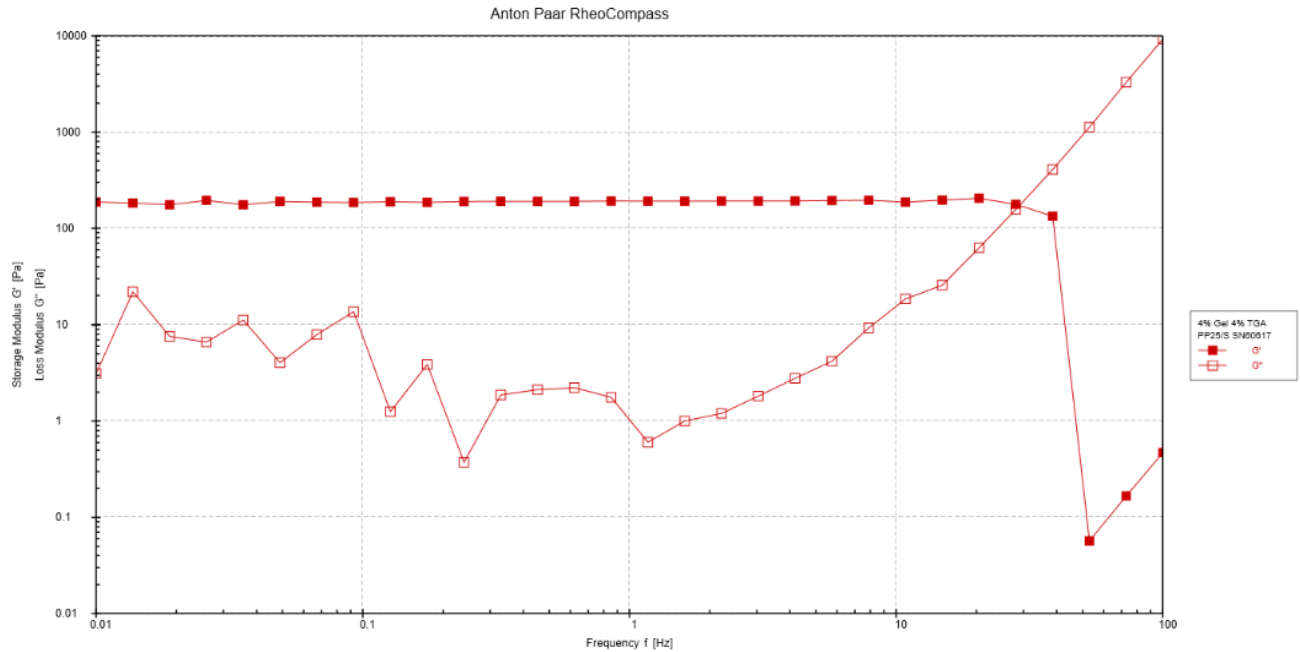
Figure 15: Representative graph of frequency sweep performed on 4% TGA with 4% Gelatin hydrogel sample.

Preliminary rheological testing was performed on the 4% TGA and 4% Gelatin diluted with DPBS(-) hydrogel. Frequency sweeps of 0.01 - 100 Hz showed a linear viscoelastic region of storage moduli where the average stiffness could be approximated to be 190.23 Pa (Figure 15). The stiffness is significantly lower than expected due to only trace amounts of TGA being extracted from the Moo Gloo. Upon further inspection of the product, the content of TGA in the Moo Gloo product before extraction was <1%. Therefore, the amount of actual TGA extracted from the supernatant after centrifugation would be <<1% making extraction of TGA unreliable and unusable if the hydrogel present in the model was to have a high stiffness representative of fibrosis (> 2 kPa).

After determining that the TGA hydrogel would not reach the stiffness values of the fibrotic peritoneum, alternatives were sought. After consulting with manufacturer Advanced Biomatrix about which collagen hydrogel would be best in order to achieve an average stiffness range of 8 kPa, they recommended Bovine Type 1 Collagen hydrogel TeloCol-10 diluted to a concentration of 8 mg/mL using 0.01 M HCl and neutralized following the manufacturer's standard neutralization protocol. They recommended TeloCol-10 as it is easy to work with, used

more in clinical research, and able to reach stiffness ranges of 8 kPa according to tests performed by the manufacturer.

4.4.3 Hydrogel Seeding

The Telocol-10 hydrogel was first prepared and mixed in a tube as explained in section above. Then, using a 1000 μL positive displacement pipette with a volume of 170 μL, the hydrogel was seeded into its respective chamber. The chip with the seeded hydrogel was then placed for 60 minutes in the 37℃ incubator before proceeding to adding the fluids.

The goal in the three chamber chip design for seeding the hydrogel was to evenly and fully fill up its chamber without leakage. By preliminary seeding trials, it was observed that the hydrogel filled its respective chamber smoothly, and further leakage tests would need to be performed to confirm uniform filling of the chamber

The goal in the lumen design when it came to hydrogel seeding was to only fill up the lower half of the chamber that is in contact with the media channels, leaving the upper half for the dialysate fluid. However, when the hydrogel was seeded in this design, the hydrogel only filled the half side of the chamber where the hydrogel was being seeded. This could have been caused by high viscosity and high surface pressure of the hydrogel. The chip was placed in refrigeration to check if the gel stabilized and spread through the chamber, but this was not achieved. Therefore, this design was discarded, and the three chamber design was pursued further.

4.4.3.1 Hydrogel Seeding Feasibility Test - Dye Leakage

To further assess hydrogel retention and leakage, the hydrogel was dyed in blue and then seeded in the hydrogel chamber. If the blue dye was observed to leave the desired chamber, the retention failed. Later different colored dye was placed in both the dialysate (yellow) and blood analog (red) channel, to assess if there was immediate mixing of the solutions, as that would indicate there was some leakage. When adding the red blood analog no leakage was observed. However, when the yellow dialysate was added, the pressure difference pushed some liquid through and some blood analog was pushed out of its chamber through the inlet and outlet. In order to avoid this, plugs were placed in this inlet and outlet. Additionally, a hole was punched at the end of the dialysate chamber to release some pressure and let the air in the chamber escape. These adjustments were successful, as no leakage was observed in the second run. The findings are shown in Figure 16 below.

Figure 16: Hydrogel retention and leakage test
(a) Hydrogel retention testing using blue dye, (b) unsuccessful hydrogel leakage test, (c) and successful hydrogel leakage test after adjusting the fluid addition method.

4.4.4 Final Design Selection

After going through the final design selection process, the three-chamber chip ultimately emerged as the final design over the lumen multi-microfluidic design. Although this design was not successful in the soft lithography manufacturing step, as the hydrogel retention features could not be peeled off of the resin mold successfully, the addition of a pre-wrap foam membrane allowed for the same function as these retention features that ultimately outperformed the lumen multi-microfluidic model in hydrogel retention. As such, it appeared as though only the three-chamber chip design would allow for the desired mechanical and transport properties to mimic ultrafiltration in peritoneal dialysis.

5.0 Final Model Manufacturing and Formulation

After it was determined that the three-chamber chip could be manufactured using the desired methods and the hydrogel could be seeded and retained, additional fluids needed to be added to the microfluidic model in the dialysate and vascular channels. For the vascular channel, flow at a rate that mimicked capillary flow in the peritoneum is needed. A syringe pump system with connections to the chip inlets was designed to allow for flow over the dwell period, for continuous addition of waste products to be filtered by the dialysate.

5.1 Final Manufacturing Process

The three chamber chip master mold, shown in Figure 11(d), was used to manufacture all final design three chamber chips following the mold treatment process described above. Using the soft lithography, membrane addition, and plasma bonding methods described above, chips with the final design were manufactured. As discussed in section 4.4.4, the final hydrogel that was added to these chips was a collagen hydrogel. This hydrogel was seeded into the chips according to methods described in section 4.4.5. Following hydrogel addition, the model was ready for addition of a dialysate fluid in the dialysate chamber and addition of a blood analog

solution in the vascular channel. In order to mimic blood flow in a capillary with the blood analog in the vascular chamber, a syringe pump system was attached to the inlet of the blood analog channel to provide a constant flow of blood analog solution.

5.2 Fluid Addition

Fluids were added to the vascular channel and dialysate channel to allow for transport of waste products across the collagen hydrogel to mimic *in vivo* conditions. The blood analog solution for the vascular chamber and the dialysate solution for the dialysate chamber were formulated using the methods described below and added to their respective channels through the channel inlets.

5.2.1 - Dialysate Fluid Formulation

A low osmolarity lactate-based peritoneal dialysis (PD) solution was prepared utilizing aseptic technique in a biosafety cabinet. This formulation has been proven to be an adequate substitution for commercially available dialysate when treating patients with acute kidney injury [24]. Lactate-based PD solution is also the most commonly used formulation for patients undergoing continuous ambulatory peritoneal dialysis [25]. Therefore, it is highly likely that the clinical success in achieving ultrafiltration of waste products from the blood with this formulation will translate to our microfluidic chip. It is expected that the dialysate fluid in the dialysate chamber within the microfluidic chip will be able to filter urea out of the blood analog as it diffuses through the stiffened hydrogel environment.

1L of Ringer's lactate solution and 30 mL of 50% dextrose solution were added to a 2L glass storage bottle using a serological pipette. The storage bottle was inverted several times to ensure adequate mixing of the two solutions. A 5 mL sample was removed from the prepared dialysate and transferred to a conical tube. The pH of the solution was then tested using an Apera Instruments pH20 pH meter as a checkpoint to see if the batch prepared matched the expected values of batches prepared in literature, affirming the recipe was followed correctly. The accepted pH range for lactate-based PD solution is between 5.2 and 6.5, and the pH of the prepared solution was determined to be just within range at a pH of 6.5 [25, 26]. After verification of pH, the storage bottle was placed out of direct sunlight at room temperature until use of the solution in the microfluidic chip.

5.2.2 Blood Analog Fluid Formulation

The simulated body fluid must have the same properties as blood which are a density of 1060 kg/m3, a dynamic viscosity between 2.9 – 4.37 mPa*s, and a kinematic viscosity between 2.75-4.12 x 10^{-6} m^2/s [27]. In order to formulate 100 grams of a fluid with these properties, 34.5 grams of 100% glycerol were added in a glass bottle and mixed with 44.1mL of DI water. To this solution 21.41 grams of urea were added, and everything was well mixed. The pH of the

formulated body fluid analog was measured to be 7.4. After pH verification, the glass bottle was closed and stored at room temperature hidden from the sunlight. The concentrations used to formulate this solution were obtained from literature [27].

5.3 Syringe Pump Flow Setup

In order to flow the blood analog through the proposed system, a syringe pump with a 5mL syringe was used. The syringe was connected to a tubing and a hose adaptor connected the tubbing to the blood analog input (Figure 17). At the output a hose adapter was placed and connected to a tube which led into a container reservoir that collected the blood analog. This was set up in a small incubator oven so the chip could stay at $37℃$ for the dwell time duration (Figure 17). The syringe pump was placed outside with the tube leading into the incubator where the rest of the set up was placed. The flow rate of the blood analog was calculated to be 9 µl/min from a scaled-down version of the blood flow in the peritoneum. The scaled-down calculations can be found in Appendix D.
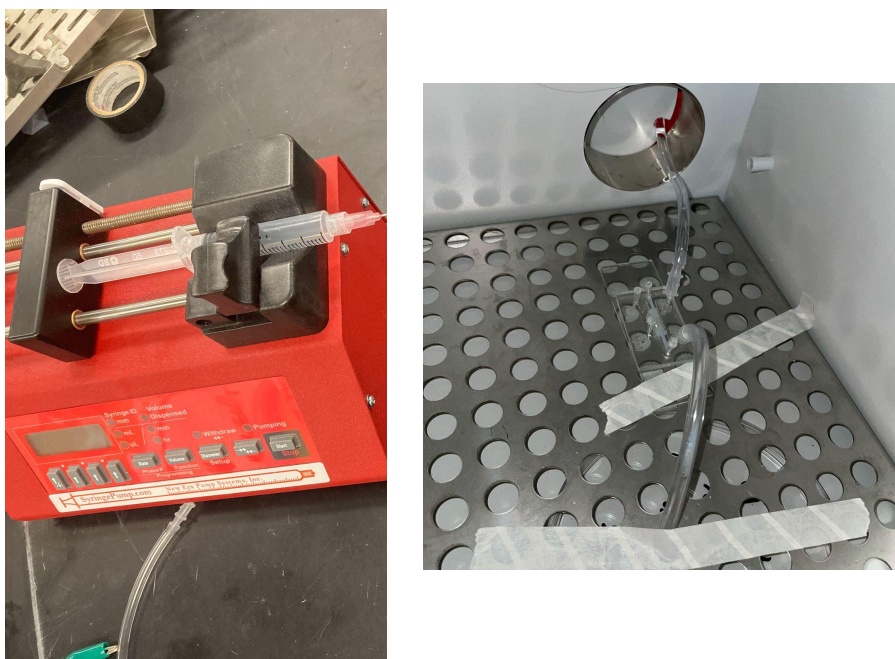
Figure 17: Syringe pump set up on the benchtop (left) and in the incubator oven (right)

6.0 Final Model Verification Testing

Where the microfluidic model was fully assembled with the desired fluids in each channel and the connection to the syringe pump flow setup, verification testing was needed to see if the model did indeed meet the desired objectives. To evaluate if the model met the objective 'representative of *in vivo* conditions,' the hydrogel was characterized using rheology to

determine stiffness. The hydrogel was characterized further using a transwell permeability system to determine the permeability coefficient and, in turn, the diffusion coefficient. To further determine transport properties, the mass transfer area coefficient for urea across the hydrogel was calculated using a standard peritoneal permeability assay. The mass transfer area coefficient obtained experimentally was compared to a simulated value obtained using a simulation of the chip in COMSOL. To evaluate if the model met the objective 'accessible for research purposes,' a direct transfer sterility test was used to assess if different sterilization methods eliminated pathogenic growth to allow for future cell culture experiments in the chip. While these two objectives were the main objectives that required verification testing, the other three objectives were still considered and are represented in testing. For example, 'production' is partially evaluated using the direct transfer sterility test, as this test evaluates if the production method is feasible given it is done under benchtop conditions and requires an additional sterilization step. 'Reusability' is also partially evaluated using the sterility test, as identifying an appropriate sterilization method that works initially could also be used for re-sterilization of chips following an experiment. 'Cost effectiveness' is evaluated through the characterization testing, as the choice of materials was made with the desired properties in mind. If the properties are achieved, it can be said the low cost materials successfully create a cost effective system.

6.1 Stiffness Characterization of Hydrogel Using Rheology

To ensure the hydrogel is an appropriate model for the fibrotic peritoneum, parallel-plate rheological testing was performed to determine the hydrogel stiffness. This verification test is intended to assess the design objective 'representative of *in vivo* conditions,' and specifically peritoneal stiffness as a result of fibrosis. The first round of this type of testing served as a sort of feasibility testing for using the TGA-gelatin hydrogels in the model; these results can be found in Appendix F. Further verification testing was performed on the TeloCol-10 (Advanced BioMatrix) collagen hydrogel diluted to a concentration of 8 mg/mL.

6.1.1 - Rheology Testing Methods

Using prior knowledge of the behavior and rheological testing of collagen hydrogels as a starting point, a strain value of 0.1% was selected to run frequency sweeps in oscillatory shear (Table 5). A frequency range of 0.01 Hz to 100 Hz was chosen based on literature values [53]. A gap size of 1 mm was assumed and measurements were taken at 37℃ to mimic *in vivo* conditions. Samples were run in triplicates and consisted of 300 μL samples where the final composition was 8:1:1 10 mg/mL Collagen to 0.01 N HCl to 0.1 N NaOH. The pH of the sample was confirmed to be in the range of 7.0 - 7.5 using standard pH strips after each dilution. Once the sample was prepared, the stage of the rheometer was brought to a temperature of 4°C where the sample was then loaded onto the stage. The stage was then brought up to a temperature of 37℃, a solvent trap was placed on the sample to avoid evaporation, the parallel plate tool was

lowered and a 15 minute rest period was allowed for the sample to gel. Following the 15 minute rest period, measurements were taken.

6.1.2 A Stiffness Greater Than the Stiffness in the Healthy Peritoneum is Achieved
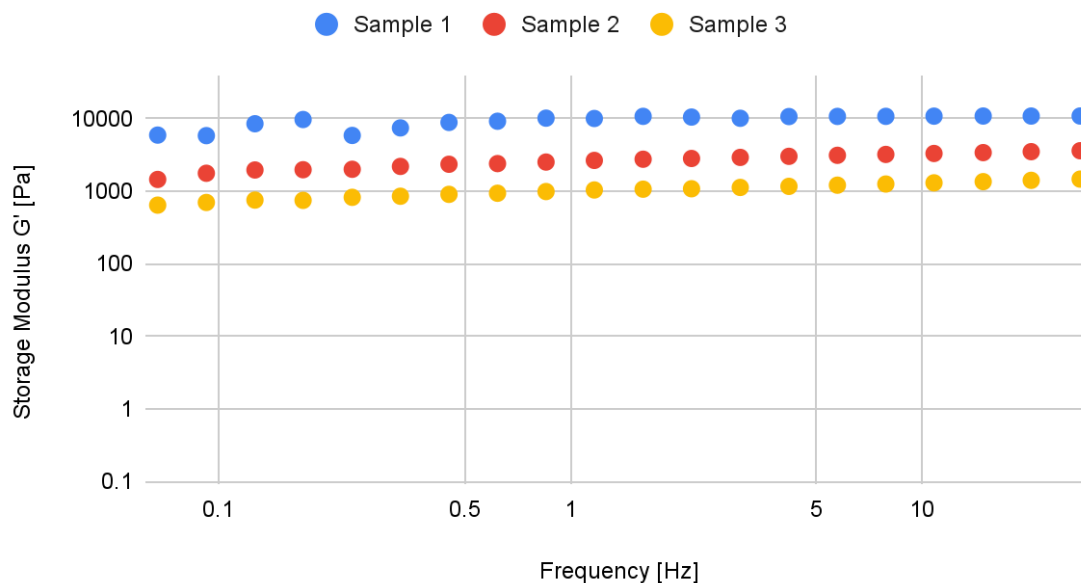
Figure 18: **Storage moduli obtained during frequency sweeps for collagen hydrogel.**

Storage and loss modulus vs. frequency plots were generated using the data from the frequency sweeps. Storage modulus refers to a material's ability to store energy elastically while loss modulus refers to dissipate stress through heat. Since hydrogels are viscoelastic materials, rheological tests must be performed to accurately account for both their solid and liquid behavior. In making the connection between storage modulus and stiffness, it is important to consider the relationship between the storage modulus and the elastic modulus. In the linear viscoelastic region of a stress vs. strain graph, Young's modulus is approximated as the slope and describes the stiffness. The linear region of a storage modulus vs. frequency graph generated during the frequency sweeps at the strain of interest identifies the linear viscoelastic region also, and the storage modulus in this region can be assumed to be equal to Young's modulus and equal to stiffness. A plot of storage moduli at different frequencies for the three samples tested reveals the average stiffness achieved across the three samples in the linear viscoelastic region is approximately 5.044 ± 4.916 kPa (Figure 18). The linear region occurs around a frequency of 0.06 - 28.1 Hz, which is visualized using a log scale (Figure 18).

6.2 Permeability Characterization of Hydrogel using Transwell System

In order to validate whether the model is able to accurately replicate the in vivo conditions of peritoneal fibrosis, the transport properties of the hydrogel needed to be evaluated. Finding key metrics such as the diffusion coefficient allowed the model to be compared to in-vivo values for the evaluation of the chip's capabilities.

Table 5: Parameters used to run frequency sweeps for rheological tests.

Parameter	Value
Temperature	37℃
Gap Size	300 μL
Frequency	0.01 - 100 Hz
Strain rate	0.1%

6.2.1 Permeability Characterization of Hydrogel Methods

The permeability of the experimental hydrogel was evaluated using a transwell system. This system allowed for the experimentation and observation of the behavior of representative solutes such as fluorescein salt through the hydrogel. Fluorescein salt was used as it was verified as an appropriate stand in for the modeling of low-molecular weight solutes such as urea [28]. A protocol for this experiment is included in Appendix G.
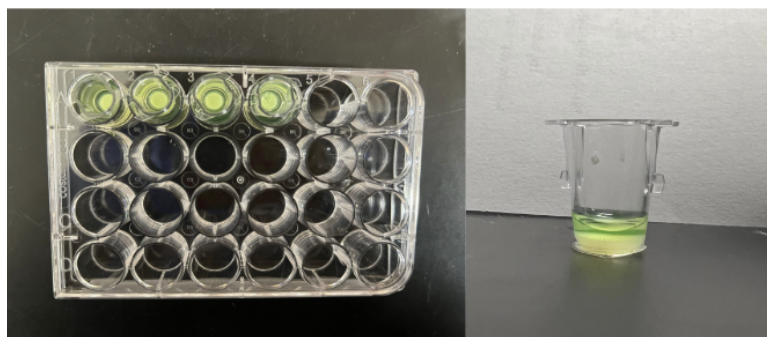
Figure 19: Transwell system set up with seeded hydrogel and fluorescein solution

6.2.1.1 Transwell Permeability Assay

Fluorescein salt (MW 412.3) was mixed with dialysate solution to a concentration of 0.0125 μg/ml. Telcol-10 was diluted using 0.1M NaOH and 0.01M HCL in a ratio of 8:1:1 to achieve an estimated stiffness of 8 kPa and pH of 7. 67 μL of the hydrogel was loaded into the dish of a transwell system and allowed to gel at 37°C. The experimental set up is pictured in figure 19. Once gelation occurred the outer well was filled with 1000 μL of PBS and the inner well was filled with 205 μL of the fluorescein salt solution as seen in figure 19. The volumes of

these solutes were calculated based on the dimensions of a 24-well plate with the thickness of the hydrogel set to match the thickness of the original procedure using a 12-well plate (Appendix H). The media was allowed to sit for a period of five hours with 20μL samples of the outer well taken at time points of one hour. These samples were then run on a plate reader set to an absorbance wavelength of excitation 495 nm 530 emission to find the concentration of salt within the samples using a standard curve. Once the concentrations were found, a concentration vs. time graph was built for each transwell and the linear region of this graph was isolated with its slope taken as dc_A/dt in (Eq. 2). Using this value, the permeability of the hydrogel was calculated [57].

6.2.1.2 Transswell COMSOL Simulation

In order to further evaluate the hydrogels transport properties the change in concentration across the hydrogel in the transwell system was utilized by a A COMSOL Multiphysics simulation. The COMSOL Multiphysics simulation was used to recreate the permeation process across the membrane using the experimental data. Then, by running a parameter optimization, the diffusion coefficient was estimated from Fick's second law equation ,

$$\frac{\partial c}{\partial t} + \mathbf{u} \cdot \nabla c = \nabla \cdot (D\nabla c) + R$$

(Eq. 1)

where c is the concentration of fluorescein salt, t is the time, u is the velocity, D is the diffusion coefficient, and R is the reaction rate [57]. The reaction rate was neglected because no chemical reaction occurred in the diffusion process.

First, the 24-well transwell geometry was replicated with the addition of the collagen membrane acting as a barrier, the inner well with high fluorescein concentrations as the donor, and the outer well receiving fluorescein in the outer well as the receptor. Then, the "Transport of diluted species" physics was selected, with two different 'transport properties' subsections, one for the donor and other for the receptor. Here the parameter specifications for both solutions were determined including the initial conditions such as fluorescein salt concentration. All these parameters and dimensions can be found in the tables in Appendix I. Finally the parameter optimization was added by inputting the experimental data and running a global least-squares objectives using a SNOPT solver method with a tolerance of 10^{-9} that represents the error. Then, the simulation was computed to find the value of D that best fits the experimental data (Eq. 1).
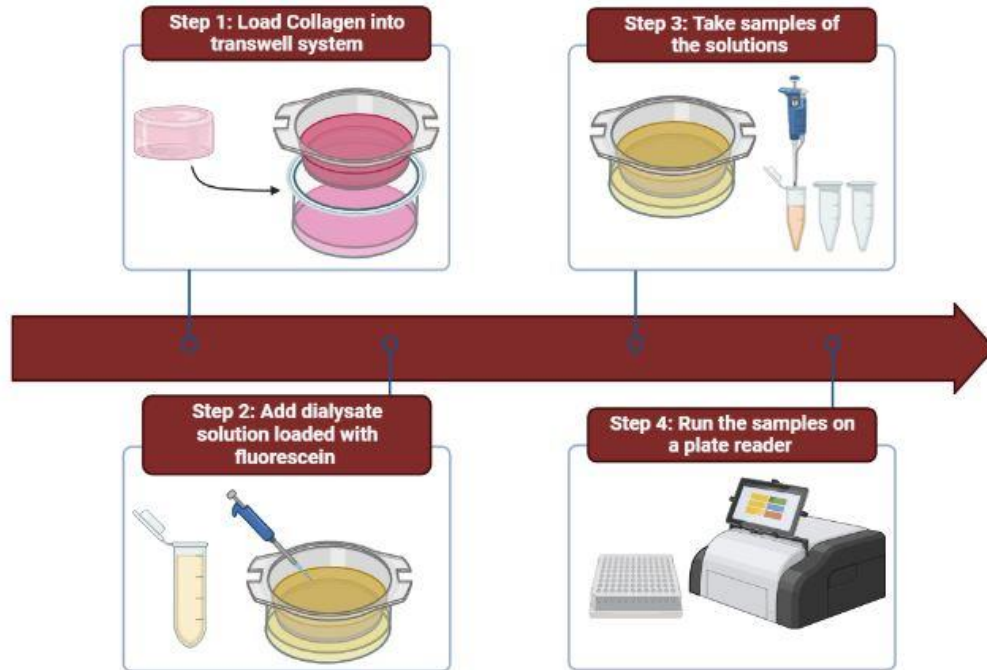
Figure 20: Schematic representation of determining the permeability experimentally using the transwell system.
Created in Biorender.com.

6.2.2 Permeability Coefficient Obtained from Transwell Assay

Once the concentrations were found, a One-Way ANOVA was run on the values between each transwell (N=3 n=10). A p-value less than 0.05 was found, thus the variance between samples is not significantly different, and it can be plotted in the simulation to find a low error diffusion coefficient. Based on data gathered, a concentration vs. time graph was built for each transwell and the linear region of this graph was isolated with its slope taken as dc_A/dt in the Eq 2.

$$\frac{dc_A}{dt} \;=\; P \; x \; A \frac{c_D}{V_A} \qquad\qquad (Eq.\ 2)$$

The permeability of the hydrogel was found to be $2.59 \times 10^{-6} \pm 1.17 \times 10^{-6}$ m/s. The calculation of this value as well as the data collected from the three trials is pictured in Appendix H.

6.2.3 Parameter Optimization in COMSOL Multiphysics Estimated the Diffusion Coefficient Across the Collagen Hydrogel

The results of the parameter optimization gave a value of $6.2484 \times 10^{-10} \pm 2.338 \times 10^{-18}\ m^2/s$ for the diffusion coefficient. This value will be used in further testing to find the

transport properties of the proposed model. In addition to this it displayed the concentration of fluorescein over time in the transwell system as shown in Appendix H.

6.3 Standard Peritoneal Permeability Assay

In order to ensure that the proposed model is representative of *in vivo* conditions and can be used for research purposes, this must be able to mimic the permeability of the peritoneum as it happens during peritoneal dialysis. The gold standard for peritoneal model analysis is the standard peritoneal permeability analysis (SPA). SPA is an adaptation of the peritoneal equilibrium test which is used to evaluate the peritoneal transport characteristics in patients. 3.86% glucose is added to the dialysate along with dextran. The dextran serves as both a volume marker and for a marker of fluid kinetics, for applications such as determining the lymphatic absorption rate [30]. The mass transfer coefficient of low molecular weight solutes such as urea can be calculated using this method, as well as the change in the intraperitoneal volume [31].

6.3.1 Experimental MTAC Methods

Lactate-based peritoneal dialysate solution was used to perform a standard peritoneal permeability assay. Telcol-10 was diluted with 0.1M NaOH and 0.01M HCl at the ratio described previously. Using a 1000 μL positive-displacement pipette, the hydrogel was seeded into the middle chamber of a three chamber chip. The hydrogel was allowed to polymerize in a 37°C incubator for 30 minutes. The dialysate solution and blood analog fluid were then introduced to fill their respective channels. To mimic blood flow through the capillaries, a pump system was attached to the blood analog channel, flowing the solution through the channel at a velocity of 1.82 mm/min and a flow rate of 9 μL/min. Time zero was designated by the time at which each fluid had fully filled their channels. At this time, the dialysate solution sat for a dwell time that was determined during the diffusion coefficient optimization process . A 50 μL sample of the dialysate solution was taken from the inlet using a pipette and was analyzed to find the mass transfer area coefficient (MTAC) of urea using Equation 3 below [30]. The urea content of the dialysate was measured via a colorimetric assay at 340 nm (Stanbio Urea Nitrogen (BUN) Liqui-UV®). The protocol for the assay and all calculations are included in Appendix G. A schematic representation of this sampling process is seen in Figure 21.

$$MTAC \; (mL/min) \;\; = \frac{V}{t} \; ln(\frac{V_{10}^{0.5} \, (P - D_{10})}{V_{t}^{0.5} \, (P - D_{t})}) \qquad\qquad (Eq. \; 3)$$

In the MTAC equation, V denotes the total average volume of the dialysate found as the area under the curve of a time vs. dialysate volume graph. V_{10} denotes the volume at time 10 minutes and V_t represents the final volume of the dialysate solution. P and D represent the urea concentration of the blood analog and dialysate solutions, respectively, at the times of 10 and 60 minutes.

Choosing MTAC as a value to measure transport properties is beneficial in future cellularization of the chip, as it allows for consideration of dialysate volume loss from lymphatic capillary uptake that is representative of *in vivo* conditions. However, the acellular model of the chip has a constant volume, assuming no leakage from the chambers. As such, the MTAC equation can be simplified, where V_{10} and V_t are equal if the volume is constant and V_{10}/V_t simplifies to 1 (Eq. 4). Instead of 10 and 60 minutes, the initial concentration of urea in the dialysate, D_i, and the final concentration of urea in the dialysate after the dwell time, D_f, are used.

$$MTAC \ (mL/min) \ \ = \frac{V}{t} \ ln(\frac{(P - D_i)}{(P - D_f)}) \qquad\qquad (Eq. \ 4)$$

The MTAC of urea was calculated using equation 4 and compared to the values found in the literature for standard peritoneal permeability assay as described by Zweers et al [31]. This procedure helps validate the model by illustrating the ability to meet the objective of being representative of *in vivo* conditions. Once the MTAC was found for our model, it could be compared to the baseline value of 22.9 mL/min. A direct comparison would not be possible, as MTAC is directly proportional to dialysate volume (Eq. 3). The value of 22.9 mL/min is based on a 2 L dialysate volume used in a typical human dwell [31]. This value was scaled down approximately 25,000 times to account for the 78 μL dialysate volume in the microfluidic chip. Therefore, the target scaled down MTAC was determined to be 1.49 x 10^{-11} m^3/s based on the difference in dialysate volume between a human and microfluidic chip. This MTAC was found in studies examining healthy peritoneal environments. The MTAC of urea was found to not change a statistically relevant amount from a diseased to healthy peritoneum. Because it does not change, this MTAC allows the chip to be evaluated without the use of a control or healthy peritoneum model. A statistically similar value gathered from the chip of a fibrotic environment chip would validate our model as representative of *in vivo* conditions and a possible fibrotic peritoneal environment.
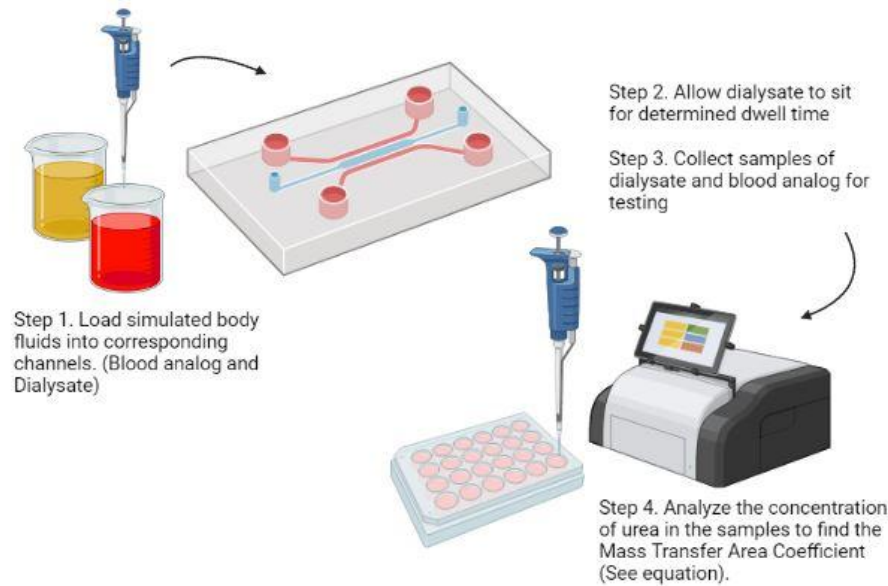
Figure 21: Schematic representation of determining the MTAC experimentally in the microfluidic model.
Created in Biorender.com.

6.3.2 Simulated MTAC in COMSOL Multiphysics Estimates Dwell Time of 6 Hours

To estimate the best dwell time for the experimental set up, a simulation of this test was performed in COMSOL multiphysics using the diffusion coefficient found in the permeability characterization of the hydrogel. This provided the concentration in each chamber over time, which was used to find the respective simulated MTAC over time.

The 2D geometry of the proposed model was imported into COMSOL and the "laminar flow" physics platform was used along with the platforms used in the transwell system simulation previously described in section 6.2.1 to account for flow through the vascular channel. The fluid properties and parameters were added as shown in Appendix J . The initial conditions for this simulation include the urea concentration in the blood analog and dialysate chamber as well as the velocity at the inlet of the vascular channel, which are also outlined in the Appendix J.

After computing the experiment, the velocity field and concentration gradients across the surface of the chip were given by the simulation (Appendix J). The average concentration in each chamber over time was also an output of the simulation, this data was used to find the simulated MTAC at the different timepoints (Figure 22).
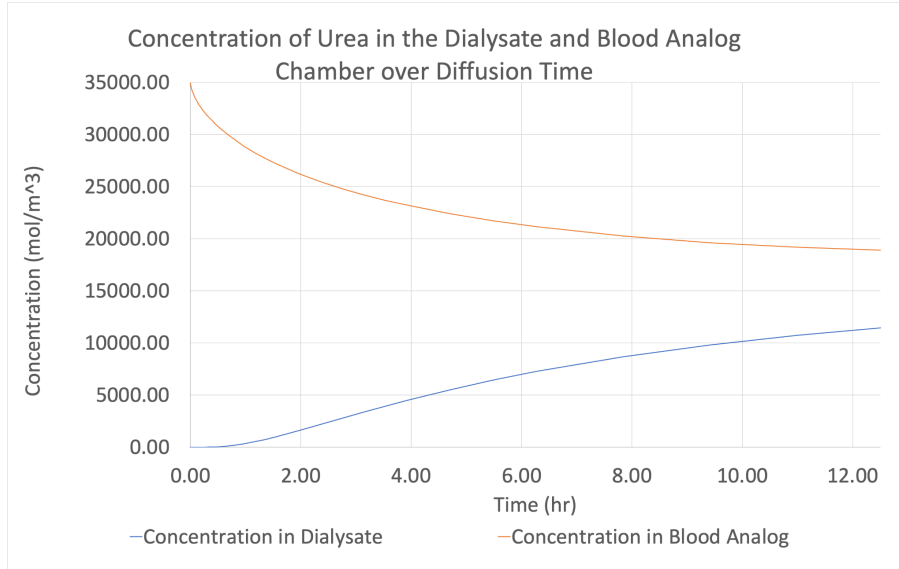
Figure 22: Concentration of urea in the dialysate and blood analog chambers over time

The MTAC value peaked after 6.28hr of diffusion time with a value of $7.87 \times 10^{-13} m^3/s$ as seen in Figure 23. The MTAC was calculated in Excel using equation 4 in the section above with an initial time of 0 seconds (Eq. 4).
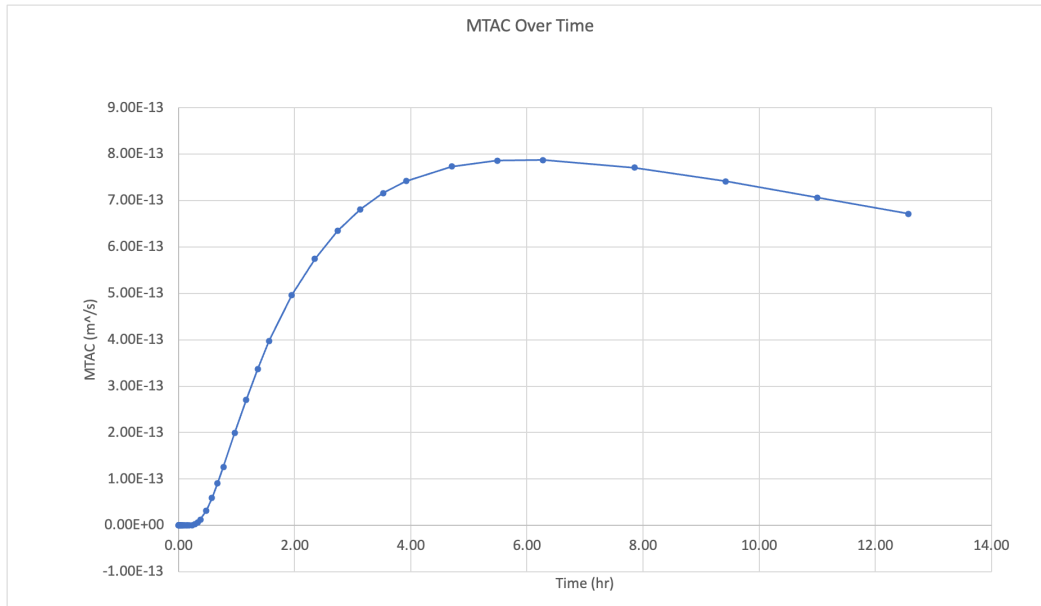
Figure 23: MTAC value over diffusion time

6.3.3 MTAC in the Microfluidic Model Differs from Predicted Values in the Simulation

As described in section 6.3.1, a sample of the dialysate was taken after the desired dwell time and the urea concentration was determined using a blood urea nitrogen (BUN) assay. The

protocol for calculating urea concentration from the change in absorbance value at 340 nm over 90 seconds of the sample once it is added to the assay working reagent is included in Appendix G. The change in absorbance at 340 nm of the sample in the working reagent over 90 seconds is compared to the change in absorbance of a standard solution, provided with the assay kit. The absorbance values obtained for triplicate samples of the standard and dialysate sample after a dwell time of 6 hours are shown in Table 6, where A_1 denotes the absorbance of the respective solution in the working reagent at 30 seconds after addition and A_2 denotes the absorbance of the respective solution in the working reagent at 90 seconds after addition.

Averages of ΔA from the triplicate samples were used to ultimately determine the urea concentration in the dialysate sample. The average ΔA for the standard was 0.040 ($\pm$ 0.007) and the average ΔA for the dialysate sample was 0.957 ($\pm$ 0.300). Using the calculations in Appendix G and plugging in these average ΔA values, the urea concentration in the dialysate after a dwell time of six hours was determined to be 256.51 mmol/L, which is equivalent to 256.51 mol/m^3.

Table 6: Absorbance results from BUN assay

Sample Type	Sample Number	A_1	A_2	ΔA (A_1-A_2)
Standard Solution	1	1.691	1.644	0.047
	2	1.681	1.641	0.040
	3	1.716	1.683	0.033
Dialysate Sample	1	1.537	0.367	1.17
	2	1.607	0.992	0.617
	3	1.485	0.396	1.089

A comparison of this urea concentration at the six hour time point measured from the dialysate sample to the predicted urea concentration in the dialysate from the COMSOL simulation is shown in Figure 24. The concentration obtained from the BUN assay is significantly lower than predicted by the COMSOL simulation. The experimentally determined concentration was plugged into the MTAC equation (Eq. 4) and a MTAC of 2.61 x 10^{-14} m^3/s was calculated. This differs from the predicted peak MTAC of 7.87 x 10^{-13} m^3/s.
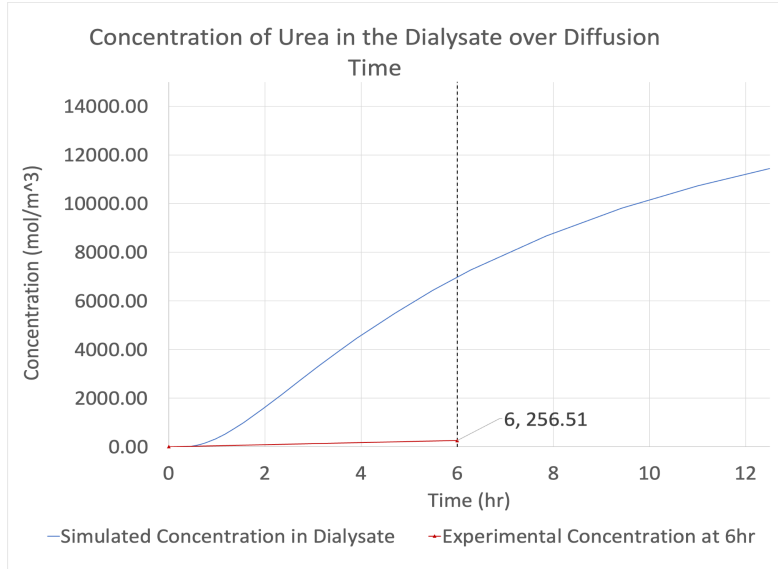
Figure 24: Simulated vs. experimental concentration of urea in dialysate chamber.

6.4 Sterility Testing

Where the microfluidic chip is intended to be used for research with cell culture applications and specifically seeding LECs, it is crucial that the chip can be adequately sterilized to reduce the chance of contaminating the culture. Testing adequate sterilization falls under the design objective "representative of *in vivo* conditions," as development of a physiologically accurate system to study the role of lymphatic absorption of dialysate in ultrafiltration failure is dependent on cell culture in the microfluidic chip. Where the goal of this project is not to cellularize the system but instead create a tool for researchers to use for cell culture studies, it is crucial to verify that adequate conditions can be created in the chip for the desired experiments and modeled in vivo conditions. Thus explains the importance of identifying an adequate sterilization method through sterility testing. Additionally, as an extension of this type of testing, future research groups could test the adequacy of re-sterilization methods after cleaning the chips out of experimental contents for reuse of the chips for multiple experiments. So, a foundation for sterility testing is needed.

6.4.1 Sterility Testing Methods

Several sterilization methods have been evaluated for PDMS-based microfluidic chips. Sterilization with UV irradiation in a biosafety cabinet with such capabilities has been shown to increase the modulus of elasticity and stress relaxation of PDMS [28]. PDMS with these modified properties constitutes a stiff environment for cells to adhere to and leads to increased cell proliferation over ethanol-sterilized PDMS, which does not experience this alteration of mechanical properties [28]. However, use of 70% ethanol is a widely recognized method for surface sterilization and the adequacy of sterilization using ethanol for the microfluidic chips

developed in this project is still a topic of interest. With this in mind, two experimental groups emerged: chips sterilized with UV irradiation and chips sterilized with 70% isopropyl alcohol, which is comparable to 70% ethanol. While literature provides insight into the preferred method of sterilization, it is still necessary to verify that either this method or the alternative ethanol sterilization method will adequately prevent growth of bacteria and fungi within the novel design.

An overview of testing methods is shown in Figure 25. Additionally, a protocol for this experiment is included in Appendix G. PDMS chips bonded to glass slides were prepared using the protocol described previously up to the point of plasma bonding, but no addition of hydrogel or fluids occurred. The first experimental group of chips was placed in individual sterile culture dishes glass side down with the lids removed (n=3). Subsequently, the culture dishes were placed in a UV irradiation chamber for one hour to allow for sterilization and new sterile lids were replaced. The second experimental group of chips was again placed in individual culture dishes glass slide down (n=3). The culture dishes were transferred to the biosafety cabinet with the lids on. 70% isopropyl alcohol was pipetted into the chips, allowed to sit in the channels for one minute, and aspirated using a pipette. The lids were partially replaced on the culture dishes for a period of 15 minutes to allow for drying of excess ethanol while preventing contaminants from falling into the culture dishes. A control group of n=3 chips did not undergo any sterilization treatment, but was placed in separate, sterile culture dishes. A second control group of n=3 culture dishes containing sterile Luria broth (no microfluidic chips) was included to study potential contamination from incubation. Each group of culture dishes was placed in a separate, surface-sterilized Tupperware container prior to incubation to reduce airflow around the dishes and potential contamination from opening and closing the incubator.

Miller's Luria broth was prepared by mixing 25 g of a pre-mixed powder concentrate with 1 L of deionized water that was brought to a boil to ensure complete dissolution of the powder. The broth was autoclaved for 15 minutes at 15 lbs pressure and 121℃ to sterilize. The broth was first pipetted into the channel of each chip on the benchtop to ensure the broth was in contact with the channels for the experiment duration. More broth was added into each culture plate to completely immerse the microfluidic chips. Each group of culture dishes was placed in a separate, surface-sterilized Tupperware container prior to incubation to reduce airflow around the dishes and potential contamination from opening and closing the incubator. The incubator used had temperature control only at 37℃.
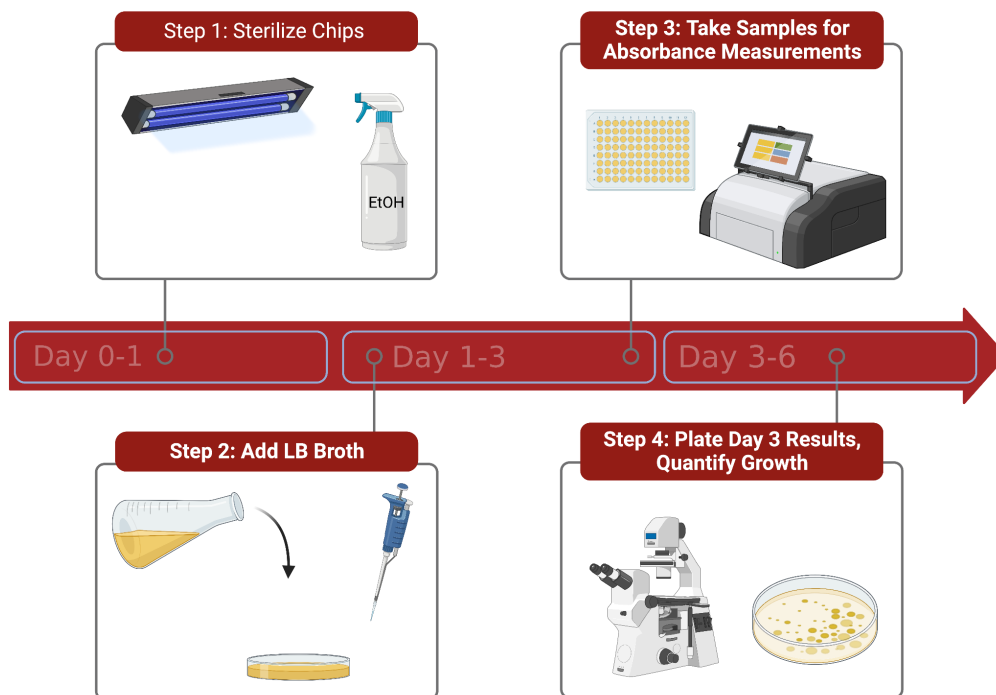
Figure 25: An overview of the direct transfer sterility test methods with experiment timeline.
Created in Biorender.com.

100 μL samples of the broth in each culture plate in triplicate were removed just after addition, after 24 hours, after 48 hours, and after 72 hours and placed in a well plate to measure absorbance. The timeline was chosen after speaking with an expert in the field, as this would allow an opportunity to determine both bacterial growth and fungi growth. The experimental setup is meant to be consistent with USP 71 standards of sterility testing using the direct transfer method in the absence of the highly specialized setups that are used to run these types of tests for pharmaceuticals. The timeline is expedited compared to the recommended timeline from USP 71, but includes the first time point of interest, as this is sufficient to determine the presence of pathogenic growth.

Absorbance at 600 nm was measured using an absorbance plate reader for each sample collected to determine optical density, which is a commonly used measurement to determine bacterial growth (OD_{600} measurements). Optical density and absorbance are terms used interchangeably with the same definition, where both terms are mathematically defined by a logarithmic relationship to the percent transmittance of light at a specified wavelength [40]. Typically, OD_{600} measurements are used to determine specific numbers for growth and growth rates within a culture, as optical density correlates with bacterial growth and standard curves can be generated for optical density vs. cell density for different species of bacteria [39]. In this experiment, any absorbance reading that varied by more than one standard deviation from the average absorbance measurement of the sterile Luria broth identified bacterial growth. Where the contaminating species could theoretically be any number of bacterial species present in the incubation environment or even a mix of species, specific growth numbers could not be

determined from these measurements alone. Thus, absorbance measurements were semi-quantitative results that simply determined the presence of bacteria or not. To further quantify results, day 3 broth from plates with the lowest absorbance readings in each group was plated on LB agar plates at a 10^4 times dilution and incubated for three days. Following incubation, plates were examined to quantify colony growth and identify bacterial and/or fungal species that were the source of contamination. Ideally, zero colonies (no pathogenic growth) should be seen if the sterilization method was effective. A positive number of colonies counted during microscopy suggests an inadequate sterilization method that most likely needs to be adjusted for adequate sterilization. Colony morphology can also be studied, where branching colonies would be indicative of fungal growth and rounder colonies of varying sizes are likely indicative of bacterial growth.

6.4.2 Higher Absorbance Measured in Non-Sterile Control Chips Compared to Sterilized Chips

The experiment was run two times with the three-chamber chip design. A summary of the absorbance measurements taken for each group at each time point is included in Figure 26. For both runs, the absorbance measurements for all groups studied are relatively consistent around 0.05 for the Day 0 sampling time point, with little deviation between measurements within a group (Figure 26).

Significant differences between absorbance measurements from the Day 0 sampling time point to the Day 1 sampling time point are seen with both runs. Similar trends exist on Day 1 between the two runs, but absorbance is higher overall for all groups for run #2 relative to run #1. The non-sterile control group has the highest absorbance of all the groups for both runs on Day 1. Between the sterilized groups, for run #1, the UV-sterilized group has a lower absorbance compared to the isopropyl alcohol-sterilized group. However, for run #2, the isopropyl alcohol-sterilized group has a lower absorbance than the UV-sterilized group, showing an inconsistent result in the sterilized groups across runs for this time point. The sterile broth group has the lowest absorbance relative to all groups and remains unchanged from the value seen on Day 0.

Differences are seen again between absorbance measurements from the Day 1 sampling time point to the Day 2 sampling time point with both runs. Absorbance is still higher overall for all groups for run #2 relative to run #1. Again, the non-sterile control group has the highest absorbance of all the groups for both runs on Day 2. Amongst the sterilized groups, the UV-sterilized group has a lower absorbance compared to the isopropyl alcohol-sterilized group for both runs on Day 2, showing a consistent result. The sterile broth group again has the lowest absorbance relative to all groups and remains unchanged from the value seen on Days 0 and 1.
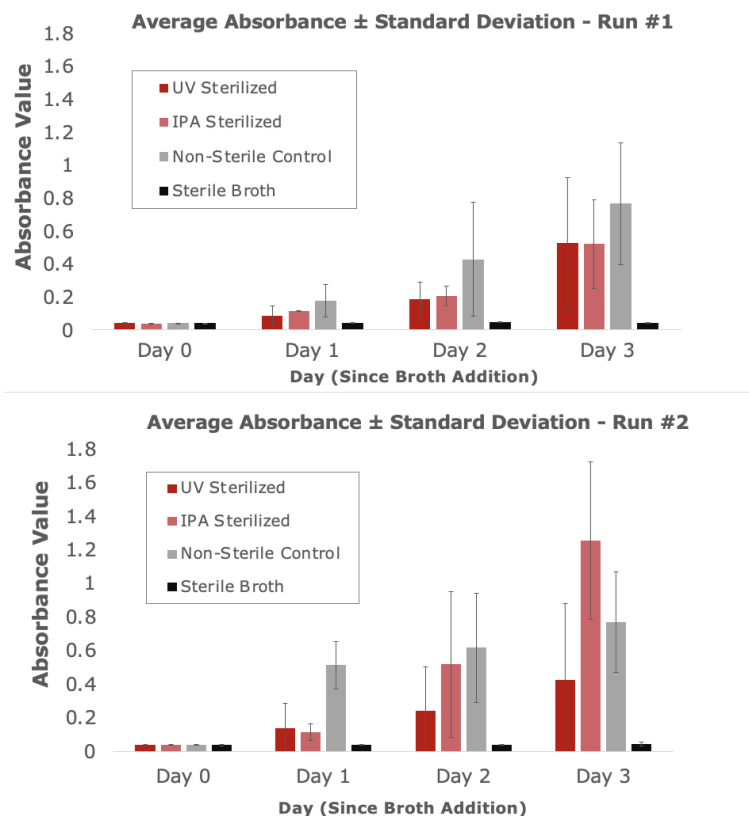
Figure 26: Average absorbance values obtained from direct transfer sterility testing.
In the key, IPA sterilized is the isopropyl alcohol-sterilized group and UV-sterilized refers to chips sterilized with ultraviolet light exposure. The error bars represent ± standard deviation and each group has n=3 chips (or broth plates, in the case of the sterile broth group).

Lastly, there are differences in the absorbance values seen on the Day 2 sampling time point compared to the Day 3 sampling time point with both runs, with the exception of the sterile broth group. The non-sterile group has the highest absorbance of all the groups for run #1, but the isopropyl alcohol-sterilized group has the highest absorbance of all the groups for run #2. Amongst the groups with chips, the isopropyl alcohol-sterilized group has the lowest absorbance for run #1 and the UV-sterilized group has the lowest absorbance for run #2.

While the results can be discussed relative to each other as a certain group has a higher or lower absorbance relative to another group for a given time point, it is important to do a statistical analysis to determine where there are significant differences between the groups. A two-way ANOVA test using a p value of 0.05 was performed using GraphPad Prism software to determine if there were differences between absorbance measurements of each group and across the sampling time points. Based on this significance level, the two-way ANOVA determined there were significant differences between either some of the groups or some of the time points, and multiple comparison testing was needed. The Holm-Šídák method of multiple comparisons was used for this process, as it is a powerful method that assumes each comparison is independent of the others. The results of this testing are summarized in Appendix K. In short, it

is of interest to note there is no significant difference between the UV-sterilized and sterile broth plates for Days 0-1 for run #1 and for Days 0-3 for run #2. Additionally, there is a significant difference seen between the non-sterile control group and the sterile broth plates for Days 1-3 for both runs #1 and #2.

6.4.3 High Number of Round Colonies Seen in Agar Plating of All Groups

The results of agar plating of broth samples of the plate from each group with the lowest absorbance measurements on Day 3 are seen in Figure 27. With the exception of the sterile-broth plates for both runs, too many colonies appear to accurately count and quantitatively connect an absorbance value with a bacterial cell density. However, colony morphology on the agar plates gives some insight into what type of pathogenic growth is contributing to high absorbance measurements over the experiment duration and for each sterilization method. The presence of round colonies and the absence of branching colonies suggests that bacterial growth is present and fungal growth is absent.
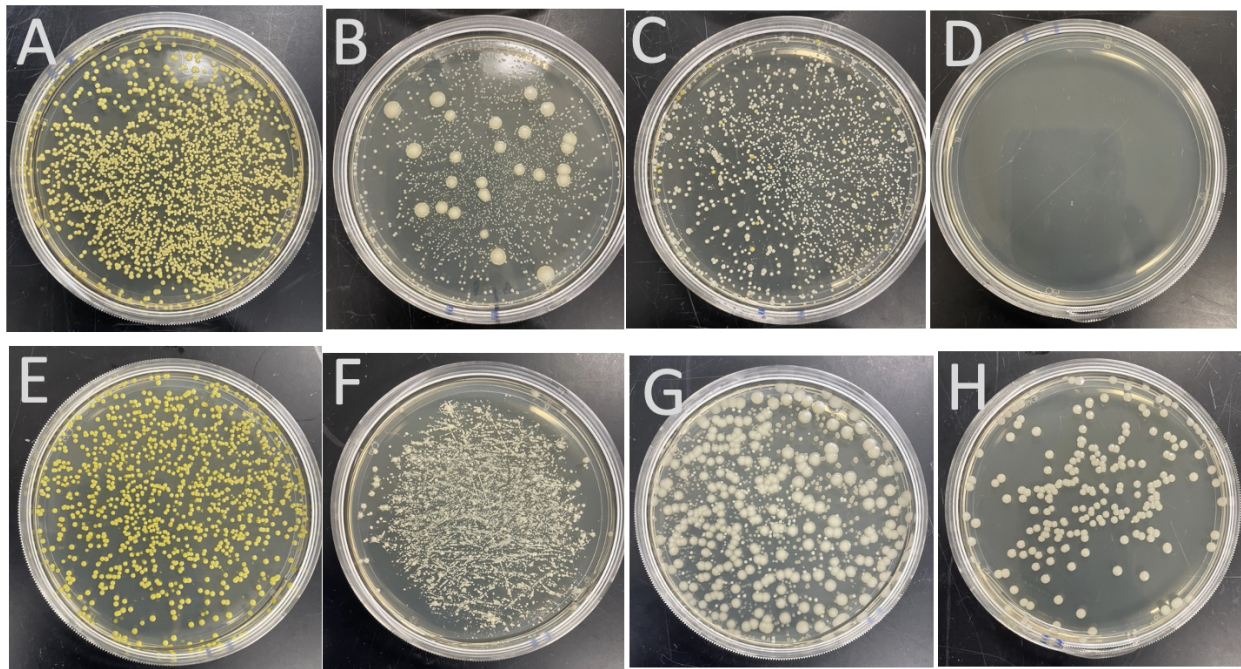
Figure 27: Results of agar plating broth samples of each group for direct transfer sterility testing.
A - UV-sterilized group, run #1; B - isopropyl alcohol sterilized group, run #1; C - non-sterile control group, run #1; D - sterile-broth plate, run #1; E - UV-sterilized group, run #2; F - isopropyl alcohol sterilized group, run #2; G - non-sterile control group, run #2; H - sterile-broth plate, run #2.

Across both runs, the colonies seen on the UV-sterilized group plates appear small (around 1 mm in diameter), opaque and yellow. For the isopropyl alcohol sterilized groups, there are hundreds of especially small (less than 1 mm in diameter) gray, opaque colonies, with some larger (2-3 mm in diameter) gray, opaque colonies in the run #1 plate. The non-sterile control plates across both runs include a mix of colonies seen in the UV-sterilized and isopropyl-alcohol

sterilized groups. The sterile broth plate for run #1 shows no colony growth, while the sterile broth plate for run #2 unexpectedly shows several large (1-2 mm in diameter) gray, opaque colonies.

7.0 Final Design and Validation

The results from verification testing allow for an assessment of objectives to determine if each was fully achieved, partially achieved, or not achieved. Additionally, a discussion of the impact of the design and ethics surrounding the product created is included.

7.1 Assessment of Objectives

The meeting of each objective was evaluated using at least one of the validation testing methods and through completing the manufacturing process in some cases. It was determined that all objectives were met at least in part and some objectives were fully achieved based on the definitions set forth at the beginning of the engineering design process. Subsequent chapters of this report provide insight into what else could be done in the future to fully meet the remaining objectives.

7.1.1 Representative of *in vivo* Conditions

Representative of *in vivo* conditions was found to be the most important objective to meet for the creation of preliminary designs as well as for considering design alternatives. Based on this objective, the chip needed to include elements to achieve stiffness characteristic of fibrosis and allow for interstitial flow. More specifically, the chip needed to be able to replicate the filtration and transport of waste seen in peritoneal dialysis. Using these criteria, this objective was partially achieved. Creating a stiff matrix was key to replicating the mechanical properties that arose from a fibrotic peritoneum. Including a collagen hydrogel in the hydrogel chamber was found to be the best option to satisfy the matrix stiffness criterion. Using a diluted collagen mixture the chip was able to replicate a stiffness of 5.04 ± 3.935 kPa. The healthy peritoneum has a stiffness of 2kPa on average and based on this, the chip was successfully able to incorporate a stiff matrix.

Interstitial flow is defined as the movement of solutes across a membrane based on their concentration gradient. This objective is paramount as the incorporation of interstitial flow is needed to not only ensure the future cellularization of the chip but also its function as a disease state. Using the transwell system, transport properties such as the diffusion coefficient were characterized. The transwell system and chip had similar dimensions in terms of thickness 2.2mm vs. 3.8mm The diffusion of the fluorescein salt was observed in the transwells lending to the expectation that interstitial flow in theory should be achieved in the chip. The SPA confirmed this to some degree. While the chip was able to accommodate interstitial flow, seen in the change

in concentration of urea in the dialysate chamber after its dwell time, this filtration was not able to model physiologically relevant values. This was due to the thickness of the hydrogel and the concentration of urea in the blood analog and samples being out of linear range of the assay. Given that the chip was unable to replicate the MTAC of urea, it cannot be claimed that the chip was able to fully be representative of *in vivo* conditions. Further optimization of the SPA would help the chip meet this objective. Additionally, changing the design of the chip to thin the hydrogel section to a more physiologically accurate thickness would cut down on the dwell time and potentially create a diffusion coefficient closer to what is seen in the body.

7.1.2 Accessible for Research Purposes

Accessible for research purposes was ranked the second to last most important design objective and it was defined so the microfluidic model could be used to test treatment options for ultrafiltration failure through future cellularization. This objective was partially achieved by incorporating different channels with different purposes as it happens during peritoneal dialysis. A chamber where dialysate is added, and different compositions could be tested; a vascular channel where different drugs could be incorporated for screening; and a hydrogel that acts like tissue and has the ability to host cells so the effect of the fluids on these can be also studied.

In order to future cellularize the chip, this needs to have a sterile environment with no microbial growth. The sterility of the device was tested using UV and ethanol sterilization, with promising results shown by the UV sterilization; however, cellular testing is needed to fully assess the ability of the proposed model to host cells successfully in the future.

7.1.3 Production

The production objective was originally defined as the device must be manufactured using techniques and lab equipment available in a standard academic lab space. The production objective was included because if the device could not be manufactured using methods available to the team, there would essentially be nothing to evaluate. Other advanced manufacturing techniques, such as photolithography, require a significant amount of training and investment into the equipment. The team did not have access to these resources and recognized that several other labs may not have access to these resources, so the team sought out to manufacture the design using soft lithography and the methods described in previous sections. This objective was fully achieved, as the microfluidic chip was able to be manufactured using these methods and passed a dye leakage feasibility test in several phases, as previously described. All solutions were able to be added to the device and the syringe pump system was successfully connected to the device.

The manufacturing method may present some issues in a future, cellularized version of the model, although the exact impact is unknown at this time. Although the hydrogel retention features were not able to be formed using soft lithography, the pre-wrap foam membrane

addition was a solution to this problem. This is sufficient for the acellular version of the model, but may present some issues in interactions with cells in a future, cellularized version of the model. If this is the case, the manufacturing method may need to be revisited to include a method that allows for formation of the original hydrogel retention features and this objective may only be partially achieved.

7.1.4 Cost Effectiveness

The cost effectiveness objective was originally defined as "the effectiveness of the microfluidic chip should justify the cost." This objective was fully achieved, as all materials purchased for the entire design process, manufacturing process, and validation testing process were purchased within a budget of $1000. There were several chips manufactured during the duration of this project, and the team estimates that approximately 100 chips were made within this budget. Validation testing verifies the effectiveness of the model, as explained in a previous section. So, the cost per chip is significantly less than the $1000 budget, which is significantly less than the cost for housing and developing one animal model. The team does recognize that other teams looking to recreate this work may not have access to some of the manufacturing equipment, such as a plasma reactor, which may be an additional investment. However, the amount of models you can develop with this initial investment is still more cost effective compared to the current gold standard.

7.1.5 Reusability

The reusability objective was originally defined as "the model has sterilization properties that allow for reuse." The reusability objective was ranked the lowest in comparison to the other objectives and was partially achieved, as a master mold was manufactured that allowed for multiple chips to be manufactured at the same time as long as the master mold permitted. While different sterility methods were tested with the hopes of finding one that allows for reuse of the chips, pathogenic growth was seen in all groups. Further cellular testing needs to be performed in order to assess if UV sterilization is an optimal method that allows for the chips to be reusable. Currently in the microfluidic modeling field, most chips are one time use aligning the project with the industry norm.

7.2 Ethical Impact of Final Designs

The development of accurate disease models helps foster better understanding of disease pathologies as well as drug treatments. Ultrafiltration failure following peritoneal dialysis affects a significant subset of the population undergoing the treatment. This condition can lead to kidney failure without the implementation of more invasive methods like hemodialysis. Ultrafiltration failure due to fibrosis and increased lymphatic uptake of the dialysate is a common problem but has not been studied extensively. Additionally, animal models fail to recapitulate some of the physiological characteristics needed to make the data retrieved from them relevant. Accurate *in*

vitro disease models are beneficial, as they reduce the need for further developing animal models. Testing with animal models requires ultimately sacrificing the animal for study, which is met with mixed reviews in the sphere of ethics. Our model will accommodate research into peritoneal fibrosis and lymphangiogenesis without the need to injure or develop an animal model. The results of the research conducted using the proposed model will also be gathered with significantly higher throughput, allowing for more efficient and accurate drug trials.

7.2.1 Economic Impact

Peritoneal dialysis is more cost-effective than hemodialysis when treating kidney failure. Survival rates have shown to be higher over a 10 year lifespan, and $16,000 cheaper in that same period of time [49]. The 10 year mean quality-adjusted life-year (QALY) of PD is 3.86, compared to a 3.25 of HD [48]. Because of this, a device that helps better understand peritoneal dialysis could lead to improvement of the current treatment, and make the breach of effectiveness between both treatment options even larger. This will affect quality of treatment, and reduce cost burden to patients and health care providers. The fact the PD is a cheaper treatment for kidney failure, an improved treatment could help reduce healthcare disparities as it would be more accessible for those that may not have the resources to afford other treatments.

In terms of current methods to study PD, which are animal testing, there is also a large cost difference in comparison with the proposed in-vitro device. According to an expert on the field that the team talked with, animal testing costs on average $35,000, and that is just for raising the testing subjects, and not including disease model development. Animal models are not only expensive, but also low throughput. Therefore, an in-vitro microfluidic device will result in a higher throughput and lower cost increasing the amount of testing performed to better understand PD.

There are no identifiable economic ethical concerns associated with the proposed microfluidic device. It will not have a significant economical effect on individuals or the economy as a whole, but the reduction cost of testing for PD, associated with future reduction of cost of kidney failure treatment.

7.2.2 Environmental Impact

The implementation of microfluidic chip models for diseases come with challenging but significant human health and environmental impacts. While microfluidic models carry great promise for urgent clinical needs as well as expands and provides opportunities for testing and diagnosis for limited laboratory facilities, the environmental impacts of the models are entirely dependent on the materials and techniques used to assemble said model. The chip housing the channels of most current microfluidic models are assembled using a combination of rigid polymers such as polydimethylsiloxane (PDMS) and inorganic glasses. While PDMS has minimal risks to aquatic ecosystems including no acute toxicity to benthos and its degradation

products have no significant effects on the soil or its microorganisms the same cannot be said about glass [51]. The main environmental impact of glass comes from the manufacturing processes since melting the raw materials produces carbon dioxide and nitrogen oxides that contribute to smog. Fortunately, material substitutions can be used to replace glass in favor of more environmentally friendly materials like PDMS and PMMA. The materials used to produce the microenvironment being modeled can also have negative environmental effects. The proposed microfluidic model uses a combination of dialysate fluid, blood analog solution and collagen to model the desired disease state. These materials commonly generate high amounts of waste and can have negative environmental impact if not disposed of correctly. To help reduce the environmental impact of these materials, the recommended strategy is to maintain close attention to materials used in literature and make material substitutions whenever possible. While microfluidic models can have significant effects on the environment, the benefits that they produce often outweigh the negatives. If in vitro models such as microfluidic models can accurately represent disease states and isolate aspects of diseases, the understanding of diseases could progress, leading to new discoveries and treatments for patients suffering from the studied diseases.

7.2.3 Social Impact

The choice to begin dialysis treatment can come with some risk. It was reported that those undergoing dialysis are more at risk for unemployment due to the serious time constraints that dialysis requires. This can lead to adverse social effects due to loss of autonomy. However, peritoneal dialysis (PD) has been shown to be less correlated to unemployment risk than hemodialysis. Additionally, patients have a better option of participating in PD at home. Despite these problems the creation of an in vitro model would not exacerbate any social problem arising from PD. The creation of an in vitro model will foster better understanding of the peritoneal membrane and could lead to increasing the time people can use PD before failure. The in vitro design will not exacerbate any withstanding social issues related to dialysis treatments. The ability to test drugs on a physiologically accurate model will allow for better dialysis fluid production and PD procedures. Additionally, because the chip is used for the study of the diseased tissue it will be used for research only as opposed to clinical use. While organ on a chip technology can be used for personalized medicine studies, diseases like peritoneal fibrosis have low variability between patient populations. The chip's use should not create healthcare disparities such as the ones concerning current personalized medicine treatments. As stated before the chip is not going to be used clinically.

7.2.4 Global Impact

Although the decision for a patient to begin PD treatment is a multifactorial decision, there is evidence to suggest the likelihood of a patient to be placed on PD treatment over hemodialysis treatment correlates somewhat to national policy, which varies across the globe. Furthermore, it may be incorrectly assumed that countries with more income may push for PD

treatment where there may be more resources for research and medical personnel education. In an analysis of the Kidney360 Global Dialysis Series where healthcare leaders in various countries shared the national strategy for dialysis care, it was discovered there is a poor correlation between a country's gross national income (GNI) and the percentage of patients on peritoneal dialysis treatment [50]. Instead, the highest percentage of patients undergoing peritoneal dialysis treatment are seen in Mexico and Guatemala and are associated with the mandated "peritoneal-dialysis first" policy [50]. Technicians in these countries are highly trained to aid in PD treatment and education gaps in other countries may help explain the prevalence of hemodialysis instead of a country's income and access to certain resources [50]. This is essentially a current global ethical issue, as disparities exist between nations in terms of access to quality PD treatment and are directly tied to national policy and willingness to invest in further research and education.

The goal of developing the proposed microfluidic model is to increase an understanding of PD and the shortfalls of the treatment method in achieving adequate filtration rates across long-term treatment. Assuming an increased understanding leads to better PD treatment methods far down the road, countries that currently have alternate dialysis policies may instead adopt the "peritoneal-dialysis first" mandate and seek to put measures in place to close the medical education gap. Countries such as Mexico and Guatemala who currently utilize this treatment more frequently may become global leaders in the PD standard of care to aid other countries' development of such criteria, which is important to consider politically. The proposed model also provides an opportunity for conducting research in an acellular manner to gain an understanding of the disease state, which may be a more viable option in cases where countries are either unwilling to invest or do not have resources to conduct cellular research. Ultimately, however, it is up to each nation to decide how government policy and funding can be used to best support patients with chronic kidney disease and they may or may not choose to use the information available to help patients.

7.2.5 Health and Safety Issues

As this is an *in vitro* device to study peritoneal dialysis, any health and safety concerns of the user are minimal. The reagents and materials used for developing this device do not pose any risk, as they are considered non hazardous. Despite the low health risks associated with this device, all reagents and materials should be properly handled, stored, and disposed to ensure safety.

As this device's purpose is to study peritoneal dialysis with the goal of improving the health conditions of the patients that undergo this treatment, users must be properly trained to use the device in order to obtain reliable data. Adequate researcher education can minimize user error and ensure the safe and effective use of the experimental setting and results. Users should be familiar with the proper sterilization techniques, fluid management, and troubleshooting to

ensure their own safety, as well as decipher proper results that may affect patients in the long term.

7.2.6 Manufacturability

Microfluidic devices are designed to control cell microenvironments and maintain tissue-specific functions to mimic human physiology. Therefore, reproducibility is key for implementation and acceptance of the device. The basic steps involved in the manufacturing of the presented device include the use of a master mold, soft lithography, and plasma bonding; and with the proper equipment and protocols, this device can be reproduced with relative ease. The resin 3D printed master mold error is negligible due to the high tolerances of the printer, and with the proper surface treatment and procedure for soft lithography, the PDMS elastomer chip obtained from the mold is also easily reproducible. The biggest source of error associated with the manufacturability of the microfluidic chip is user error, from peeling off the elastomer from the mold and subsequently bonding it to the glass slide.

7.2.8 Sustainability

Whenever a new product is manufactured, it is important to consider the sustainability impact in manufacturing the product. Specifically, the source materials for manufacturing the product are of interest. In this model, resin is used as the 3D-printing filament to produce the molds for soft lithography. Epoxy resins used for additive manufacturing are produced through oxidation of olefins, which are a petroleum-derived product [37]. Petroleum is a finite resource that is markedly unsustainable due to its extraction process. During the soft-lithography process, polydimethylsiloxane (PDMS) is used to produce the microfluidic chips themselves. PDMS is made from a polymerization reaction in which a silicone oil is the result [38]. Silicone is a derivative of silica, which is made from sand. Sand is relatively more sustainable than petroleum, yet still a finite resource. Glass is another silica derivative, so it is again relatively more sustainable.

Other components of the model besides the microfluidic chips themselves can also be assessed for sustainability. The fluids and hydrogel are mainly composed of water and biologically-derived material (bovine collagen) where sustainability is not necessarily a concern. However, the syringe pump setup does involve plastic tubing and is powered by electricity. The electricity is not produced using renewable energy to the knowledge of the research team, which presents concerns in the context of sustainability of this resource.

In order to increase sustainability, alternative material choices could be explored, particularly for the resin molds that are used to produce the microfluidic chips. A limitation that existed for this project in additive manufacturing was access to 3D-printing equipment with a high enough resolution to accurately print the channels and hydrogel chamber division features. The resin 3D printer had this resolution and was thus the best choice for manufacturing the

molds to achieve the desired functionality. Future research teams could assess the feasibility of switching to a filament material that is not derived from petroleum to increase sustainability in this area. If this was not possible, it would be ideal to reduce the amount of source material needed to produce the amount of units needed to conduct the desired research. If the chips themselves were able to be washed out, resterilized and reused, less chips overall would have to be produced, increasing sustainability of the model system itself. Additionally, if the chips and models were going to be mass produced, it would be the recommendation of this research team for researchers using the chips to consider renewable energy sources when powering their flow setups to reduce the demand of non-renewable electricity.

8.0 Discussion

The results from validation testing revealed that some objectives were achieved with the final iteration of the microfluidic model. However, some of the results were not as expected. It is important to discuss why these results were not as expected in order to identify future design changes that could optimize the model and allow for a more useful research tool.

8.1 Discussion of Stiffness Results

The average stiffness ranges across all samples for the collagen hydrogel varied greatly with sample 1 having the highest stiffness, with an average storage modulus of 10.593 kPa within the linear viscoelastic region. The average stiffness ranges of samples 2 and 3 decrease greatly with samples 2 and 3 having an average storage modulus of 3.310 kPa and 1.231 kPa within the linear viscoelastic region, respectively. This disparity in average storage moduli can be attributed to sample preparation, as visible air bubbles increased between each sample and were likely induced by the gradual viscous loss throughout the sample dilution protocol. When preparing the diluted samples, the exact amount of final solution that would be loaded onto the rheometer was prepared. While positive displacement pipettes were used to minimize viscous loss, ultimately small amounts of viscous solution remained at the walls and tips of the pipette. Therefore, when loading the sample onto the rheometer, the final volume of the solution would be less than the intended volume, resulting in air bubbles in the samples due to viscous loss.

The average stiffness across all of the collagen hydrogel samples after dilution was found to be 5.044 ± 4.916 kPa. From these results, while the average stiffness of the samples did not reach the intended 8 kPa value, the aforementioned results suggest that the material is a promising choice for modeling the mechanical stiffness of the fibrotic peritoneum, as sample 1 had an average stiffness of 10.593 kPa. While the goal of 8 kPa stiffness was not met, the reached stiffness value of 5.044 kPa is still representative of the fibrotic peritoneum during PD treatment, as a study conducted in 2023 by Diao *et al.* revealed the stiffness of patients' peritoneum, determined via shear wave elastography, 3 months to 5 years into PD was 6.4 kPa

[52]. The study also determined the physiological stiffness of the peritoneum was 2 kPa. Therefore, while the collagen hydrogel did not reach the intended 8 kPa stiffness, the hydrogel is still a suitable model for peritoneal fibrosis as it is approximately 2.5 times stiffer than a healthy peritoneum.

8.2 Discussion of Permeability Results

The diffusion coefficient of the fluorescein salt was found to be $6.2848 \times 10^{-10} \pm 2.33 \times 10^{-18}$ m^2/s as seen in section 6.2.1.2. The diffusion coefficient is defined as the amount of a particular substance that diffuses across a unit area per one second. Based on this value, the relative permeability of the hydrogel to low molecular weight solids can be estimated. In a study published by Lee *et al.* the diffusion coefficient of fluorescein was measured across the peritoneum and the change in this value was compared between the different organs covered by the peritoneum [56]. The diffusion coefficient of fluorescein through these membranes can be found by multiplying the values by their free diffusion in water. The diffusion coefficient for the different organs was found to be 8.37×10^{-7} for the liver, 1.23×10^{-6} for the kidney, and 9.16×10^{-7} for the cecum. The diffusion coefficient of our system is 1000-10,000 times smaller than the *in vivo* literature values.

This was expected given the differences in the dimensions and composition of the membranes. The peritoneal membranes used in the study are more than 10x thinner than the hydrogel used in the transwell plate, additionally the surface area of the *in vivo* peritoneum is much larger than the surface area of the transwell. Finally, the experimental hydrogel is modeled to mimic a stiffer peritoneal ECM. All of these factors correlate to the diffusion of fluorescein salt being lower in the transwell model than *in vivo*. The experimental diffusion coefficient being lower than the in-vivo value could potentially be indicative of a fibrotic matrix causing changes in its transport properties. The change in dimensions between these two values must be taken into account. Lee *et al.* also found the diffusion coefficient of fluorescein through a collagen gel with the same thickness as the experiment but using a 12-well system as opposed to a 24-well [56]. The difference in surface area and volume is still present however much less compared to the in-vivo study. The diffusion coefficient of this experiment is much closer to the experimental values $(1.22 \pm 0.06 \times 10^{-10})$ [57]. Based on this value it cannot be claimed that the stiffer hydrogel was able to elicit different transport properties without repeating the study with a control hydrogel. Including a group with hydrogel stiffness's comparable to the healthy peritoneum and transwell dimensions would produce a better understanding of how the thickness of the hydrogel affects the diffusion coefficient. Additionally, having a healthy peritoneum model would allow for the better estimation of values like comparable dwell times between a human and microfluidic chip.

8.3 Discussion of Standard Peritoneal Permeability Assay and MTAC Results

As stated in section 6.2.3, there was a difference between the MTAC calculated experimentally after a 6 hour dwell time, 2.61 x 10^{-14} m^3/s, and the MTAC calculated using the COMSOL simulation, 7.87 x 10^{-13} m^3/s. Both of these values differ from the target scaled MTAC of 1.49 x 10^{-11} m^3/s that the microfluidic model should be designed towards in order to allow for an appropriate rate of transport to be comparable to the function of the peritoneum in a human patient. First, the MTAC calculated using the COMSOL simulation is lower than the target scaled MTAC by two orders of magnitude. Where the simulation was created based on an input of all design parameters and represents a system operating at 100% efficiency under ideal conditions, the MTAC value obtained from the simulation can be assumed to be a good prediction of what should be seen in the microfluidic chip if it is functioning as intended. It is not ideal that this predicted value differs by two orders of magnitude, and it is likely that design changes are necessary in order to optimize the transport function of the model. For example, the MTAC is dependent on the volume of dialysate and is directly proportional to MTAC according to the MTAC equation (Eq. 4). A higher volume of dialysate in the chip would likely allow the model to achieve a higher MTAC, and the dialysate chamber dimensions could be increased to accommodate a higher volume of dialysate. Additionally, reducing the hydrogel chamber width would reduce the diffusion distance and reduce the dwell time needed in the chip. Reducing the dwell time to achieve the target MTAC would increase the ability of the model to be a high throughput testing device for its intended uses and would be beneficial in consideration of several design objectives.

The MTAC calculated with the experimentally obtained urea concentration results is smaller than the target scaled value by three orders of magnitudes, and two times smaller than the expected value from the simulation. Although this suggests that the experimental microfluidic model achieves less rates of urea transport than the simulation and the peritoneum in a human, there may be issues with this conclusion drawn from the calculated value based on a few factors. First, the urea concentration calculated using the BUN assay is likely not accurate. The range of linearity for the BUN assay used is from 2-140 mg/dL for calculations of BUN. Using the change in absorbance value obtained from the dialysate sample and dividing by the change in absorbance of the standard, the BUN calculated for the sample was 717.75 mg/dL. This is well outside the range of linearity and the secondary calculation for urea concentration based on this value is likely not valid because of this. So, the urea concentration calculated from the sample (256.31 mol/m^3) is likely not a good representation of the urea concentration that was actually in the sample and is much lower than expected at this time point based on the predicted value from the simulation (7262.5 mol/m^3).

The BUN value was likely out of range of linearity for the assay because the urea concentration in the sample itself was too high to be measured accurately. Where the BUN assay

is traditionally used to test blood samples from human patients, this range of linearity is assumed to be the typical range for BUN values that would be seen clinically. The blood analog solution is formulated with a concentration of urea that is higher than values that would be representative of *in vivo* conditions. This was done intentionally. The urea concentration in the blood analog is representative of the concentration of all waste products, not just the concentration of urea. These other waste products could be added to the blood analog, but would add significantly to the cost for this solution. Originally, it was thought that the lowest cost option would be the best and help achieve the 'cost-effectiveness' objective. However, based on the outcome of the experiment and the fact that this objective is weighted lower than 'representative of *in vivo* conditions,' a smarter design choice for future iterations of the design may be to reevaluate the blood analog composition and reformulate with a lower urea concentration. A secondary option would be to explore alternative assays with a larger range of linearity to accommodate the high urea concentration, although these may be more expensive than the assay chosen for this experiment and again reduce the ability for the model to achieve the 'cost-effectiveness' objective.

Where the urea concentration started off much higher than the physiological concentration, it is reasonable to assume the amount that diffused across the hydrogel into the dialysate may also be higher than the highest physiological concentration that would be measured by the assay. Additionally, some observations during the sampling process at the six hour mark led the team to believe that the sample taken from the dialysate chamber is not necessarily representative of transport across the hydrogel only by diffusion. If some of the blood analog mixed into the dialysate by bulk motion across the chip, the concentration would be even closer to the exceptionally high concentration measured in the dialysate. Another observation driven from the sampling process at six hours of dwell time was that the hydrogel changed its color from white translucid to fully transparent, being hard to distinguish from the other fluids in the microfluidic chip. This could suggest that the mechanical and structural properties of the collagen hydrogel may have been affected by the constant fluids in its surrounding. This could have led to loss of integrity allowing for more urea transport than anticipated, thus the effect of these fluids in the hydrogel needs to be better studied. Finally, another observation from the test set up was leakage at the inlet of the blood analog channel. This was assumed to be caused by the pressure of the hose adapter against the chip, thus being easier for the fluid to exit the channel around it.

Overall, more runs of this test need to be performed to draw a conclusion on the transport properties of the proposed microfluidic device. In addition, some experimental changes are needed to improve the accuracy of the data being obtained from the test and prevent the observable failures listed above.

8.4 Discussion of Sterility Test Results

As presented in section 6.3.2, there is generally a higher absorbance seen with the non-sterile control group relative to both sterilized groups for all sampling time points past Day 0 for both runs of the experiment. With OD_{600} measurements, a higher absorbance correlates to a higher pathogenic growth. This is due to the concept of the more growth that there is within the broth, the cloudier the broth and the higher the absorbance at 600 nm [39]. So, the higher absorbance with the non-sterilized group suggests more pathogenic growth relative to the sterilized groups and also suggests that sterilization worked to some degree to eliminate some pathogenic growth.

Interestingly, the agar plating results are somewhat consistent with this suggestion. The non-sterile control group plates show a mix of colony types that appear exclusively on the UV-sterilized plates and the isopropyl-alcohol sterilized plates. UV-sterilization appears to have eliminated the gray, opaque colonies of various sizes and only yellow colonies remain. On the other hand, isopropyl-alcohol sterilization appears to have eliminated the yellow, opaque colonies and only the gray, opaque colonies remain. So, the sterilization methods tested seem to be effective at reducing, but not completely eliminating, some pathogenic growth. Each sterilization method appears to be effective at reducing a specific, but different, type of bacterial growth. Further quantification of the agar plating step is necessary to derive accurate conclusions about specific bacterial cell densities seen with the broth in each experimental group. This would help connect absorbance values to a specific amount of bacterial growth and put results into context more. Although the colonies could not be hand counted, automated colony counting technology may be a solution that could help obtain the numbers needed in future runs of the experiment.

While the higher absorbance values are seen relatively consistently across time points and across runs for the non-sterile control group, there is not a statistically significant difference between absorbance values for the non-sterile groups and either of the sterilized groups, based on a p value of 0.05 and the two-way ANOVA testing method described previously. This could be due to high standard deviations within the absorbance measurements for each group at each time point across the three chips studied. In some cases, a biofilm would form on top of the broth of some of the plates (Appendix L). It would become impossible to take broth samples using the method described without picking up some of the biofilm material, which was very opaque. The wells containing the biofilm samples had extremely high absorbances and contributed to a high standard deviation for that experimental group at that time point. In future experiments, removing the biofilm and testing the broth itself may give a more accurate representation of the broth absorbance and reduce standard deviation within an experimental group.

The fact that there is no statistically significant difference between the non-sterile groups and sterilized groups suggests pathogenic growth to some degree in all plates containing chips, regardless of sterilization. The source of this pathogenic growth is confirmed to be from the

chips themselves and not from accidental contamination after Day 0 in either the sampling or incubation process, as the sterile broth plates did not see any pathogenic growth based on low absorbance values throughout the experiment that are consistent with Day 0 values and the results of the agar plating showing no colonies for run #1. The colonies that appear in the sterile broth sample agar plate for run #2 are thought to be from a mixup of samples during the dilution process and the fact that the non-sterile control group broth may have gotten added to the centrifuge tube labeled for the sterile broth plate sample dilution. However, more runs of the experiment are needed to confirm that this is indeed the case and rule out that there are bacteria growing in the sterile broth without producing any degree of cloudiness in the broth.

Although the fact that there was pathogenic growth in all plates with chips seems to discount the sterilization methods tested, it is important to remember that the prime environment for bacterial growth was created using the Luria broth and incubation at 37℃. If mammalian cells were seeded in the chip, cell culture media would be used to provide nutrients to the cells for growth and proliferation. Often, there are antibiotics like streptomycin and penicillin typically included in cell culture media that are intended to combat bacterial growth. If sterilization eliminates most bacterial cells and proper aseptic technique is used to culture cells within the chip, antibiotics in the media may sufficiently reduce pathogenic growth for the duration of the mammalian cell culture experiment. While this is a theory, further experiments with cell culture media would be needed to confirm if this is indeed the case.

The statistically relevant results for this test include the fact that there is no significance between absorbance measured for the UV-sterilized group and the sterile broth plate across multiple days, suggesting low enough pathogenic growth in the UV-sterilized group's broth to be comparable to no pathogenic growth in the sterile broth. This was not the case with the isopropyl-alcohol sterilized group, suggesting growth overall was lower with the UV-sterilized group compared to the isopropyl alcohol-sterilized group. The UV-sterilization method is also significantly easier for researchers to perform, as they only need to place the chips in a chamber and not work to pipette alcohol into the chips in a biosafety cabinet. This coupled with the absorbance results suggests UV-sterilization is the sterilization method that should be used going forward with cell culture experiments in the chip.

9.0 Conclusion and Recommendations

The microfluidic model was able to achieve all of the desired design objectives at least in part. However, there are several areas of future work where the device could be improved and optimized to create a tool for researchers looking to develop solutions for peritoneal dialysis in response to the physiological changes that happen during the treatment duration. These ideas for future work are outlined in the following sections.

9.1 Future Work - Permeability Assay

To better optimize the permeability assay, new trials should be run using both the fibrotic hydrogel model and a healthy hydrogel model with properties closer to the 2 kPa. These trials would benefit from using the same thickness dimension as previously used. Obtaining these values would allow for the estimation of how dimensionality affects the transport properties of the hydrogel. As well as confirm that there will be observable diffusion changes with the increase in matrix stiffness. After this study permeability trials using the chip should be done so that better dwell times can be estimated. The current dwell time used is optimized based on the hydrogel thickness of a transwell system which works for the current chip due to their similar thickness dimensions, however there is still a difference in surface area and volume. Being able to find the diffusion through the actual chip would optimize dwell time.

9.2 Future Work - Optimize Pump Set Up

Although the syringe pump setup did successfully allow for the desired flow rate of blood analog in the vascular channel, there was leakage from some of the inlets and outlets observed. This suggests that there was some pressure in the chip that was pushing the fluid out of the inlets and outlets. A likely source of this was the syringe pump system. The Luer adaptor used to connect the tubing from the syringe holding the blood analog solution to the chip may have constricted the flow too much and introduced turbulence in the flow. The adaptor also may have created pressure at the inlet, where the adaptor was vertical and constantly pushing the fluid down, where it then had to flow horizontally across the channel. ISO 22916:2022 may give some insight in how to reduce turbulence at the connections between the pump and the chip, as there are guidelines pertaining to these connections in the standard. It is the recommendation of this team to refer to this standard and potentially redesign this connection to reduce pressurization of the chip and leakage from inlets.

9.3 Future Work - Device Cellularization

Cellularization of the chip would be the next step in evaluating the validity of the model; this would also allow for processes that needed to be modeled mechanically to be done biochemically such as the creation of a stiffer matrix. The addition of fibroblast with growth factors such as those in the TGFβ category would potentially induce a stiffer and more physiologically accurate hydrogel as they are seen in inflamed ECM. The addition of lymphatic endothelial cells would allow for the study of both lymphangiogenesis and for mimicking events of increased fluid uptake due to lymphatic vessels.

9.4 Future Work- Reducing Dwell Time and Further SPA Experimentation

The dwell time for the current chip is 1.5 times longer than the dwell time found in a human even with the scaled down MTAC. This dwell time is due to the size of the hydrogel chamber and difference in hydrostatic pressure between the dialysate and ECM which would be much larger in a human. Replicating the thickness of the peritoneum would be the first step in reducing this dwell time. Additionally in order to also have a more accurate MTAC, the volume of the dialysate chamber needs to be enlarged, thus increasing the expected MTAC measurement.

Running the SPA with urea gives a good idea of the movement of small molecular weight solids however the MTAC of these solids is not affected to a statistically significant degree by peritoneal stiffness due to their small size. Adding larger proteins such albumin is suggested to be able to observe changes in the MTAC as proteins are larger. Additional values such as the restriction coefficient which is the membrane's general permeability to either high or low weight molecular solids would also help evaluate the chip's ability to represent in-vivo conditions. These values are all based on diffusion instead of fluid loss allowing for testing that does not hinge on lymphangiogenesis. If lymphangiogenesis is achieved, further studies using values such as the transcapillary ultrafiltration rate will further validate the model as ultrafiltration failure is also caused by the increased uptake of dialysis fluids.

9.5 Future Work - Reusability

In terms of reusability of the model there are further evaluations that need to be performed after cellularization of the chip. Currently, the proposed model is produced with reusable master molds that can produce batches of four chips, this could be easily expanded to more chips with the goal of faster manufacturing. However, when it comes to the reusability of the microfluidic device itself, testing should be performed after usage. The main aspects that should be investigated include, washing off the chambers and removing every component, cleaning it up, and re-sterilize them. After sterilization of the used chip, verification testing should be re-run to test the performance of the chip in comparison to an unused chip.

References

[1]   Centers for Disease Control and Prevention, "Chronic Kidney Disease in the United States,2021," 2021, https://www.cdc.gov/kidneydisease/publications-resources/ckd-national-facts.html.

[2]   R. T. Kredeit, "Ultrafiltration failure is a reflection of peritoneal alterations in patients treated with peritoneal dialysis," Front Physiol., vol. 9, pp. 1815, 2018. DOI: 10.3389/fphys.2018.01815.

[3]   M. Sacchi, R. Bansal, and J. Rouwkema. "Bioengineered 3D models to recapitulate tissue fibrosis," *Trends in Biotechnology*, vol. 38, no. 6, pp. 623- 636, 2020. https://doi.org/10.1016/j.tibtech.2019.12.010.

[4]   Harvard Stem Cell Institute, "Kidney fibrosis study reveals causes, potential therapeutic target," 2019. https://hsci.harvard.edu/news/kidney-fibrosis-study-reveals-causes-potential-therapeutic-target#:~:text=A%20final%2C%20common%20pathway%20in,fail%20to%20repair%20themselves%20completely.

[5]   D. J. Jafree and D. A. Long, "Beyond a passive conduit: implications of lymphatic biology for kidney diseases," Journal of the American Society of Nephrology, vol. 31, no. 6, pp. 1178 - 1190, 2020, DOI: https://doi.org/10.1681/ASN.2019121320.

[6]   K. D. Nolph, R. Mactier, R. Khanna, Z. J. Twardowski, H. Moore, and T. McGary, "The kinetics of ultrafiltration during peritoneal dialysis: The role of lymphatics," Kidney Int, vol. 32, no. 2, pp. 219–226, 1987, doi: 10.1038/KI.1987.195.

[7]   M. Bartosova, S. G. Zarogiannis, C. P. Schmitt, and P. P. Biobank, "How peritoneal dialysis transforms the peritoneum and vasculature in children with chronic kidney disease-what can we learn for future treatment?", *Molecular and Cellular Pediatrics*, vol. 9, no. 9, 2022, doi: 10.1186/s40348-022-00141-3.

[8]   S. Larocco, "CLINICAL FEATURE: Treatment Options for Patients with Kidney Failure," *The American Journal of Nursing*, vol. 111, no. 10, pp. 57–62, 2011.

[9]   Z. Zhang, N. Jiang, and Z. Ni, "Strategies for preventing peritoneal fibrosis in peritoneal dialysis patients: new insights based on peritoneal inflammation and angiogenesis", *Front. Med.* vol. 11, no. 3, pp. 349-358, 2017, doi: 10.1007/s11684-017-0571-2.

[10]   I. Teitelbaum, "Ultrafiltration Failure in Peritoneal Dialysis: A Pathophysiologic Approach," *Blood Purif*, vol. 39, pp. 70–73, 2015, doi: 10.1159/000368972.

[11]   H. Kinashi *et al.*, "Connective tissue growth factor is correlated with peritoneal lymphangiogenesis", *Nature Scientific Reports,* vol. 9, pp. 12175, 2019, doi: 10.1038/s41598-019-48699-9.

[12]   M. Terri *et al.*, "Mechanisms of Peritoneal Fibrosis: Focus on Immune Cells–Peritoneal Stroma Interactions," *Front Immunol*, vol. 12, Mar. 2021, doi: 10.3389/fimmu.2021.607204.

[13]   P. Pattanayak *et al.*, "Microfluidic chips: recent advances, critical strategies in design, applications and future perspectives," *Microfluidics and Nanofluidics*, vol. 25, no. 12. Springer Science and Business Media Deutschland GmbH, Dec. 01, 2021. doi: 10.1007/s10404-021-02502-2.

[14]   S. Xiang *et al.*, "Rapamycin inhibits epithelial-to-mesenchymal transition of peritoneal mesothelium cells through regulation of Rho GTPases," *FEBS J*, vol. 283, no. 12, pp. 2309–2325, Jun. 2016, doi: 10.1111/febs.13740.

[15]   G. T. González-Mateo *et al.*, "Paricalcitol Reduces Peritoneal Fibrosis in Mice through the Activation of Regulatory T Cells and Reduction in IL-17 Production," *PLoS One*, vol. 9, no. 10, p. e108477, Oct. 2014, doi: 10.1371/journal.pone.0108477.

[16]   B. Yang, M. Wang, X. Tong, G. Ankawi, L. Sun, and H. Yang, "Experimental models in peritoneal dialysis (Review)," *Exp Ther Med*, vol. 21, no. 3, p. 240, Jan. 2021, doi: 10.3892/etm.2021.9671.

[17]   Y. Cho, K. Na, Y. Jun, J. Won, J. H. Yang, and S. Chung, "Three-Dimensional In Vitro Lymphangiogenesis Model in Tumor Microenvironment," *Front Bioeng Biotechnol*, vol. 9, Oct. 2021, doi: 10.3389/fbioe.2021.697657.

[18]   L. I. Ibrahim, C. Hajal, G. S. Offeddu, M. R. Gillrie, and R. D. Kamm, "Omentum-on-a-chip: A multicellular, vascularized microfluidic model of the human peritoneum for the study of ovarian cancer metastases," *Biomaterials*, Sep. 2022, doi: 10.1016/J.BIOMATERIALS.2022.121728.

[19]   O. Mastikhina *et al.*, "Human cardiac fibrosis-on-a-chip model recapitulates disease hallmarks and can serve as a platform for drug testing," *Biomaterials*, vol. 233, p. 119741, Mar. 2020, doi: 10.1016/j.biomaterials.2019.119741.

[20]   International Organization for Standardization "INTERNATIONAL STANDARD ISO 10993-5," Switzerland, Nov. 2009.

[21]   PreciGenome, LLC. "Cross flow membrane chip cell." (2021). https://www.precigenome.com/product-page/crow-flow-membrane-chip-cell.

[22] Wang X, Phan DT, Sobrino A, George SC, Hughes CC, Lee AP. Engineering anastomosis between living capillary networks and endothelial cell-lined microfluidic channels. Lab Chip. 2016 Jan 21;16(2):282-90. doi: 10.1039/c5lc01050k. PMID: 26616908; PMCID: PMC4869859.

[23] Dogru, Aydemir, D., Salman, N., Ulusu, N. N., & Alaca, B. E. (2020). Impact of PDMS surface treatment in cell-mechanics applications. Journal of the Mechanical Behavior of Biomedical Materials, 103, 103538–103538. https://doi.org/10.1016/j.jmbbm.2019.103538.

[24] Cullis B., Abdelraheem M., Abrahams G., et al. (2014). Peritoneal Dialysis for Acute Kidney Injury. *Peritoneal Dialysis International 34*(5),494-517. https://doi.org/10.3747/pdi.2013.00222.

[25] Fischer, Schenk, U., Kiefer, T., Hübel, E., Thomas, S., Yatzidis, H., Mettang, T., & Kuhlmann, U. (1995). In vitro effects of bicarbonate- versus lactate-buffered continuous ambulatory peritoneal dialysis fluids on peritoneal macrophage function. *American Journal of Kidney Diseases 26*(6), 924–933. https://doi.org/10.1016/0272-6386(95)90057-8.

[26] Chak, Wong, K.-M., Wong, A., Choi, K.-S., Chan, Y.-H., Cheung, C.-Y., Chau, K.-F., & LI, C.-S. (2000). Effects of peritoneal dialysate acidity on the net ultrafiltration and solute removal in patients on intermittent peritoneal dialysis. *Hong Kong Journal of Nephrology 2*(1), 50–53. https://doi.org/10.1016/S1561-5413(09)60034-X.

[27] Brindise MC, Busse MM, Vlachos PP. Density and Viscosity Matched Newtonian and non-Newtonian Blood-Analog Solutions with PDMS Refractive Index. Exp Fluids. 2018 Nov;59(11):173. doi: 10.1007/s00348-018-2629-6. Epub 2018 Oct 30. PMID: 31745378; PMCID: PMC6863344.

[28] Dogru, Aydemir, D., Salman, N., Ulusu, N. N., & Alaca, B. E. (2020). Impact of PDMS surface treatment in cell-mechanics applications. Journal of the Mechanical Behavior of Biomedical Materials, 103, 103538–103538. https://doi.org/10.1016/j.jmbbm.2019.103538.

[29] D. Aydemir, S. Dogru, B. E. Alaca, and N. N. Ulusu, "Impact of the surface modifications and cell culture techniques on the biomechanical properties of PDMS in relation to cell growth behavior," Int. J. Polym. Mater. Polym. Biomater., vol. 71, no. 12, pp. 886–897, 2022, doi: 10.1080/00914037.2021.1919670.

[30] Y. T. Ho, G. Adriani, S. Beyer, P.-T. Nhan, R. D. Kamm, and J. C. Y. Kah, "A Facile Method to Probe the Vascular Permeability of Nanoparticles in Nanomedicine

Applications," Sci. Rep., vol. 7, no. 1, p. 707, Dec. 2017, doi: 10.1038/s41598-017-00750-3.

[31]   M. M. Zweers et al., "The Standard Peritoneal Permeability Analysis in the Rabbit: A Longitudinal Model for Peritoneal Dialysis," Perit. Dial. Int. J. Int. Soc. Perit. Dial., vol. 19, no. 1, pp. 56–64, Jan. 1999, doi: 10.1177/089686089901900110

[32]   Y. T. Ho, G. Adriani, S. Beyer, P.-T. Nhan, R. D. Kamm, and J. C. Y. Kah, "A Facile Method to Probe the Vascular Permeability of Nanoparticles in Nanomedicine Applications," Sci. Rep., vol. 7, no. 1, p. 707, Dec. 2017, doi: 10.1038/s41598-017-00750-3.

[33]   M. G. Barbato, R. C. Pereira, H. Mollica, A. Palange, M. Ferreira, and P. Decuzzi, "A permeable on-chip microvasculature for assessing the transport of macromolecules and polymeric nanoconstructs," J. Colloid Interface Sci., vol. 594, pp. 409–423, Jul. 2021, doi: 10.1016/j.jcis.2021.03.053.

[34]   L. F. Alonzo, M. L. Moya, V. S. Shirure, and S. C. George, "Microfluidic device to control interstitial flow-mediated homotypic and heterotypic cellular communication," Lab on a Chip, vol. 15, no. 17, pp. 3521–3529, 2015, Sep. 2016, doi: 10.1039/c5lc00507h

[35]   U.S. Centers for Medicare & Medicaid Services. "ESRD Quality Incentive Program." Dec. 2022, https://www.cms.gov/medicare/quality-initiatives-patient-assessment-instruments/esrdqip.

[36]   T. Lee, J.E. Flythe, & M. Allon. "Dialysis care around the world: a global perspectives series," Kidney360, vol. 2, no. 4, pp. 604–607, Apr. 2021,. https://doi.org/10.34067/KID.000108202.

[37]   M. Peerzada, S. Abbasi, K. T. Lau, & N. Hameed, "Additive manufacturing of epoxy resins: materials, methods, and latest trends," Ind. Enj. Chem. Res., vol. 59, no. 14, pp. 6375 - 6390, Mar. 2020, https://doi.org/10.1021/acs.iecr.9b06870.

[38]   M. Meissner, A. M. Seddon, and C. P. Royall, "Colloidal Microfluidics," *Frontiers of Nanoscience*, vol. 13, pp. 125–166, Jan. 2019, doi: 10.1016/B978-0-08-102302-0.00006-7.

[39]   G. Sezonov, D. Joseleau-Petit, & R. D'Ari. "Escherichia coli Physiology in Luria-Bertani Broth," Journal of Bacteriology, vol. 189, no. 23, Dec. 2007, https://doi.org/10.1128/JB.01368-07.

[40]   J. X. J. Zhang and K. Hoshino, "Optical transducers: Optical molecular sensing and spectroscopy," *Molecular Sensors and Nanodevices*, pp. 231–309, Jan. 2019, doi: 10.1016/B978-0-12-814862-4.00005-3.

[41] D. Gupta, J. W. Santoso, and M. L. Mccain, "Characterization of Gelatin Hydrogels Cross-Linked with Microbial Transglutaminase as Engineered Skeletal Muscle Substrates," *Bioengineering*, vol. 8, no. 1, pp 6, Jan. 2021, doi: 10.3390/bioengineering.

[42] X. Wang, D. T. T. Phan, A. Sobrino, S. C. George, C. C. W. Hughes, and A. P. Lee, "Engineering anastomosis between living capillary networks and endothelial cell-lined microfluidic channels," *Lab Chip*, vol. 16, no. 2, pp. 282–290, Jan. 2016, doi: 10.1039/C5LC01050K.

[43] *Microfluidic devices — Interoperability requirements for dimensions, connections and initial device classification*, ISO 22916:2022, 2022.

[44] *Micro process engineering — Vocabulary,* ISO 10991:2009, 2009.

[45] *Biological evaluation of medical devices — Part 5: Tests for in vitro cytotoxicity,* ISO 10993-5:2009, 2009.

[46] *Biological evaluation of medical devices — Part 4: Selection of tests for interactions with blood,* ISO 10993-4:2017, 2017.

[47] U.S. Pharmacopeia, "USP<71>Sterility tests", p 5984–5991. *2018 United States Pharmacopeia and National Formulary, USP 41-NF 36 U.S. Pharmacopeial Convention, Rockville, MD,* pp. 5984-5991. 2018.

[48] Nakayama, M., Ishida, M., Ogihara, M., Hanaoka, K., Tamura, M., Kanai, H., Tonozuka, Y., & Marshall, M. R. (2015). Social functioning and socioeconomic changes after introduction of regular dialysis treatment and impact of dialysis modality: A multi‑centre survey of Japanese patients. Nephrology, 20(8), 523–530. https://doi.org/10.1111/nep.12482.

[49] Klomjit N, Kattah AG, Cheungpasitporn W. The Cost-effectiveness of Peritoneal Dialysis Is Superior to Hemodialysis: Updated Evidence From a More Precise Model. Kidney Med. 2020 Dec 30;3(1):15-17. doi: 10.1016/j.xkme.2020.12.003. PMID: 33605939; PMCID: PMC7873827.

[50] T. Lee, J.E. Flythe, & M. Allon. "Dialysis care around the world: a global perspectives series," *Kidney360*, vol. 2, no. 4, pp. 604–607, Apr. 2021, https://doi.org/10.34067/KID.000108202.

[51] Environmental behavior and ecological effect of polydimethylsiloxane: a review https://pubmed.ncbi.nlm.nih.gov/23189715/#:~:text=PDMS%20has%20less%20risk%20to,%2C%20soil%20animals%2C%20and%20crops.

[52] Diao, X., Chen, Y., Lin, J., Xu, M., Cao, P., Peng, Y., Wu, H., Guo, Q., Huang, F., Mao, H., Yu, X., Xie, X., and Yang, X. (2023). Mesenteric elasticity assessed by shear wave elastography and its relationship with peritoneal function in peritoneal dialysis patients, Clinical Kidney Journal vol.16, no.1, pp. 69–77, https://doi.org/10.1093/ckj/sfac192.

[53] Zuidema JM, Rivet CJ, Gilbert RJ, Morrison FA. A protocol for rheological characterization of hydrogels for tissue engineering strategies. J Biomed Mater Res B Appl Biomater. 2014 Jul;102(5):1063-73. doi: 10.1002/jbm.b.33088. Epub 2013 Dec 6. PMID: 24357498.

[54] Alonzo LF, Moya ML, Shirure VS, George SC. Microfluidic device to control interstitial flow-mediated homotypic and heterotypic cellular communication. Lab Chip. 2015 Sep 7;15(17):3521-9. doi: 10.1039/c5lc00507h. Epub 2015 Jul 20. PMID: 26190172; PMCID: PMC4855298.

[55] Selgas, R., Bajo, M. A., Cirugeda, A., del Peso, G., Valdés, J., Castro, M. J., Sánchez, S., Fernández-Reyes, M. J., Hevia, C., Gil, F., Aguilera, A., Ortiz, J., Alegre, L., Alvarez, V., & Sánchez-Tomero, J. A. (2005). Ultrafiltration and small solute transport at initiation of PD: questioning the paradigm of peritoneal function. Peritoneal dialysis international, vol. 25, no 1, pp. 68–76. https://doi.org/10.1177/089686080502500113.

[56] Lee, D., Kim, J. C., Shin, E., Ju, K. D., Oh, K.-H., Kim, H. C., Kang, E., & Kim, J. K. (2015). In Vivo Measurement of Site-Specific Peritoneal Solute Transport Using a Fiber-Optic-based Fluorescence Photobleaching Technique. Journal of the Optical Society of Korea, 19(3), 228–236. https://doi.org/10.3807/JOSK.2015.19.3.228

[57] Hsu, H. H., Kracht, J. K., Harder, L. E., Rudnik, K., Lindner, G., Schimek, K., Marx, U., & Pörtner, R. (2018). A Method for Determination and Simulation of Permeability and Diffusion in a 3D Tissue Model in a Membrane Insert System for Multi-well Plates. *Journal of visualized experiments : JoVE*, (132), 56412. https://doi.org/10.3791/56412.

Appendix A - Rubric for Pugh Selection Matrix Rankings

SCORE	-1	0	0.5	1
Representative of In Vivo Conditions	Does not accurately model blood flow with capillary channel, stiffness of fibrotic tissue, interstitial flow between lymphatic capillaries and hydrogel, and dialysate addition/dwell	Models conditions listed, but not for human anatomy (similar to some extent in the rat, but not fully)	Includes all conditions previously mentioned and designed with human anatomy in mind but does not include a channel for lymphatic capillaries (just seeding cells, fluid absorbed cannot go anywhere but is held onto by cells)	Includes all conditions previously mentioned and designed with human anatomy in mind; includes lymphatic channel
Production	Cannot fabricate or produce	Able to produce a model with significant input of resources, highly specialized facilities and trained professionals (rat model - vivarium)	Able to manufacture using synthetic materials and machines/resources available at WPI but with not previously well-defined methods ("sandwich technique" to create multiple layers; this was not discussed extensively in literature)	Able to manufacture using synthetic materials and machines/resources available at WPI but with previously well-defined methods, significant input from literature
Cost Effective	Takes more of a time/money investment compared to the rat model	Takes a significant input of time and money to raise the rats, modify the anatomy/physiology, study time, collect tissue/dissection of rats for study results	Takes less of a time/money investment compared to the rat, but this investment may be outside our time and money budget for the MQP	Takes less of a time/'money investment compared to the rat and the investment is within the time and money budget for the MQP
Accessible for Research Purposes	Results cannot be measured/gathered through imaging or some other commonly used technique	Study results can be gathered at the conclusion of the study through harvesting and studying tissues	Study results can be gathered in real time using imaging methods, but image quality may not be	Study results can be gathered in real time using imaging methods, and image quality is of high resolution

| Reusable	Model has a negative environmental impact through use of toxic materials that cannot be adequately disposed of and is not reusable	Model is not reusable and results can only be gathered once using one unit of the model (ex. one rat)	ideal due to multiple layers of material	
			Model may have the potential to be "reused" in the sense there are multiple setups on one unit to test multiple experimental conditions, reducing environmental impact	Model has the potential to be reused and test multiple experimental conditions using a single unit as well as the capability to be completely sterilized for multiple experiment runs, greatly reduces environmental impact and cuts down on waste generated during experiments

Appendix B - Final Design Selection Criteria
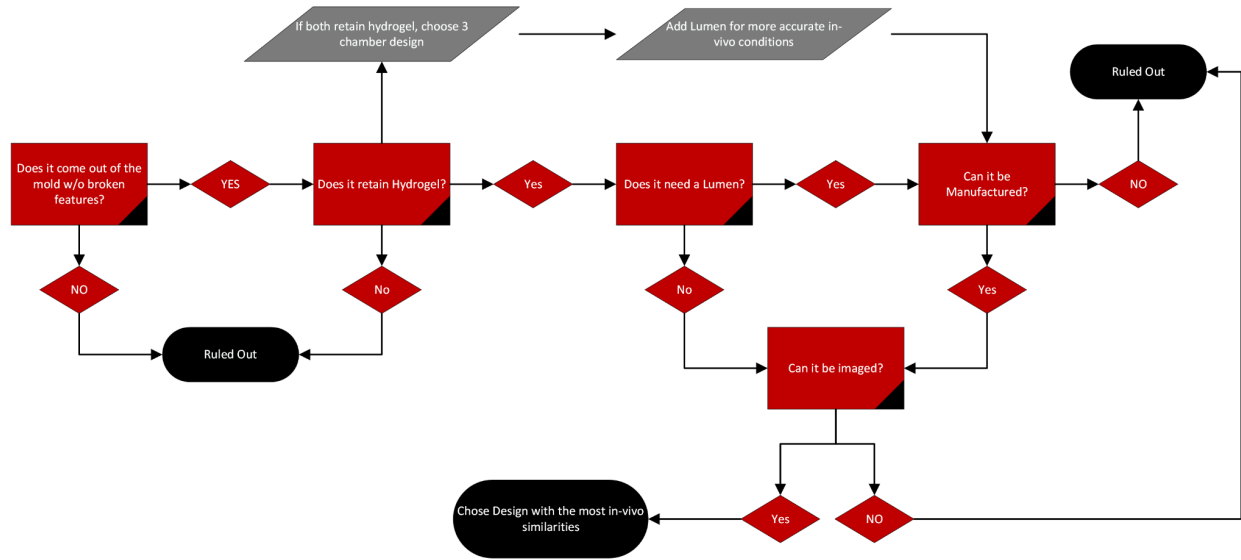
Figure 28: Final design decision flowchart
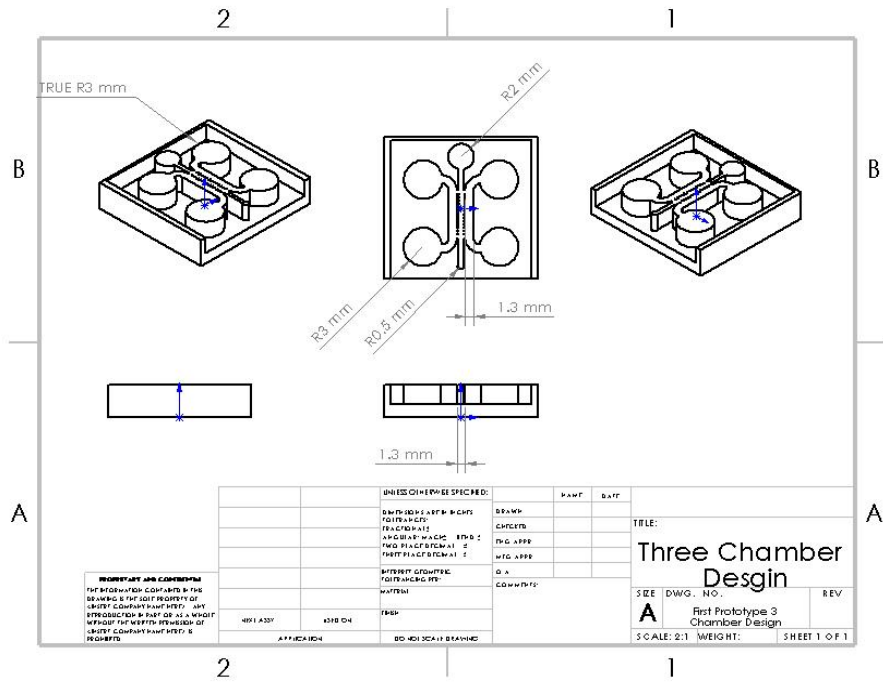
Appendix C - Mold Design CAD Drawings
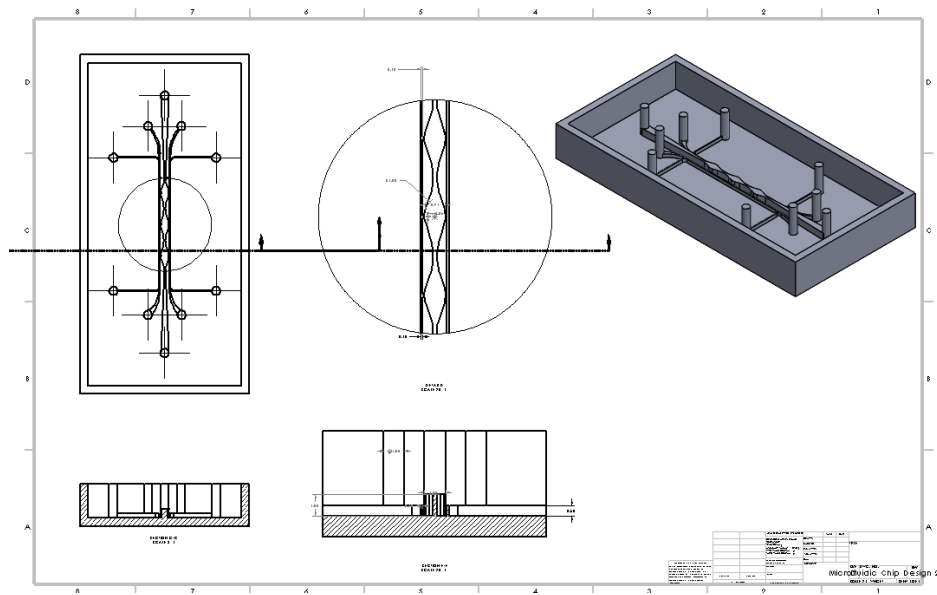

Figure 29: Three chamber chip first iteration
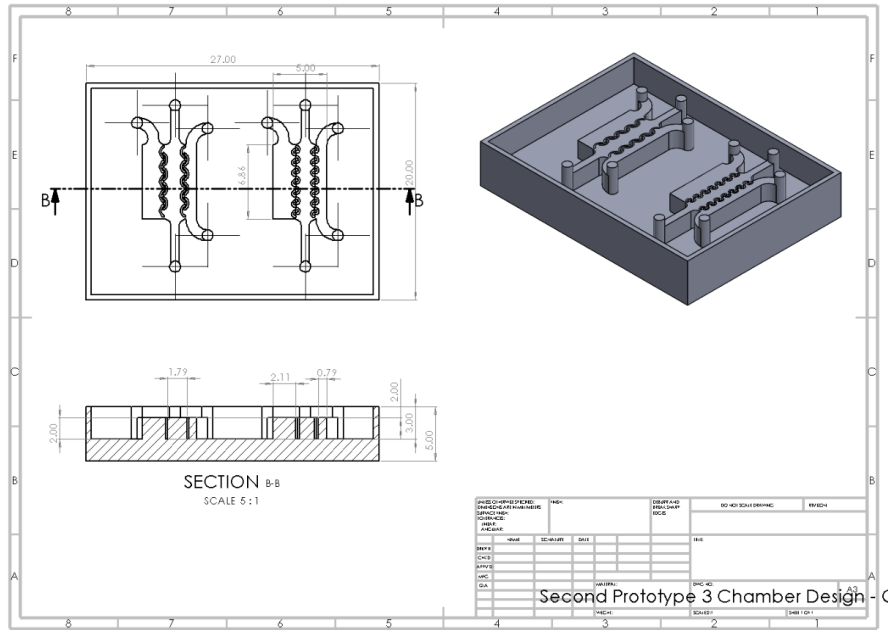

Figure 30: Lumen chip first iteration

Figure 31: Three chamber chip second iteration
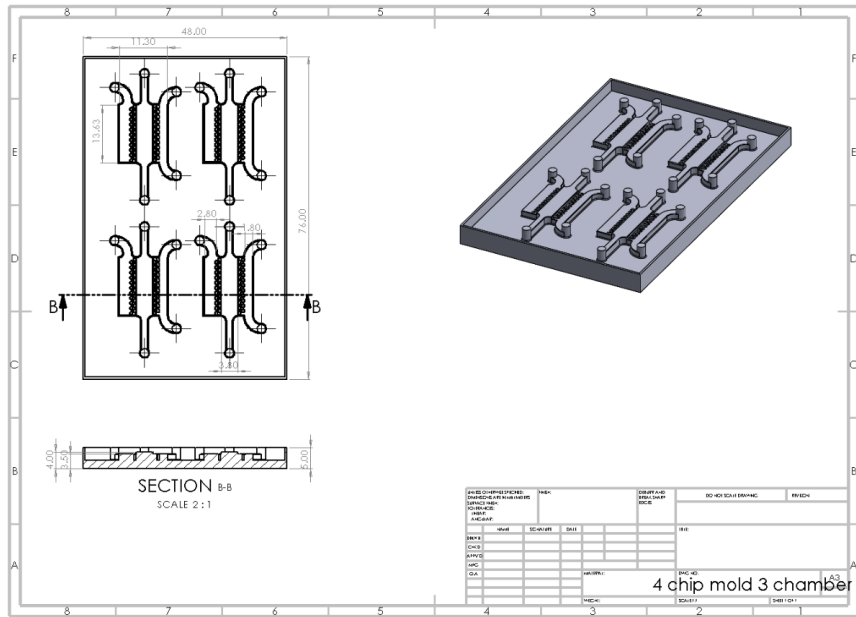
Figure 32: Three chamber chip final iteration

Figure 33: Lumen chip final iteration

Appendix D - Flow Rate Calculations for Syringe Pump Set Up

Based on physiological values of 6 mL/min of blood per 100 g of tissue:

- Hydrogel approximate weight was 150mg
- If 6 mL of blood go through 100g of tissue in one minute then:
    - $Vol = 6mL \: x \: 0.150g \: / \: 100g = 0.009mL$
- of blood will go through 0.15g of tissue in one minute thus:
    - Q = 9uL/min
    - V = Q/A = 1.82mm/min

Appendix E - Frequency Sweep Data for TeloCol-10 Hydrogel

Figure 34: Storage and Loss Modulus vs Frequency (Frequency Sweep) graph for sample 1 of Collagen TeloCol-10 hydrogel
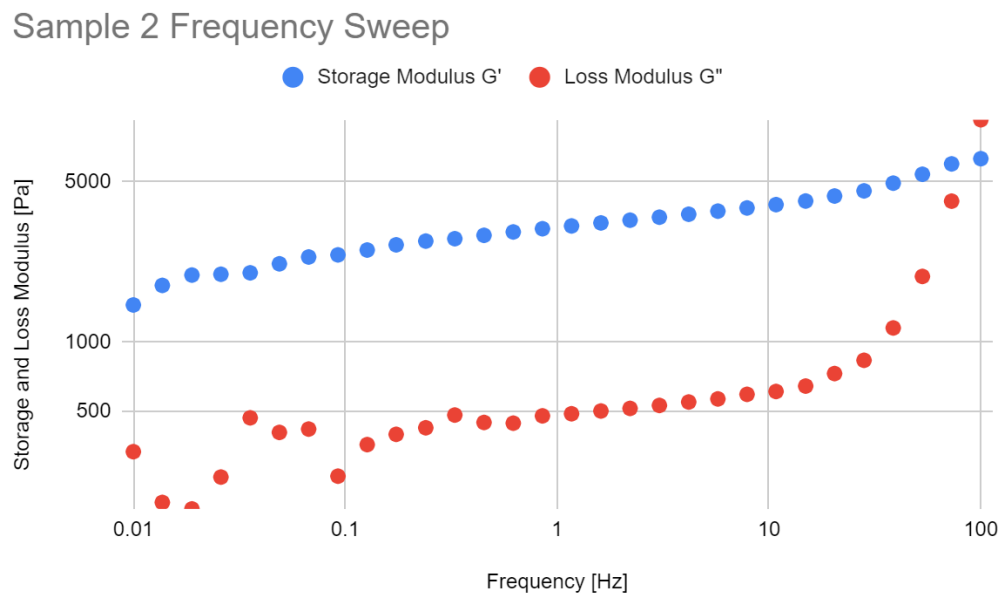
Figure 35: Storage and Loss Modulus vs Frequency (Frequency Sweep) graph for sample 2 of Collagen TeloCol-10 hydrogel
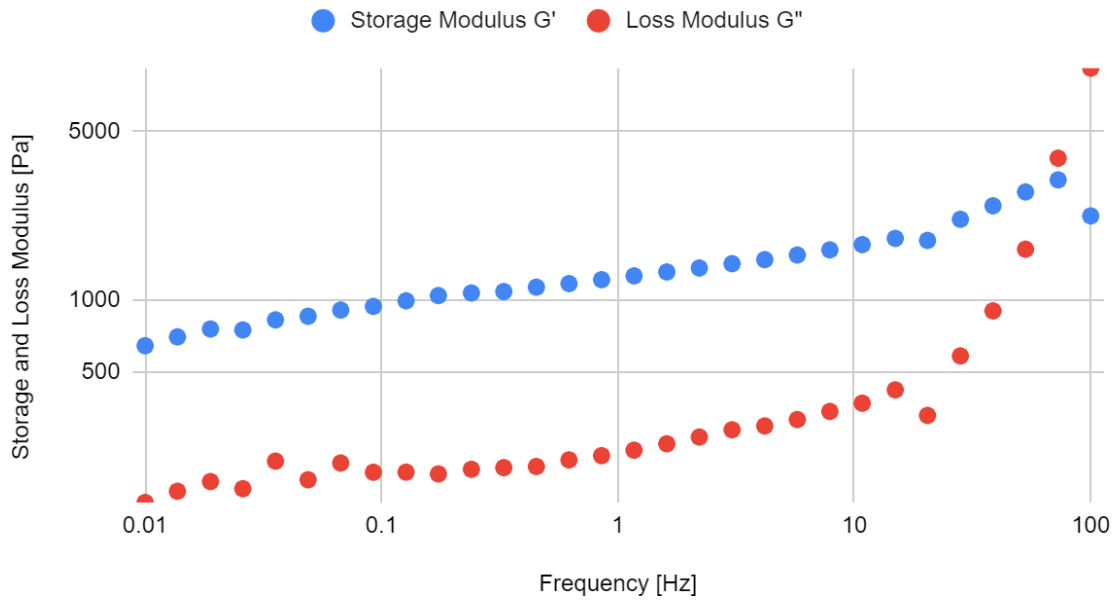
Figure 36: Storage and Loss Modulus vs Frequency (Frequency Sweep) graph for sample 3 of Collagen TeloCol-10 hydrogel

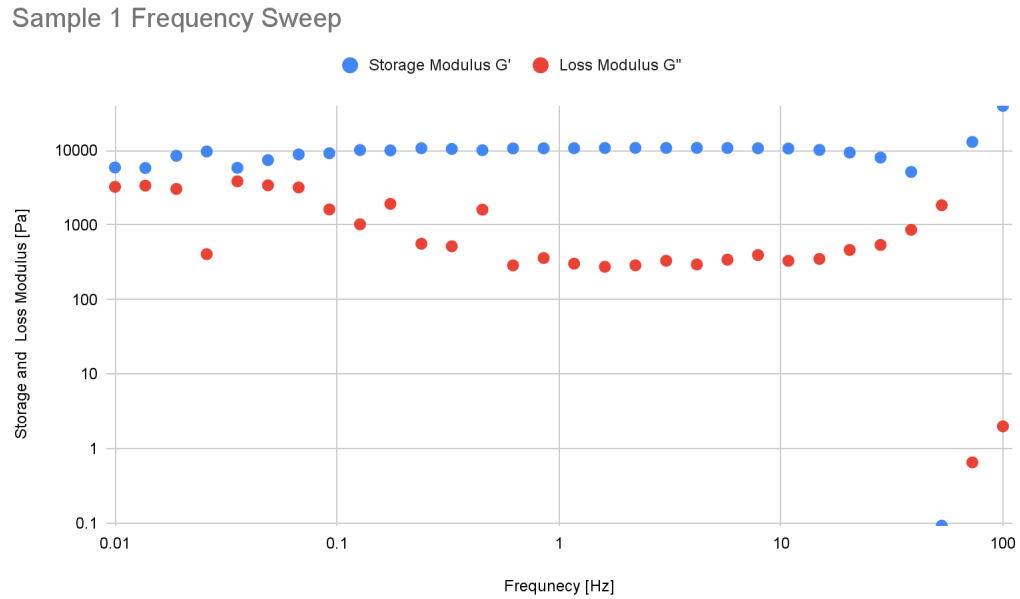# Appendix F - Frequency Sweep Data for Gelatin-TGA Hydrogel

Figure 37: Storage and Loss Modulus vs Frequency (Frequency Sweep) graph for sample 1 of Gelatin-TGA hydrogel

Figure 38: Storage and Loss Modulus vs Frequency (Frequency Sweep) graph for sample 2 of Gelatin-TGA hydrogel

Figure 39: Storage and Loss Modulus vs Frequency (Frequency Sweep) graph for sample 3 of Gelatin-TGA hydrogel

Appendix G - Experimental Protocols
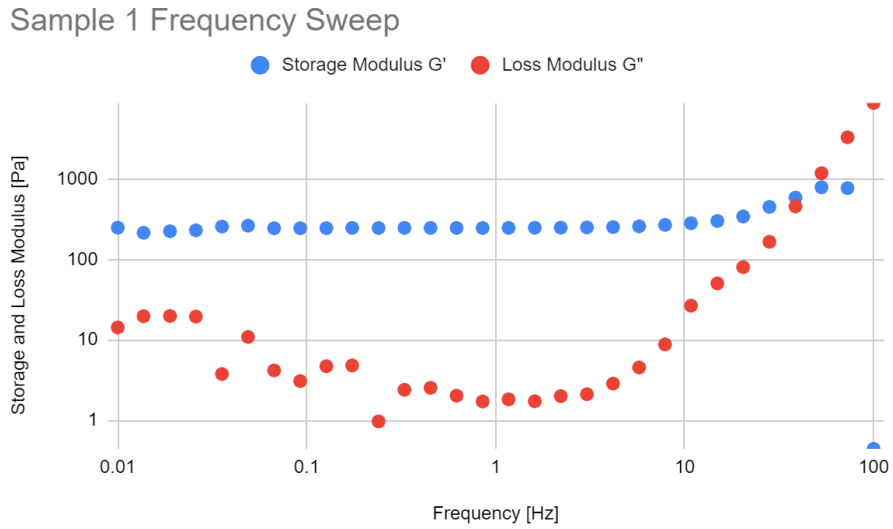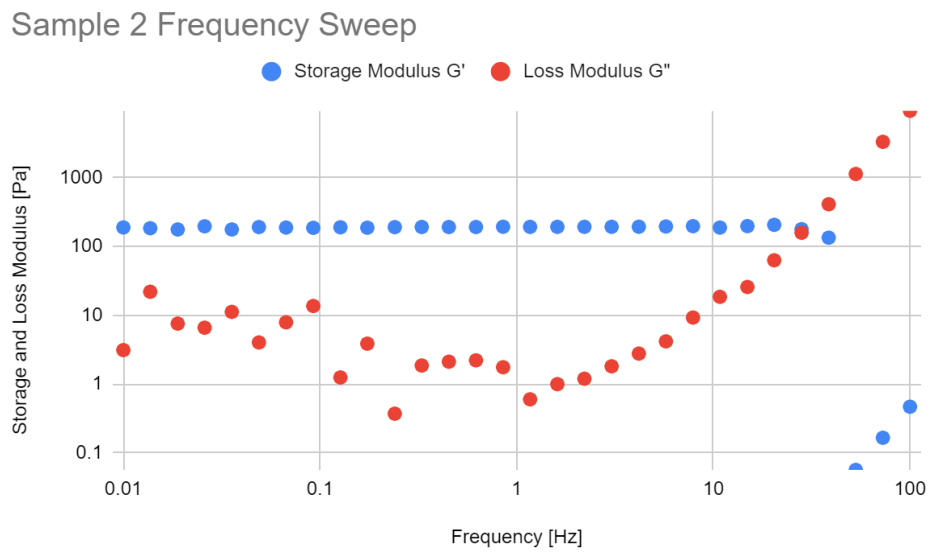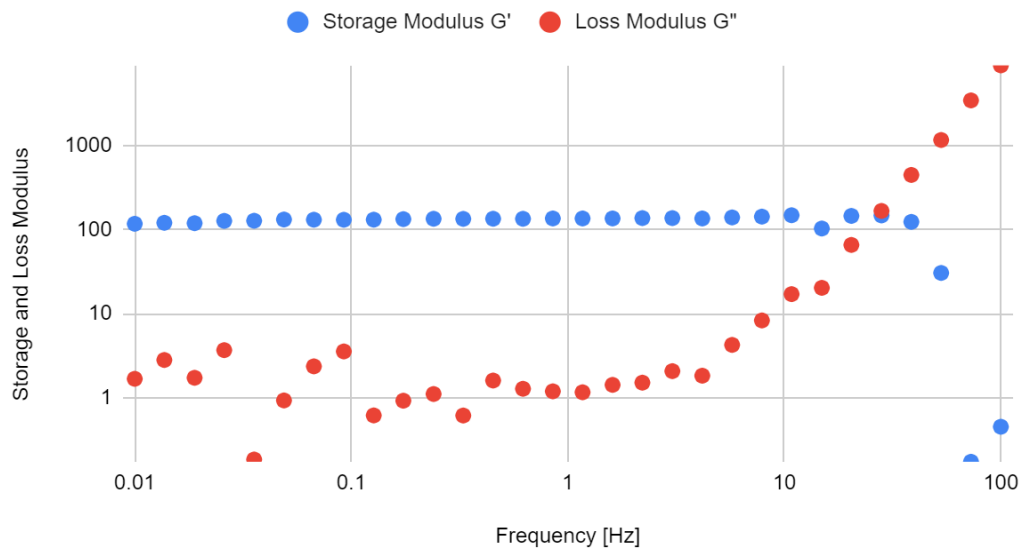
Permeability Characterization Using Transwell System

Preparing The Sample for Permeability Studies:
1. Collect the aliquots of chosen collagen (Telcol-10) and keep them on ice to avoid polymerization
2. Collect aliquots of 0.01M HCL and 0.1M NaOH
3. Mix the collagen at an 8:1:1 ratio checking to make sure the ph is in the range of 7.0-7.6
4. Apply 68µl of designated collagen to the 24-well membrane insert system and place it in 24 well plate
5. Place in the incubator at 37 degrees celsius for 30 minutes

Permeability studies in the membrane insert system:
1. Create a stock solution of 2 mL/mL NaFl (fluorescein sodium salts) PBS or DPBS (-)
2. Take an aliquot of the stock solution and dilute this stock solution down to 0.0125mg/ml making sure to make enough for each transwell
3. Using the 0.0125mg/ml solution, create a standard curve in a 96-well plate with 1:64, 1:128, 1:256, 1:512, 1:1024, 1:2048, and 1:4096 dilutions in order to establish a linear range. The final volume in the well should be 100µL. Read the curve at 485 nm excitation 535 nm emission for 20ms44
4. Add 1000µL of DPBS or PBS to the outside of the transwell system (the acceptor compartment)
5. Carefully add 205µL of the donor solution (0.0125mg/mL) to the transwell insert
6. Transfer the entire system to the incubator
7. Take 20µL samples of the acceptor solution periodically every hour
8. Run this assay for 5 hours
9. Once all samples have been collected run them dilute them in 480µL of DPBS and run them on a plate reader

Experimental Determination of Mass Transfer Area Coefficient (MTAC)

Materials needed:
- Three chamber chip with membrane addition, plasma bonded to a glass microscope slide
- Blood analog solution
- Dialysate solution
- Collagen hydrogel
- Syringe pump
- Luer adaptors
- Plastic tubing
- Stanbio blood urea nitrogen (BUN) assay kit
- Cuvettes
- Microcentrifuge tubes
- Pipette tips

Setup:

1. Seed collagen hydrogel into the three-chamber chip with the membrane addition using a positive displacement pipette.
2. Draw blood analog into a 1 mL syringe and attach the end to plastic tubing. Using Luer adaptors, place the opposite end of tubing in the inlet for the blood analog chamber on the chip. Place another Luer adaptor and plastic tubing piece on the outlet of the blood analog chamber.
3. Place the chip in an incubator with temperature control at 37℃. Feed the plastic tube connected to the syringe through the back outlet of the incubator.
4. Place the syringe into the syringe pump. Gently fill the blood analog chamber by hand. Set the syringe pump to 9 µL/min.
5. Fill the dialysate chamber at the inlet using a pipette with the dialysate fluid.
6. Start the syringe pump.
7. Run the setup for 6 hours.

Preparation/Performance of BUN assay (adapted from the manufacturer - Stanbio):

1. Prepare the working reagent in a 5:1 ratio of buffer (R1) to enzyme (R2). Suggested volumes for this experiment: 5 mL buffer R1 : 1 mL enzyme R2. Let the reagent stand for at least 30 minutes at room temperature.
2. Take a 50 µL sample of the dialysate solution from the dialysate chamber in the microfluidic chip using a pipette inserted into the dialysate chamber outlet. Pipette slowly. Deposit the sample in a microcentrifuge tube.
3. Prepare 50 µL of the BUN standard 30 mg/dL solution in a microcentrifuge tube. Label accordingly.
4. Zero spectrophotometer at 340 nm with distilled water.
5. Add 1.0 mL working reagent to the cuvette and warm to 37℃ for three minutes using an incubator.
6. Add 10µL of the dialysate sample to the 1.0 mL working reagent in the cuvette after three minutes. Swirl gently to mix.
7. After exactly 30 seconds, read and record absorbance at 340 nm, A1.
8. At exactly 60 seconds after reading A1, read and record absorbance A2.
9. Calculate change in absorbance by subtracting A1-A2.
10. Repeat steps 4-9 with the standard solution. (and any subsequent samples + standards).

Calculation of BUN/Urea concentration:

1. Determine the serum BUN with $([(A1-A2)_{sample}]/[(A1-A2)_{standard}])*30$ = BUN (mg/dL)
   a. If BUN exceeds 140, samples should be diluted 1:1 with distilled water. Then multiply results by a factor of 2.
   b. Calculate urea concentration in mg/dL with urea (mg/dL) = BUN (mg/dL) * 2.14
   c. Calculate urea concentration in mmol/L with urea (mmol/L) = urea (mg/dL) * 0.167
   d. Convert mmol/L urea concentration to mmol/m^3 urea concentration.

e. Use MTAC calculation from the COMSOL simulation data to get scaled MTAC value for the chip.

i. $MTAC\ (mL/min)\ = \frac{V}{t}\ ln(\frac{(P - D_i)}{(P - D_f)})$

Direct Transfer Sterility Test

Materials Needed:
9 PDMS chips prepared using soft lithography method and plasma-bonded to glass slides
Luria broth, prepared according to package instructions and autoclaved according to package instructions
Cell culture plates or petri dishes (12), sterile
96 well plate(s) for absorbance readings/sampling
Pipette with capability of pipetting 100 μL
70% isopropyl alcohol or 70% ethanol
Luria agar plates

Instruments Needed:
UV sterilization box/chamber
Plate reader
Incubator with temperature control
Microscope with imaging capabilities

Phase I: Sterilization of Chips
- Punch inlets into all of the chips using a 200 μL disposable pipette tip.
- Group #1: Control:
    a. Put a sleeve of sterile culture plates in the biosafety cabinet. Remove three plates and bring to the benchtop. Place one chip in each plate to form the control group (n=3). These plates will not be sterile. Label accordingly.
- Group #2: UV sterilization
    a. Remove three plates from the sleeve in the biosafety cabinet. Place one chip in each plate to form the first experimental group (n=3). Label accordingly.
    b. Place the plates in the UV sterilization chamber. Remove and discard the lids of the plate prior to closing the chamber door to ensure more direct UV exposure to the PDMS. Close the chamber door and set the timer for 1 hour.
    c. Following UV sterilization and prior to opening the door, remove three plates from the sterile package in the biosafety cabinet. Open the door and quickly replace the lids on each sterilized plate with the new lids. Discard the remaining plates.
    d. Label each plate accordingly.
- Group #3: Isopropyl/Ethanol Sterilization
    a. Remove three plates from the sleeve in the biosafety cabinet. After spraying each chip with isopropyl alcohol to transfer to the biosafety cabinet, place one chip in each plate to form the second experimental group (n=3). Label accordingly.

b. Remove the lids and balance on the edge of each plate, so each lid is still mostly covering the chip.
c. Using a pipette, pipette 100 μL of ethanol/isopropyl alcohol into the chambers of each chip (or equivalent volume to fill channels).
d. Spray the entire chip with ethanol/isopropyl alcohol.
e. Wait approximately 1 minute before aspirating as much fluid from the channels as possible.
f. With the lids balanced on the plates, and chips balanced on plates to allow for the bottom to dry,wait 15 minutes for remaining alcohol to dry.
g. Replace lids fully and label accordingly.

Phase II: Luria broth addition

- Bring the luria broth into the biosafety cabinet. Fill four sterile 50 mL conical tubes with 30 mL Luria broth prior to addition to any chip. One will be used for the 'blank' samples during absorbance readings using the plate reader. The other three will be used for addition to the control group plates. Label accordingly.
- Bring the experimental group chips into the biosafety cabinet.
- Pipette 100 μL of luria broth into the chambers of each chip (or equivalent volume to fill channels).
- Add enough luria broth to each plate to cover the chips completely (estimated 30 mL of broth).
- Repeat broth addition steps for control group chips on the benchtop.
- Make three plates of sterile broth in sterile plates as a sterile broth control group. Use same volume of broth as chips (~30 mL).
- Place all chips in Tupperware containers with the lids balancing on them in the incubator at 37℃ (to prevent accidental contamination from incubator airflow).

Phase III: Sampling

- 15 minutes after initial incubation following broth addition, take D0 samples. Place 100 μL samples of broth from each plate into the designated 96 well plate spot and three 'blank' samples.
- Run samples on the plate reader at 595 nm using the procedure in the Gen5 software.
- Export results/take a picture of results.
- Repeat procedure in 24 hour increments for D1, D2, and D3 samples. Get average and standard deviation for all plate absorbance values. Compare absorbance to determine optical density.

Phase IV: Agar plating of broth

- If absorbance values differ significantly from the blank samples for any group studied (statistical significance determined through ANOVA method) plate at least one sample from one of the plates in that control group.
- Dilute the broth sample using an appropriate dilution factor in sterile Luria broth. Take a 100 μL sample and pipette onto a Luria agar plate, previously prepared. Use glass beads and gently swirl to have the sample cover the plate entirely.

- Replace lid and place in incubator at 37℃ for three days.
- On day 3, remove plates from the incubator and examine them under the microscope. Take images of contaminants (bacteria, fungi) to quantify.

Appendix H - Transswell Permeability Assay Data

Table 7: A Complete table of collected fluorescence and concentration values taken from the transwell system

| Trial 1-Fluorescence RFU	Hours	well 1	well 2	well 3		Trial 1-Concentration (mg/ml)	Well 1	Well 2	Well 3	
	1	290894	484490	468600			1.01E-04	1.70E-04	1.64E-04	
	2	767044	615905	1508511			2.71E-04	2.17E-04	5.36E-04	
	3	1603654	1774849	2607870			5.70E-04	6.31E-04	9.29E-04	
	4	2372979	2296316	2671674			8.45E-04	8.17E-04	9.51E-04	
	5	2885419	2897895	3346075			1.03E-03	1.03E-03	1.19E-03	
Trial 2-Fluorescence RFU	Hours	Well 1	well 2	well 3		Trial 2-Concentration (mg/ml)	Well 1	Well 2	Well 3	
	1	227465	306752	815345			7.84E-05	1.07E-04	2.88E-04	
	2	1228214	1088388	841750			4.36E-04	3.86E-04	2.98E-04	
	3	1430542	2360075	2083430			5.08E-04	8.40E-04	7.41E-04	
	4	2416770	2854779	2285258			8.60E-04	1.02E-03	8.13E-04	
	5	2695110	3768215	2241221			9.60E-04	1.34E-03	7.98E-04	
Trial 3-Fluorescence RFU	Hours	Well 1	Well 2	Well 3	Well 4	Trial 3-Concentration (mg/ml)	Well 1	Well 2	Well 3	Well 4
	1	700860	352808	418474	403360		8.25E-06	3.27E-06	4.21E-06	4.00E-06
	2	2173620	1087630	1953420	976314		2.93E-05	1.38E-05	2.61E-05	1.22E-05
	3	2416115	2053335	4212973	2587009		3.28E-05	2.76E-05	5.84E-05	3.52E-05
	4	3868078	3316580	4017733	3351945		5.35E-05	4.56E-05	5.56E-05	4.61E-05
	5	4577741	3962074	4695955	3651331		6.36E-05	5.48E-05	6.53E-05	5.04E-05
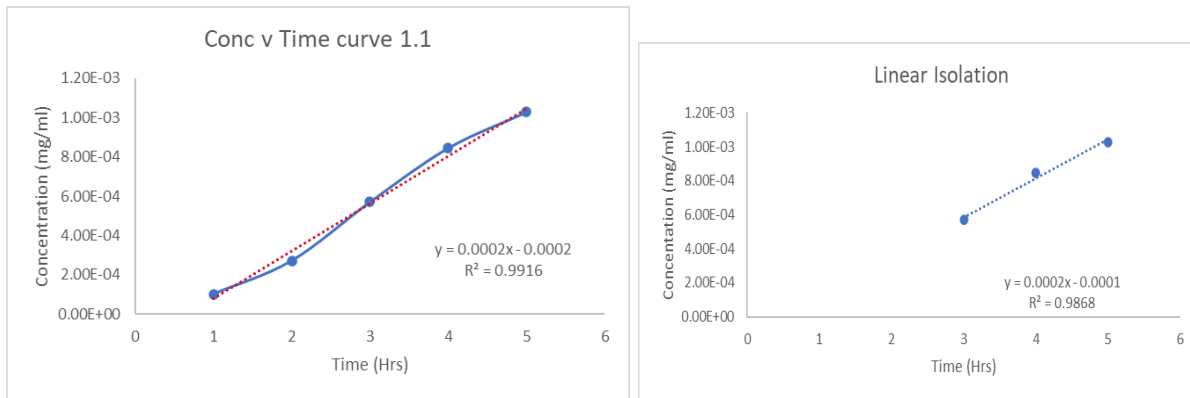
Figure 40: Representative concentration vs. time graphs of trial one with linear isolation

Table 8: Collected concentrations vs. time slopes with averages

Concentration/time- slopes	Trial 1	Trial 2	Trial 3
	0.0002	0.0002	0.0004
	0.0002	0.0004	0.0004
	0.0002	0.0004	0.0007
Averages	0.0002	0.000333	0.0005

Table 9: Permeabilities derived from respective concentration vs. time slopes and well dimensions

Premeability	Area	Conc	Volume	Conc/time
1.48148E-06	0.3	0.0125	1	0.0002
2.44444E-06	0.3	0.0125	1	0.00033
3.7037E-06	0.3	0.0125	1	0.0005
2.96296E-06	0.3	0.0125	1	0.0004
5.18519E-06	0.3	0.0125	1	0.0007

Table 10: Final permeabilities for each trial with one-way ANOVA P-value

Permeabiltiy Coefficent (m/s)	Trial 1	Trial 2	Trial 3
p-value<0.05	1.48E-06	1.48E-06	2.96E-06
	1.48E-06	2.96E-06	2.96E-06
	1.48E-06	2.96E-06	5.18E-06

Volume Calculations:

12 well:

- Volume of collagen used: $226\mu L \rightarrow .226ml \rightarrow .226cm^3$
- Volume=cross sectional area*height $\rightarrow$ Height = volume/area
- cross sectional area: $.985.3cm^2$
- Height= $(.226cm^3)/(.985.3cm^2)$
    - = **.229cm**

24 well:

- Volume of collagen needed = (Cross sectional area 24-well) * (.229cm)
- Cross sectional area: $.3cm^2$
- Volume = $(.3cm^2)*(.229cm)$
    - = **68.7µL**

Appendix I - COMSOL Data for Diffusion Coefficient Optimization

Table 11: Geometry parameters for simulation

Name	Expression for 24 well System in mm	Description
d_tran	6.5 [mm]	Diameter of the well
d_a	8.0 [mm]	Diameter of the Membrane
d_w	15.6 [mm]	Diameter of the Acceptor
h_b	2 [mm]	Height of the Barrier
h_sp	1 [mm]	Distance between well and Bottom
h_a	5 [mm]	High of the Acceptor
b	h_b/2	Immersion Depth
r	((d_a)^2+4*b^2)/(8*b)	Radius of Immersion Ball+
r_z	r+h_b	z-Position of the Immersion Ball+

Table 12: Chemical properties

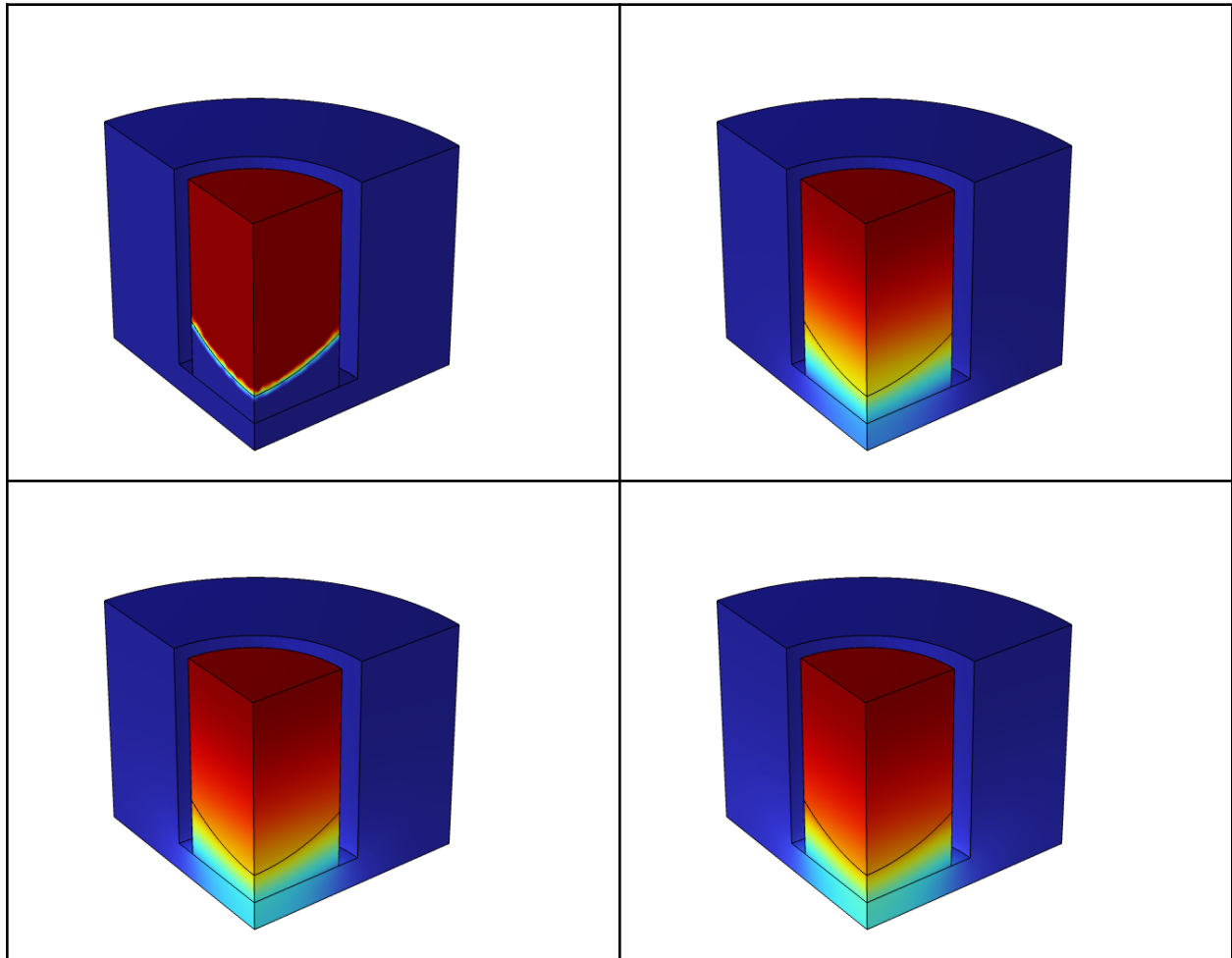| Name	Expression	Description
Dif_w	1e-9 [m^2/s]	Diffusion Coefficient of water
C_f	0.03322 [mol/m^3]	Fluorescein Salt Concentration

Figure 41: Concentration of urea over time in transwell system
at t 0, 1.5, 3, and 5 hr (left to right, to to bottom)

Appendix J - COMSOL Parameters for Microfluidic device MTAC Simulation

Table 13: Simulation parameters

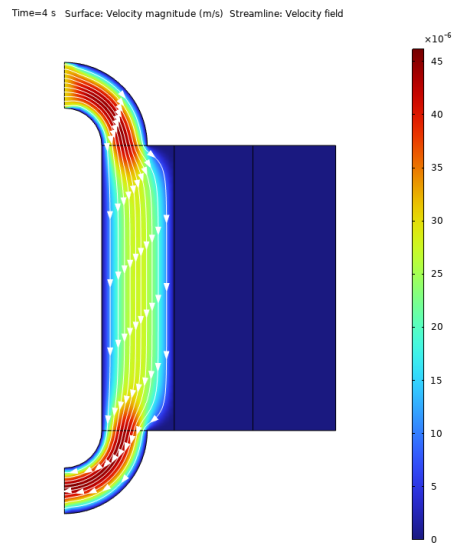| Name	Expression	Description
Diff_w	1e-9[m^2/s]	Diffusion Coefficient of water
D	6.2484e-10[m^2/s]	Collagen diffusion coefficient
C_u	2.141[g/ml]/60.06[g/mol]	Urea Concentration
eps_rho	1114[kg/m^3]	Blood analog Density
eps_mu	4.184e-3[Pa*s]	Blood analog Viscosity
V0	1.82e-3[m/min]	Initial Velocity

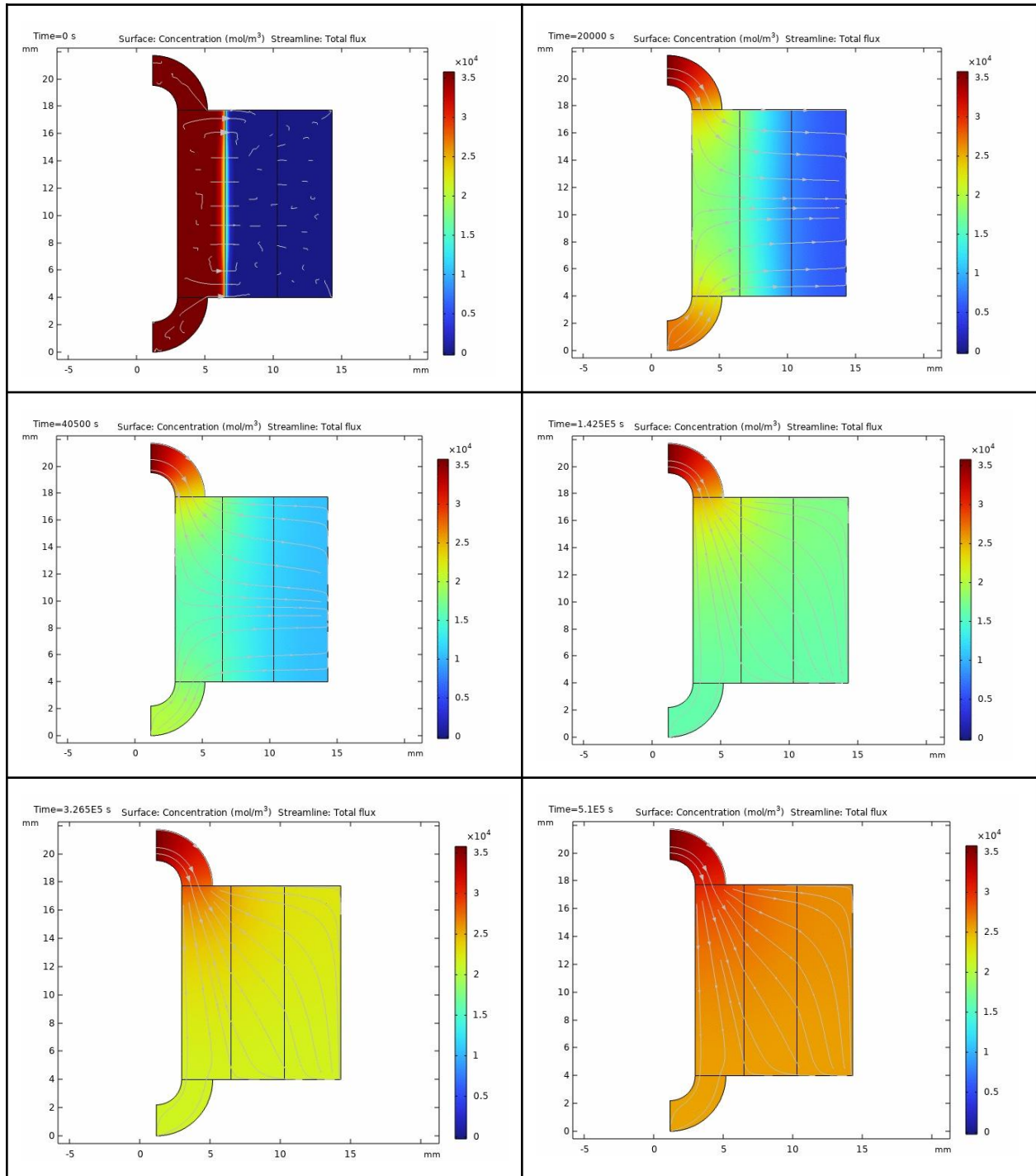**Figure 42: Velocity field in microfluidic system**

Figure 43: Concentration of urea over time in microfluidic model
at t 0, 5.5, 11.25, 39.6, 90.7, and 141.7 hr (left to right, to to bottom)

Appendix K - Multiple Comparison Testing for Direct Transfer Sterility Testing

Holm-Sidak for Significant Differences	Run #1	UV-Sterilized vs. Sterile Broth	IPA Sterilized vs Sterile Broth	UV-Sterilized vs. Non-Sterile Control	IPA-Sterilized vs. Non-Sterile Control	Non-Sterile Control vs. Sterile Broth Plates
Day 0		ns	ns	ns	ns	ns
Day 1		ns	****	ns	ns	*
Day 2		*	***	ns	ns	*
Day 3		*	**	ns	ns	**
		Target = ns (no sigificance, want the sterilized absorbance to be the same as the sterile broth, reduced pathogenic growth seen)	Target = ns (no sigificance, want the sterilized absorbance to be the same as the sterile broth, reduced pathogenic growth seen)	Target = **** (want sigificance, want the sterilized absorbance to be different from the control and lower, reduced pathogenic growth seen)	Target = **** (want sigificance, want the sterilized absorbance to be different from the control and lower, reduced pathogenic growth seen)	Target = **** (want sigificance, want the sterile broth absorbance to be different from the control and lower, reduced pathogenic growth seen)

The red boxes outline areas of interest where the result met the desired target.

Key for results: ns = no significance difference (P > 0.05) * = significant difference (P < 0.05), ** = significant difference (P < 0.01); *** = significant difference (P < 0.001); **** = significant difference (P < 0.0001)

Holm-Sidak for Significant Differences	Run #2				
	UV-Sterilized vs. Sterile Broth	IPA Sterilized vs Sterile Broth	UV-Sterilized vs. Non-Sterile Control	IPA-Sterilized vs. Non-Sterile Control	Non-Sterile Control vs. Sterile Broth Plates
Day 0	ns	ns	ns	ns	ns
Day 1	ns	**	***	****	****
Day 2	ns	ns	ns	ns	**
Day 3	ns	***	ns	ns	***
	Target = ns (no sigificance, want the sterilized absorbance to be the same as the sterile broth, reduced pathogenic growth seen)	Target = ns (no sigificance, want the sterilized absorbance to be the same as the sterile broth, reduced pathogenic growth seen)	Target = **** (want sigificance, want the sterilized absorbance to be different from the control and lower, reduced pathogenic growth seen)	Target = **** (want sigificance, want the sterilized absorbance to be different from the control and lower, reduced pathogenic growth seen)	Target = **** (want sigificance, want the sterile broth absorbance to be different from the control and lower, reduced pathogenic growth seen)

Conclusion: The only favorable consistent trend across time points studied is between UV sterilized chip broth samples and sterile broth samples in that there is no statistical difference in the absorbances, meaning the UV sterilized chip broth samples are comparable to sterile broth samples in terms of pathogenic growth.
This trend is seen across 2 days for run #1 and 4 days for run #2. The fact that there is a statistically significant difference between the non-sterile control chip broth samples and sterile broth samples past day 0 (significant pathogenic growth relative to sterile broth) for all days for both runs further reinforces this conclusion. UV-sterilization should be recommended for further testing with cell culture.

The red boxes outline areas of interest where the result met the desired target.

Key for results: ns = no significance difference (P > 0.05) * = significant difference (P < 0.05), ** = significant difference (P < 0.01); *** = significant difference (P < 0.001); **** = significant difference (P < 0.0001)

Appendix L - Biofilm Formation During Sterility Test

Figure 44: An example of biofilm formation within a Luria broth plate containing a microfluidic chip.
This biofilm was difficult to break through with a pipette tip and plates with biofilm often ended up with at least one sample to be tested for absorbance that consisted of just biofilm.